TECHNICAL MEMORANDUM

686

Progress in predicting tropical systems: The role of convection

P. Bechtold, P. Bauer, P. Berrisford,
J. Bidlot, C. Cardinali, T. Haiden,
M. Janoušek, D. Klocke, L. Magnusson,
A. McNally, F. Prates, M. Rodwell,
N. Semane, F. Vitart

Research Department

November 5, 2012

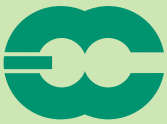

European Centre for Medium-Range Weather Forecasts
Europäisches Zentrum für mittelfristige Wettervorhersage
Centre européen pour les prévisions météorologiques à moyen terme

Series: ECMWF Technical Memoranda

A full list of ECMWF Publications can be found on our web site under:
http://www.ecmwf.int/publications/

Contact: library@ecmwf.int

European Centre for Medium-Range Weather Forecasts
Shinfield Park, Reading, RG2 9AX, England

Abstract

Progress in forecasting tropical convection with the ECMWF Integrated Forecast System (IFS) is analysed through a review of tropical errors and their evolution during the last decade as a function of model resolution and model changes. As the characterization of these errors is particularly difficult over tropical oceans due to sparse in situ upper-air data, satellite data assumes an important role for model evaluation and in data assimilation.

The evaluation of the IFS is based on the available near-surface observations and increments applied in the analysis to the short-range forecast from assimilating conventional and satellite data. A comparison with Met Office analyses is also included. Model deficiencies in the short to medium-range have been evaluated with focus on the Eastern Pacific and Indian Oceans using analyses and mostly based on the available wind observations, pointing also to problems with some observational data. A systematic underestimation of low-level wind convergence in the Inter Tropical Convergence Zone (ITCZ) in the IFS could be documented, leading to a weakening of the Hadley cell. Critical areas with strong cross-equatorial flow and large lower-level wind errors are the Indian Ocean with large interannual variations in forecast errors, and the East Pacific with persistent systematic errors that have reduced little during the last decade.

The evaluation of the model's tropical mean climate, variability and teleconnections is based on seasonal forecasts, with a particular focus on the Madden-Julian Oscillation (MJO) during the Year of Tropical Convection (YOTC). The model is shown to reproduce the observed tropical large-scale waves, oscillations and teleconnections, apart from missing teleconnection during winter between the tropical stratospheric winds and the northern-hemisphere tropospheric circulation. The major mean state error concerns the overestimation of South-East Asian summer monsoon rainfall. The recent improvements in tropical precipitation, convectively coupled wave and MJO forecasts are shown to be strongly related to improvements in the convection parameterization that realistically represents the convection sensitivity to environmental moisture, and the large-scale forcing due to the use of strong entrainment and a variable adjustment time-scale. There is however a remaining, slight moistening tendency and low-level wind imbalance in the model that is responsible for the Asian Monsoon precipitation bias and for too strong low-level easterly winds near the Equator. The diurnal cycle of precipitation is realistic over water, but the simulated maximum intensity over land precedes the observations by 3-4 hours.

Finally, preparing for the future high-resolution IFS system, where deep convection will become gradually more resolved, we currently develop a numerically efficient and generally scalable Aqua-planet system that can be applied to planets of different size and gravity. Using an equatorially symmetric sea surface temperature (SST) distribution representative for the Central Pacific, it is possible to reproduce the main tropical and midlatitude characteristics of the climate on the real Earth. The first climate simulations on a reduced Aqua-planet are promising and indicate that it is possible to realistically represent, equivalent to high horizontal resolution, the tropical wave spectra and the wave interactions between the Tropics and the mid-latitudes on small planets.

1 Introduction

Analysing the tropical convection in a forecast system is a huge and difficult task. Due to the small Coriolis force and large Rossby radius of deformation near the Equator as well as fast propagating gravity waves that export the convective heating (Bretherton and Smolarkiewicz, 1989), convection affects a vast variety of space and time scales, from the individual convective cloud to the large-scale convectively coupled waves (e.g. Simmons, 1982; Žagar *et al.*, 2005), the intraseasonal oscillations, and the Monsoon circulations.

Furthermore, it is difficult to observe convection as such or all the convective transport processes. It is therefore appropriate to describe convection by measuring the quality of the model in terms of

convection- and cloud-related quantities such as surface precipitation, outgoing longwave radiation (OLR), and observables such as the temperature, moisture and wind fields. Given these measures, it is possible to conclude on the overall forecast quality in representing convective phenomena, but not necessarily to conclude on the quality of the convection parameterization scheme itself as employed in large-scale models with horizontal resolutions larger than say 5 km. This is especially true in the Tropics where, on larger space and time-scales, the atmosphere is in radiative convective equilibrium (Held *et al.*, 1993) (see also Tompkins *et al.* (2004) Figure 3.6), so that heating processes like upper-tropospheric stratiform condensational heating and cloud radiation interaction play an important role. On synoptic scales a balance between the large-scale dynamical forcing and the convection damping prevails, while both processes strongly interact. The momentum budget is also critical, depending on an equilibrium between the large-scale pressure gradient (vertically integrated temperature anomaly), turbulent dissipation and friction due to cumulus momentum transport.

A major difficulty in evaluating tropical convection and forecasts in the Tropics resides in the sparseness of upper-air in situ data over tropical Oceans making satellite data products the main observational information source in these regions. The impact of conventional and satellite data in the analysis is defined by data density and the assigned observation errors, and thus in areas with extended cloud coverage and convection, the analysis is more strongly driven by the forecast model than by observations, and is therefore more affected by model errors. At present there is not much literature assessing the uncertainty of atmospheric analyses (Langland *et al.*, 2008; Wei *et al.*, 2010; Peng *et al.*, 2012) or studying the predictability of forecast systems (Kanamitsu, 1985; Simmons and Hollingsworth, 2002) for the Tropics, but this should change with the availability of the TIGGE archive (Park *et al.*, 2008; Bougeault *et al.*, 2010). At ECMWF, satellite observations sensitive to temperature, moisture, clouds and wind are assimilated over the Tropics. The impact of the satellite observing system on the analysis and forecasts over tropical Oceans has been outlined in Bauer *et al.* (2006), Kelly *et al.* (2007), Andersson *et al.* (2007), Geer *et al.* (2010), and Bauer *et al.* (2011). All the available studies agree in that the tropical East Pacific and East Atlantic, as well as the equatorial Indian Ocean stand out as key areas sensitive to observations. However, the impact of moisture-related observations on the dynamics is generally weaker and dissipates fairly quickly into the forecast while temperature sensitive observations are difficult to use in cloudy areas.

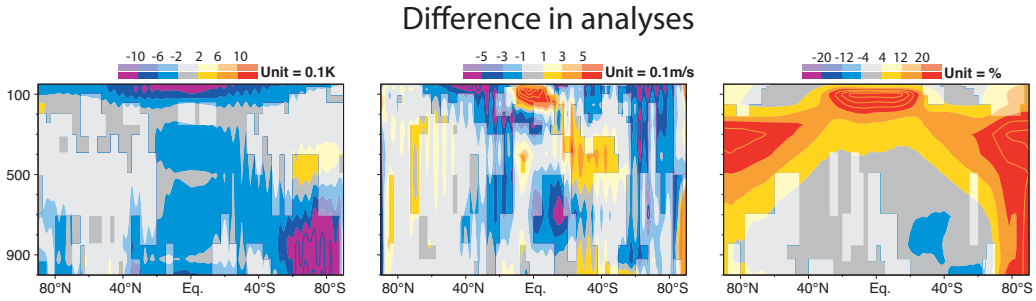

Figure 1: Vertical cross section of 2011 annual and zonal mean difference in analysis between ECMWF and UKMO: (a) temperature (K), (b) U-wind (m s^{-1}), and (c) relative humidity (%). Significant differences at the 95% level are marked by dark colours, pale shading is used otherwise.

In order to illustrate the uncertainty in tropical analysis we have plotted in Figure 1 the zonal mean analysis difference during 2011 between ECMWF and the Met Office (hereafter refered to as UKMO) for temperature, zonal wind, and relative humidity. It is evident that large differences occur in the Tropics with a tropical troposphere being around 0.5 K colder in ECMWF compared to UKMO - this difference

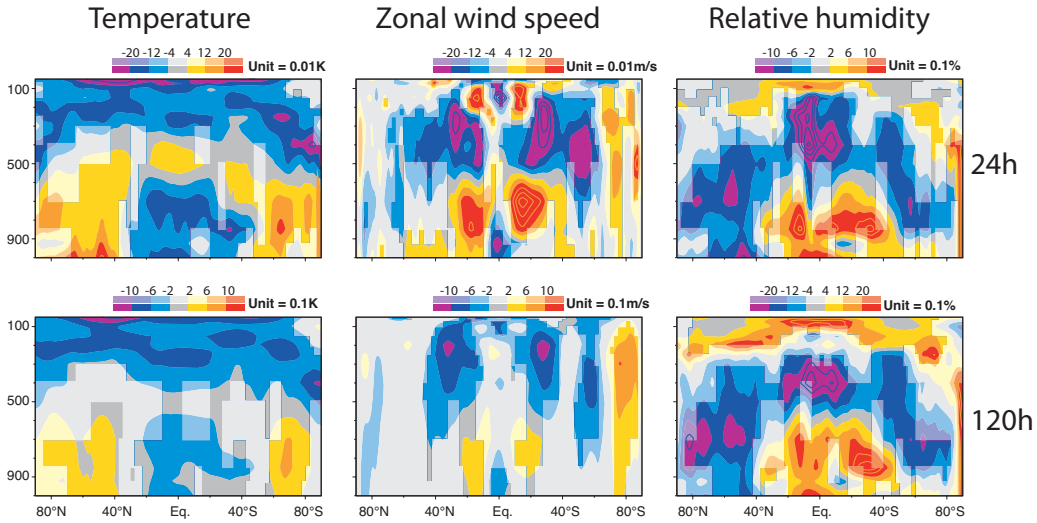

Figure 2: Mean annual ECMWF forecast errors from verification against own analysis for forecast lead times day+1 and day+5: left column, temperature (K), middle column U-wind (m s^{-1}), and right column relative humidity (%). Note the different scaling for different lead times.

is significantly larger than random errors in satellite observations which are of O(0.1-0.2 K). Wind differences amount to roughly 0.5 m s^{-1}, whereas upper-tropospheric relative humidities differ by up to 20%. Analysis differences express model, data assimilation system and observational data usage differences. Disentangling these contributions can be difficult. However, not only analysis differences are relatively large in the Tropics, also forecast errors are significant as illustrated in Figure 2 by the annual mean differences for 2011 between the ECMWF operational forecasts at lead times day+1 and day+5, respectively and the ECMWF operational analysis. Lower and upper-tropospheric tropical zonal mean errors at lead time day+5 are similar in magnitude to the analysis differences seen in Figure 1 and amount to 0.5 K for temperature and to 0.5 m s^{-1} for wind, while mid-tropospheric errors are small. The humidity errors, however are of O(2%) and therefore much smaller than the analysis difference in Figure 1 which points to differences in the model physics formulations and the moisture analysis.

Our goal is to provide a global picture of the quality of both analysis and forecasts in the Tropics, including the progress made over the last decade up to the latest model cycle Cy38r1 (operational since 19 June 2012) that gives the best results. In order to keep the overall document concise we decided to limit the discussion mainly to the high-resolution forecast system, but the results presented from monthly and seasonal integrations are based on ensemble mean statistics, and the ensemble mean forecast errors of the Ensemble Prediction System (EPS) are compared to the high-resolution system and shown to be largely similar. Instead we want to provide physical insight into recent model improvements in tropical mean state and variability, and give perspectives for current and coming developments in tropical convection and model resolution upgrades. Unfortunately, given the vast variety of convection driven circulations and oscillations, it is impossible to analyse them all, and we decided to focus mainly on the tropical oceans, and to build on previous studies.

The Indian and South-East Asian Monsoon have been looked at in Rodwell *et al.* (2010) and Molteni *et al.* (2011). The principal forecast errors pointed out by the authors concern an overestimation of rainfall over the Maritime Continent and during the Monsoon, in particular for the Indian Monsoon during June. The corrsponding overestimation in diabatic heating leads to an easterly wind bias in the equatorial Pacific affecting the prediction of ENSO in the seaosnal forecast system 4 (Molteni *et al.*, 2011). Kamga *et al.*

(2000), and more recently Agusti-Panareda *et al.* (2010) and also Molteni *et al.* (2011) focused on equatorial Africa and the Sahel and noticed a northward migration of the ITCZ with forecast lead time, and a weakening of the eastern branch of the African easterly jet. It is not yet clear if these errors are due to either an overestimation of the depth of the Saharan boundary-layer (possibly also in conjunction with radiation), and consequently to an overestimation of the Saharan heat low, or an insufficient representation of convective heating and momentum transport in relation to squall-lines forming along African easterly waves.

Model physics changes between the ERA40 (Uppala *et al.*, 2005) and the ERA-Interim (Dee *et al.*, 2011), including increased convective precipitation over land, and the effects of upper-tropospheric ice supersaturation have been reported in Tompkins *et al.* (2004). The important forecast model improvements during 2007-2008 from which also the seasonal forecast system 4 has benefited have been outlined in Bechtold *et al.* (2008) and Jung *et al.* (2010). The authors reported on improvements in model climate and its variability, in particular the MJO (Madden and Julian, 1971) and tropical wave spectra. They showed that all model physics developments contributed including the land surface scheme, the turbulent diffusion, the cloud scheme, the radiation and the convection, but that the latter had the biggest overall effect also on the midlatitude predictability. However, so far the physical mechanisms behind the improvements in the Tropics remained partially unclear.

The structure of the paper is as follows. We first document the progress in the operational high-resolution forecast system during the last decade by a comparison against available surface observations for ocean and land areas, forecasts are also evaluated against the operational analysis and the ERA-Interim. In section 3 first-guess departures (background forecast minus observation), analysis increments (analysis minus background forecast) and forecast 'errors' during 2011 are used to identify regions with major model errors, and identify the impact of key observations. These regions turn out to be those with strong cross equatorial flow. In section 4 newly developed tools and observations are used to evaluate in the latest model cycle (Cy38r1) the tropical climate, its teleconnections, and the variability of convection over land, and to relate the model climate errors to the short range forecast errors. We also look ahead to evaluate the climate impact of the next vertical resolution upgrade. The last two sections are devoted to two main research topics that concern i) the MJO predictability in relation to background relative humidity and the phase of convective heating/drying, and ii) tropical convectively coupled waves and the MJO in the current and a future high-resolution forecast system.

2 Progress during the last decade

As an overview of the evolution of the high-resolution suite of the IFS in the Tropics over the last decade, time series of a number of skill and/or error measures are presented based mainly on surface observations, but also satellite products and upper-level winds from analysis are utilized. In order to better relate changes in the forecast quality to changes in the model system, a non-exhaustive list of major model cycles including resolution changes and changes to the forecast and analysis system affecting the Tropics in particular is given in Table 1. Major cycles with changes to the data assimilation and model system include Cy24r3 (2002), Cy25r4 (2003), Cy31r1 (2006) corresponding to the ERA-Interim, Cy32r3 (2007), Cy36r4 (2010) and Cy38r1 (2012), whereas major resolution changes occured with Cy23r3 (2000), Cy30r1 (2006), and Cy36r2 (2010).

Over the tropical oceans we have available an over 20-year long time series of total column water vapor (TCWV) retrievals from the microwave SSMI (product RSSv6) that are compared in Figure 3 against the monthly mean values from the ERA-Interim and operational analysis. The significant variation of

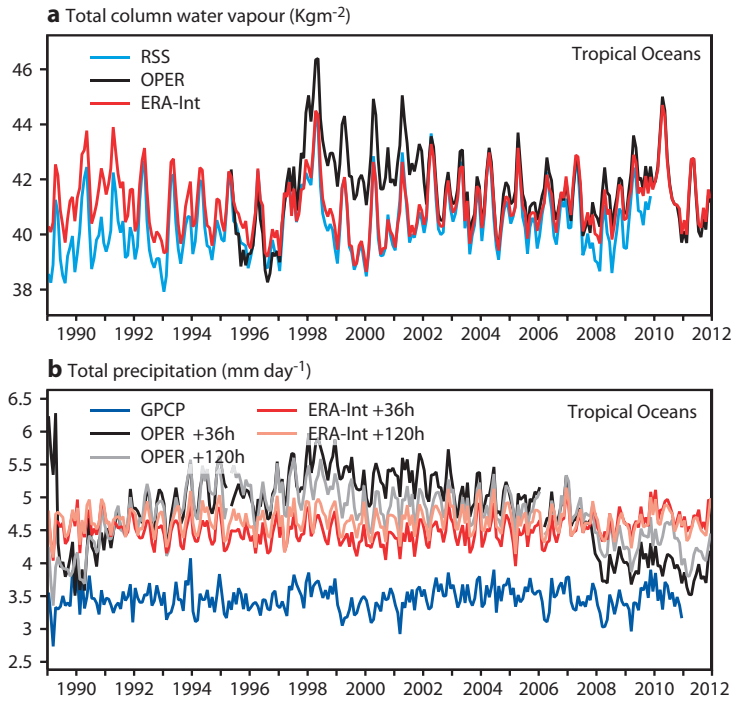

Figure 3: Time series of monthly mean Total Column Water Vapor (kg m^{-2}) over tropical oceans from observations (RSSv6 from SSMI) and ERA-Interim and operational analysis (a), and daily mean precipitation (mm day^{-1}) from the GPCP2.2, and the ERA-Interim and operational forecasts for forecast steps 12-36 hours and 96-120 hours (b).

model TCWV between 1997 and 2002 is explained by changes to the deep convection scheme in 1997 (Cy18r3), the introduction of TCWV derived from SSM/I in data assimilation in 1999 (Cy18r6) and an adjustment of the SSM/I TCWV bias correction in 1999 (Cy24r3). This period demonstrates the sensitivity to combined model-assimilation modifications. Note that from September 2006 to June 2007 both operational analysis and reanalysis use the same model cycle but different resolutions and data processing. Overall, since 2002 (Cy24r3) both analyses produce an average TCWV content of around 41 kg m^{-2} which closely fits the observations because these are assimilated and bias corrected more objectively than before.

A similar comparison was made for the daily mean precipitation over tropical oceans for forecast lead times 12-36 hours and 96-120 hours against the Global Precipitation Climatology Project (GPCP) product 2.2. With, on average, 4.5 mm day^{-1} the ERA-Interim forecasts produce much higher precipitation than the 3.5 mm day^{-1} from the GPCP2.2 product. In the ERA-Interim after 2006 there is only a small difference in the rain rates between the day+1 and day+5 forecasts. While the operational forecasts used to produce rain rates of O(5.5 mm day^{-1}) at day+1, there is a notable decrease to values of 5 mm day^{-1} in 2003 (Cy25r4), 4.7 mm day^{-1} in 2006 (Cy30r1), and an even sharper decrease in 2008 (Cy32r3) to average day+1 precipitation rates of below 4 mm day^{-1}. However, also since Cy32r3 the day+5 precipitation rates now exceed the day+1 precipitaion rates by about 0.3 mm day^{-1} due to a moistening tendency in the model (see Section 5). Overall, the tropical oceanic rain rates from the current operational forecasts at lead time day+1 are still approximately 0.4 mm day^{-1} higher than the GPCP product, but the latter likely underestimates the rain rates due to sampling errors, though the error estimate of 3% or 0.1 mm day^{-1} given by Hilburn and Wentz (2008) seems rather low.

A land-only evaluation of precipitation forecasts can be established with the aid of data from synoptic

stations. Data from roughly 600 stations reporting daily is available for the Tropics compared to about 2000 stations for the northern hemisphere extra-tropics. The evolution of the Equitable Threat Score (ETS) for precipitation events > 5 mm day^{-1} is depicted in Figure 4. The ETS is a normalised measure for correct forecasts of an event. It indicates a modest, but fairly continuous increase in precipitation forecast skill for both the Tropics and the Northern Hemisphere (NH) over the last decade. However the forecast skill in the Tropics is much lower than in the NH, with a day+4 NH forecast being as skillful as a day+1 forecast in the Tropics. Low predictability of tropical weather is related to the large Rossby radius of deformation and the weak vertical stability, and precipitation prediction over land is rendered more difficult by the mostly convective nature of precipitation and its diurnal modulation (see Section 4). Verifying the operational ECMWF forecasts during 2008 and 2009 over the Tropics and the Indian Ocean and Subcontinent in particular, Chakraborty (2010) found higher forecast skill over ocean than land.

A comparison of the ECMWF precipitation forecasts with other operational Centres following Haiden *et al.* (2012) is presented in Figure 5 based on the SEEPS score for the season 2010/2011. This score has recently been developed by Rodwell *et al.* (2010) and is the new official ECMWF 'headline score' for precipitation. It is defined in probability space and takes into account 3 categories of precipitation, namely 'dry','light',and 'heavy'. The threshold between light and heavy precipitation is defined by the local climatological distribution. The authors already evaluated the IFS extra-tropical performance with the aid of SEEPS for the period 1994 to 2008. The current results obtained from the SEEPS score (Figure 5) confirm those produced with the ETS in that a tropical day+1 precipitation forecast is of similar reliability as a NH day+4 or day+5 forecast. Figure 5 also illustrates that in the NH the forecast skill during summer is significantly lower than during winter, e.g. at lead time day+5 the summer skill is just half of that during winter, reflecting the differences in the type of precipitating systems, convective versus large-scale or stratiform. Compared to other Centres the IFS has a lead in forecast skill for both the Tropics and the NH summer and winter that is maintained throughout the forecast period. We have also added in Figure 5 results from pre-operational tests with Cy38r1[1]. This cycle shows further significant improvement for the NH and for the Tropics, where the improvement is of the same order of magnitude as the differences to the other Centres. A detailed analysis of the contributions to Cy38r1 indicates that the improvements in the NH can be attributed to the new formulation of the background errors in the analysis system. The improvements in the Tropics stem from both improvements in the analysis and improvements in the forecast system such as filtering of spurious spectral noise and tuning of the ice microphysics and the convective detrainment and downdraught strength.

An evaluation of 10m winds at analysis time and at lead times day+1 and day+5 against buoys is provided in Figure 6 for the period March 2005 to March 2012 and for different tropical areas using the scatter index (SI) and the symmetric slope (SS); see Peng *et al.* (2012) for a description of the method and the buoy locations. The scatter index is a measure of the normalized standard deviation while the symmetric slope measures the mean fit to the observations. For the whole Tropics (Figure 6a) there is a continuous improvement independent of forecast lead time of about 20% since 2005 for the SI, whereas the SS has improved by roughly 50% since 2005, with a remarkable step change in forecast skill in 2007, especially for longer lead times. Note that overall wind errors at analysis time are still significant in spite of the assimilation of the buoy data. However, 10 m wind errors vary largely between regions. The highest values of SI with the largest interannual variability in SI and SS due to the Monsoon are found for the Indian Ocean (Figure 6b). For this basin a clear improvement in SS is noticed with the introduction of Cy32r3 (2007). However, forecast errors seem to have evolved only little in the East Pacific (Figure 6c,d), in spite of improvements in the analysis since Cy36r2 (the T_L1279 system). The lowest overall values of SS, indicating a poor fit to observations, are also found in the North-East Pacific (Figure 6d). These

[1] operational since 19 June 2012

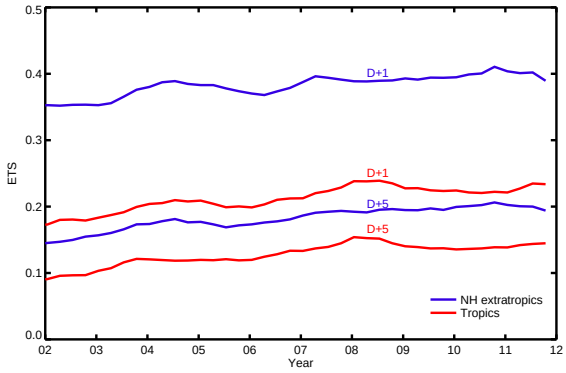

Figure 4: Time-series of 24 hours precipitation forecast skill of the ECMWF model as measured by the Equitable Threat Score (ETS) for precipitation events $>$ 5 mm for forecast lead times day+1 and day+5. A one-year running average has been applied to filter out seasonal variations. Perfect forecasts have an ETS of 1.

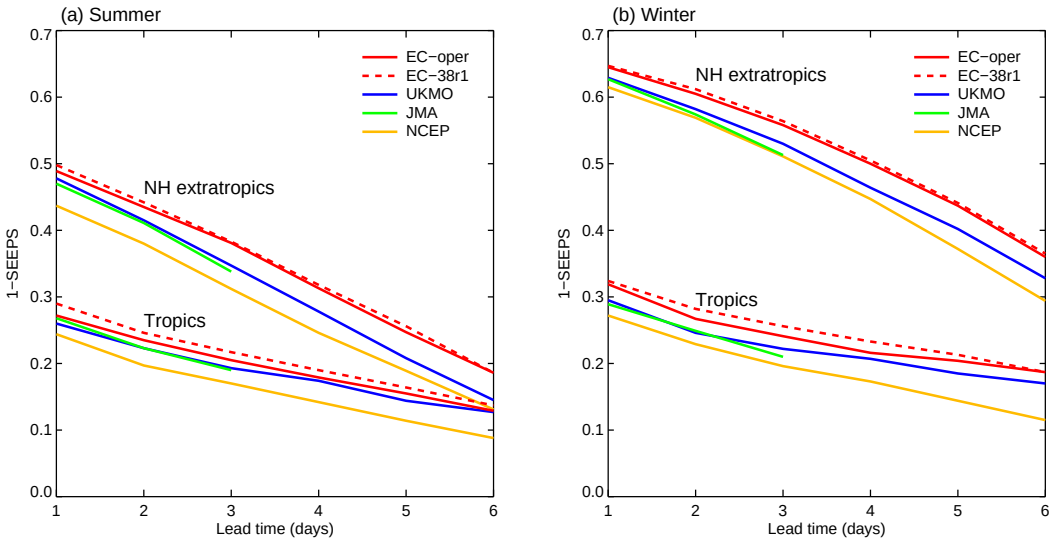

Figure 5: 24 hours precipitation forecast skill of four global models for the NH extratropics and the tropics, as measured by the SEEPS score averaged (a) over the summers of 2010 and 2011, and (b) over the winters 2010/11 and 2011/12. The boundary between tropics and extratropics is defined as 30°. A perfect forecast corresponds to 1-SEEPS=1.

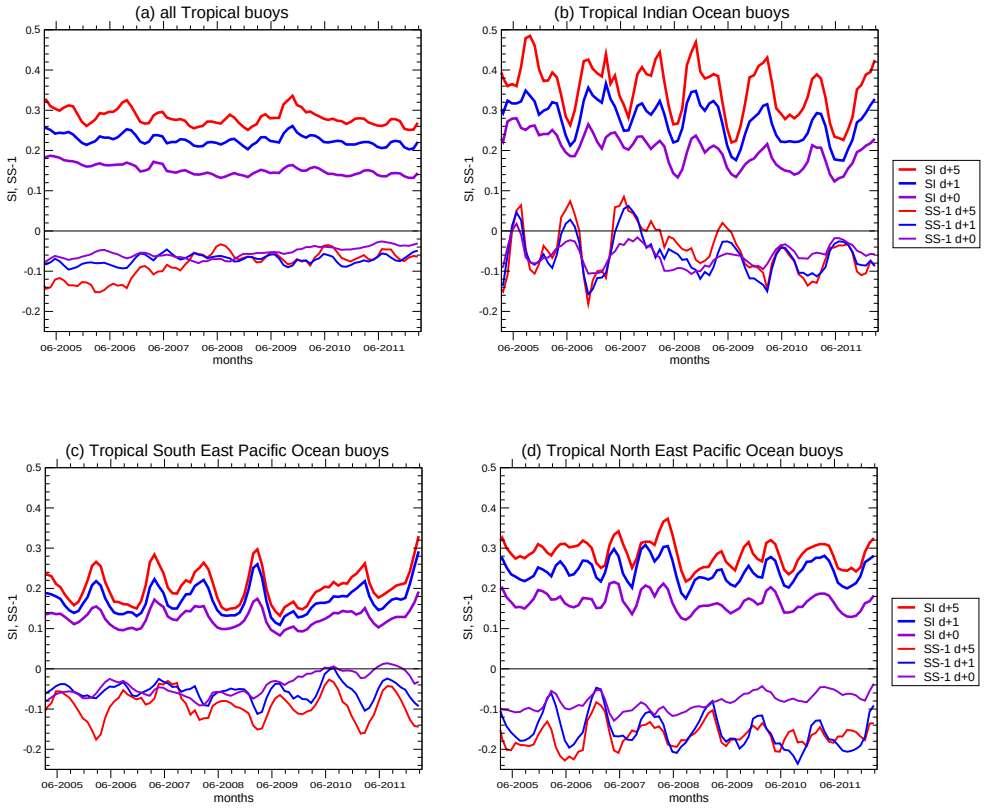

Figure 6: 3-months running mean Scatter Index (SI) (positive values) and Symmetric Slope (SS)-1 (negative values) of 10 m wind from the high-resolution forecasts at lead time day+0, day+1 and day+5 versus buoys observations during the period March 2005 to March 2012: Tropics (a), Indian Ocean (b), tropical South east and North East Pacific, (c) and (d). For a perfect forecast SI=SS-1=0.

findings are consistent with Peng *et al.* (2012) who reported large and systematic wind errors in the Central and East Pacific in different weather prediction models. Given the relatively large wind errors over the Indian Ocean and the East Pacific a special section (Section 3.3) has been dedicated to this issue for further discussions.

A more mixed picture of forecast improvement over the last decade is obtained from the upper-air verification of winds at 850 and 200 hPa against radiosondes (mainly land based) and against own analysis (Figure 7). For short lead times there is only little change in forecast quality compared to the own analysis. However, against observations the RMS error at day+1 is reduced by roughly 15% corresponding to an error reduction of 0.5 m s^{-1} at 850 hPa and of 1 m s^{-1} at 200 hPa, with the absolute errors at 200 hPa being about twice as large. For the lead time day+5 there is a significant error reduction at 200 hPa by 1.5 m s^{-1} when verified against observations and by 1 m s^{-1} when verified against own analyses. For comparison, the ERA-Interim verification is also depicted in Figures 7c-d. Recall that the ERA-Interim corresponds to Cy31r1 introduced in September 2006 (Table 1). As a consequence, operations and ERA-Interim show similar results during 2006 and the first half of 2007. Interestingly, with the introduction of Cy32r2 in June 2007 and Cy32r3 in November 2007 (Table 1). There is a marked improvement in operations compared to ERA-Interim in the day+5 200 hPa wind errors, but a degradation in the day+1 errors in particular at 850 hPa. The reasons for this are twofold. The introduction of

3 outer loops in 4D-Var and revised linear physics in the minimization (Cy32r2) as well as the revised physics in Cy32r3 contributed to more variability in the analysed and forecast fields, therefore affecting in particular the short-range verification when forecast errors are still relatively small. However, the reduced vertical diffusion in Cy32r3 affected notably the 850 hPa winds, leading to stronger vertical wind shear and consequently to an error increase over the oceanic cumulus and stratocumulus regions. The latter modification has subsequently been partly reverted due to a lack of reliable observations in these regions. Overall, there seems to be a consistent improvement in the upper-troposphere over time and for all forecast ranges. The 850 hPa level which is close to the trade-wind inversion with strong vertical wind shear is more challenging, and therefore special attention is given in Section 3 to the wind data entering the analysis (see Section 3.3).

Beyond the evaluation of mean fields, statistics on tropical cyclones are presented in Figure 8. Recently, Fiorino (2009) evaluated different global models for the period 1992 to 2008, and emphasized that tropical cyclone prediction errors strongly depend on both model resolution, and model physics. In particular, he noticed for the IFS a significant reduction in cyclone track error with the resolution increase from T_L511 L60 to T_L799 L91 in February 2006 (Cy30r1), and another step change with the revised physics package including the revised convection in November 2007 (Cy32r3). These results are confirmed in Figure 8a that displays for the period 2002 to 2012 the mean position error in the analysis and at lead time day+3 (we only consider short lead times to include all cyclone tracks with shorter lifetime). Between 2002 and 2009 the position errors have decreased from about 350 km to 200 km. Since then they remain fairly constant, and no clear impact is seen from the further horizontal resolution increase to T_L1279 in January 2010. The error growth with time of cyclone position predictions in several global models including the IFS has been investigated for the period 2006 to 2009 by Plu (2011), and he concludes from the fact that small-scale position errors roughly double in about 2 days that the current deterministic models have not yet reached their predictability limit. To conclude, tropical cyclone central pressure errors (hPa) are displayed in form of histograms for the beginning and end of the considered decade, namely 2002/2003 and 2011/2012 (Figures 8b-c). One notices for both the analysis (Figure 8b) and the day+3 lead time (Figure 8c) a strong reduction of errors in 2011/2012 with respect to 2002/2003, leading to a more symmetric error distribution. The error reduction in particular for the positive bins (too high central pressure) can be largely attributed to an increase in horizontal resolution. However, with the latest high-resolution system there seems to be a shift from a slightly positively skewed error distribution at analysis time to a quasi-symmetric distribution at day+3 to a slightly negatively skewed distribution (too deep cyclones) at longer lead times (not shown). The distribution of pressure errors will therefore require close monitoring in particular for future resolution increases.

3 Analysis and forecast

3.1 General observation impact

About 10 million observations per day, of which 95% originate from satellite data, constrain the analysis of atmospheric pressure, temperature, wind, moisture and ozone. At ECMWF, the quality of the analysis has evolved along with the model. Major milestones of algorithm developments have been the implementation of 3D-Var in 1996 and 4D-Var in 1997, and the introduction of the hybrid Ensemble of Data Assimilation (EDA) - 4D-Var system in 2011 which produces flow-dependent short-range forecast errors of the day from ensemble analyses for 4D-Var. Regarding data, instrument diversity and data volume have dramatically increased over the past 25 years so that currently observations from over 50 instruments are assimilated.

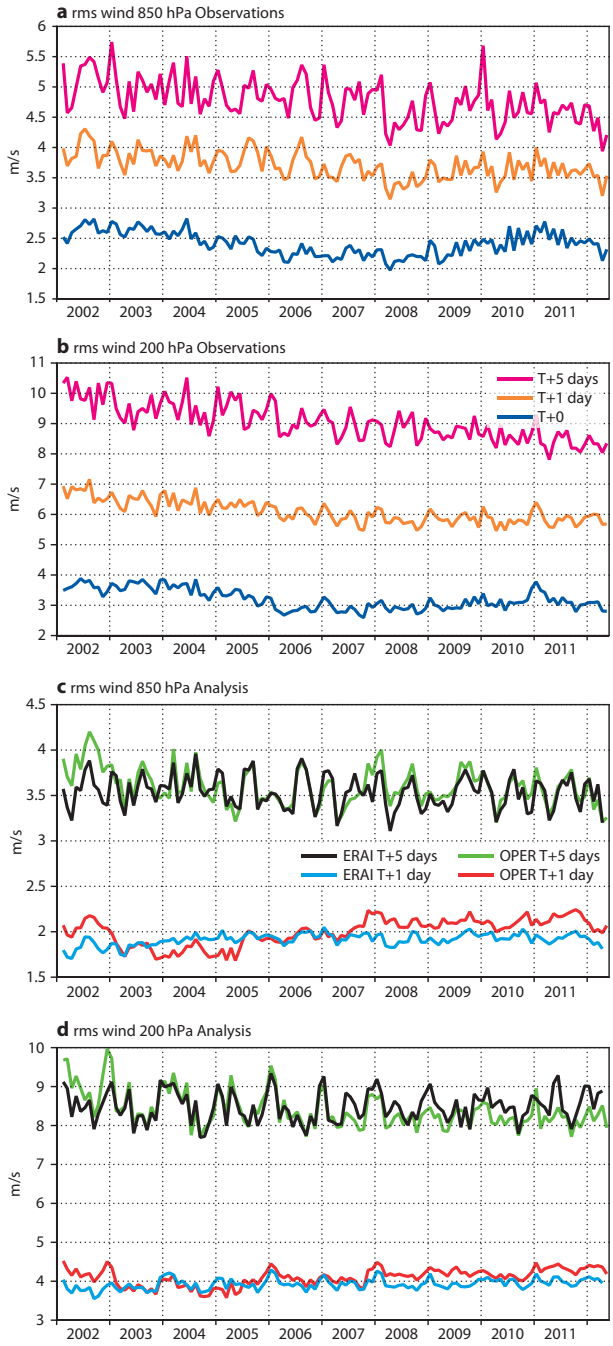

Figure 7: Timeseries of 30-day running mean RMS wind errors at 850 and 200 hPa for different forecast lead times: ECMWF operations against radiosonde observations (a)-(b), and operations and ERA-Interim against own analysis, (c)-(d).

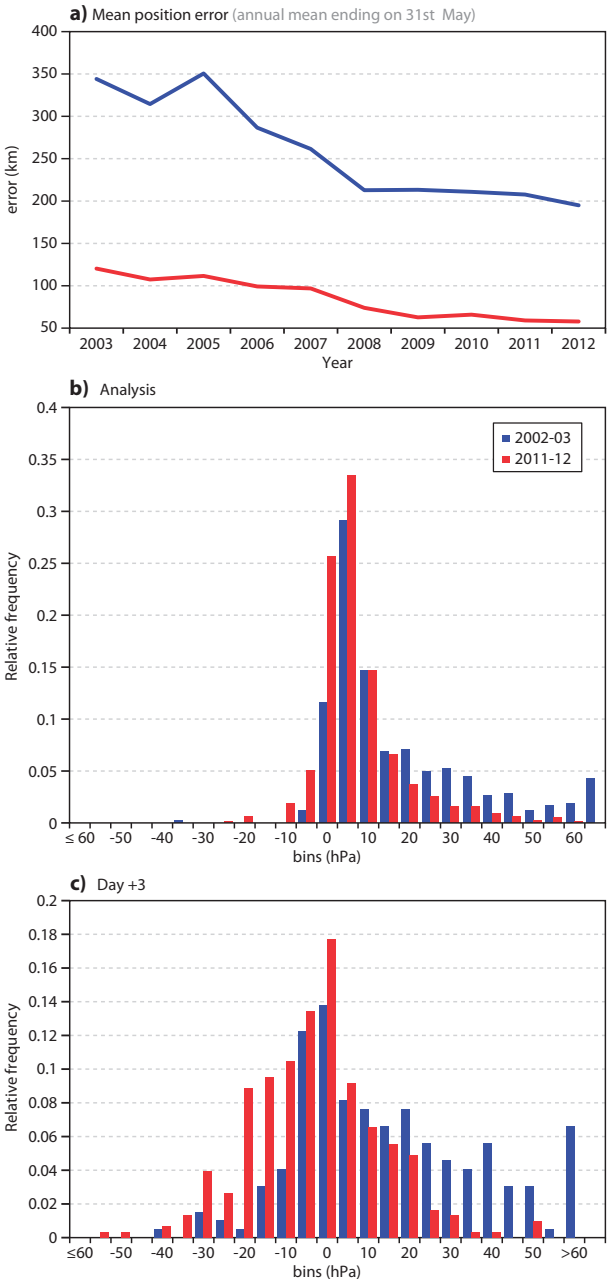

Figure 8: Annual statistics of tropical cyclone high-resolution forecast errors for the period 2002 to 2012: (a) annual mean position error at analysis time (red) and for day+3 forecasts (blue), and histograms of central pressure errors during 2002/2003 and 2011/2012 at initial time (b) and at lead time day+3 (c).

The analysis system employs a variational bias correction Dee (2005) that is applied to the majority of satellite data and selected conventional observations. This bias corrections accounts for fluctuations in instrument calibration and enhances the consistency between the rather diverse observation types, but it is also prone to absorb model bias. The other important component is the balance between observation and background errors that determine the weight given to observations in the analysis. These errors exhibit significant variations between observation types and as a function of location. These factors have to be taken into account when analysis statistics are evaluated.

The data assimilation system provides an estimate of the atmospheric state by combining meteorological observations with the 12 hour forecast (background or first-guess field). These are weighted by their respective accuracies that are characterized by their error covariance matrices. The influence of each observation in the analysis can be computed during the assimilation process from the degree of freedom for signal (DFS), which is the trace of the observation influence matrix (Tukey, 1977; Velleman and Welsch, 1981; Wahba *et al.*, 1995). The DFS quantifies the number of statistically independent directions constrained by each observation in the analysis (Cardinali *et al.*, 2004; Lupu *et al.*, 2011). The DFS depends on the accuracy assigned to observations and background as well as on the model itself that is used as a space and time propagator. The DFS is also affected by the number of assimilated observations, e.g. the more observations from a specific instrument are assimilated, the larger the DFS of that instrument will be.

Figure 9 (yellow bars) shows the relative DFS per observation type in percent over the Tropics between 30°N and 30°S in October 2011. The observation types are described in Table 2. The most influential observation type is AMSU-A radiance data providing 19% of the total observational information followed by AIRS and IASI with 15%., GPS-RO (8%) and HIRS (6%). The information content of aircraft and radiosondes (Aicraft, TEMP; 6%) is the largest among conventional observations in the Tropics followed by synoptical station (SYNOP) surface pressure data (3%). The total information provided by Atmospheric Motion Vector winds (AMVs) in the Tropics is about 7% and among the geostationary satellite platforms, Meteosat-7 is the least informative, also due to the comparably small amount of assimilated observations.

Recently, adjoint based observation sensitivity techniques have been added to measure the observation contribution to the forecast error (Baker and Daley, 2000; Langland and Baker, 2004; Cardinali and Buizza, 2004; Zhu and Gelaro, 2008; Cardinali, 2009). The observation impact is evaluated with respect to a scalar function representing the short-range forecast error (here a global dry energy norm). As for the DFS, the observation forecast error contribution (FEC) is computed for each assimilated measurement, and can also be gathered by observation type or area (Cardinali, 2009; Cardinali and Prates, 2011). As shown in Figure 9 (blue bars), the largest contribution to decreasing the forecast error is provided by AMSU-A (18%) and AMVs (16%) followed by other satellite instruments such as GPS-RO (8%), IASI (8%), AIRS (7%). Conventional observations are also important for decreasing short range forecast errors with a 12% reduction by radiosonde and 10% by aircraft data. SYNOP surface pressure and HIRS observations contribute by almost 4% and all other observations with less than 3%.

DFS and FEC are different but related quantities. They are both functions of the assigned background and observation accuracy and the model. Additionally, FEC depends on the forecast error. In an optimal and unbiased system it is expected that, given a comparable vertical distribution of the global forecast error FEC and DFS should be similar for each observation type. However, for some observation types DFS is larger than FEC, for example in the case of AIRS, IASI, HIRS and AMSU-A. A loss of forecast impact of a particular observation type with respect to the DFS can be attributed either to the observation quality (sub-optimal system) or to model errors such as model bias. For infrared observations (AIRS, IASI, HIRS) this mostly originates from temperature and moisture soundings of the lower troposphere while

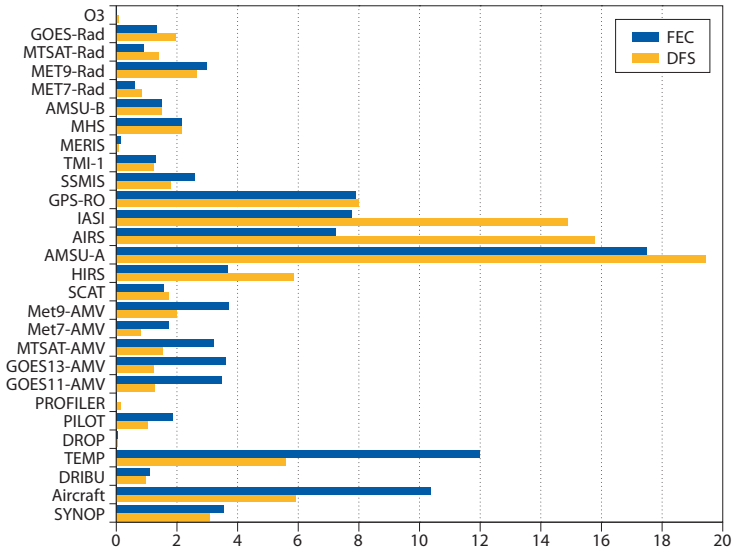

Figure 9: Degree of freedom for signal (DFS, yellow) and relative contribution to day-1 forecast error (FEC in percent, blue) per observation type assimilated in the Tropics between 30N and 30S. Data from period September-November 2011. See Table 2 for more information on observation types.

for microwave observations (AMSU-A) from soundings of stratospheric temperatures. These measures highlight that, in the Tropics, the main impact in the analysis is produced by (1) satellite data and (2) the dominance of temperature and wind observations over moisture data.

3.2 Analysis increments and forecast errors

In regions with sufficient and 'accurate' observations, model errors can be quantified by analysis increments which are the corrections the 4D-Var analysis adds to the background forecast, due to information from observations. These increments naturally have a seasonal cycle in the Tropics. As we cannot show them all, we decided to focus on the SON season in 2011 where all the areas with large errors are still apparent.

Seasonal mean of analysis increments for temperature, vector wind, as well as the RMS of the relative humidity increment are shown in Figures 10 and 11 on selected lower- and upper-tropospheric pressure levels, Figure 10 also includes the standard deviations (STDs) at 1000 hPa. A characteristic increment pattern emerges at 1000 hPa (Figure 10) where high values of the standard deviation of T and wind speed closely follow the ITCZ, but with vector wind increments that increase the convergence in the ITCZ and in particular along the southern flank of the ITCZ (situated northward of the Equator) in the Eastern Pacific. Mean wind increments and STD are both of O(1 m s^{-1}). At 850 hPa (Figure 11) the increments still tend to increase the convergence near the Equator, but now indicate a marked lack of cross-equatorial flow in the model in the East Pacific with a mean error of O(2 m s^{-1}). The largest mean temperature increments of O(0.5 K) occur in the stratocumulus areas off the West coasts of continents, but the largest RMS of relative humidity (>10%) and related STD of temperature increments (>1 K) (not shown) occur over warmer waters further West corresponding to the trade cumulus regions. At 700 hpa (Figure 11) the East Pacific stands out again with mean cross-equatorial wind increments of O(2 m s^{-1}). The mean temperature increments show large-scale structures warming the model by O(0.2 K). Similar structures persist between 700 and 300 hPa, but cooling the model by O(0.2 K) (not shown). Finally, at 200 hPa,

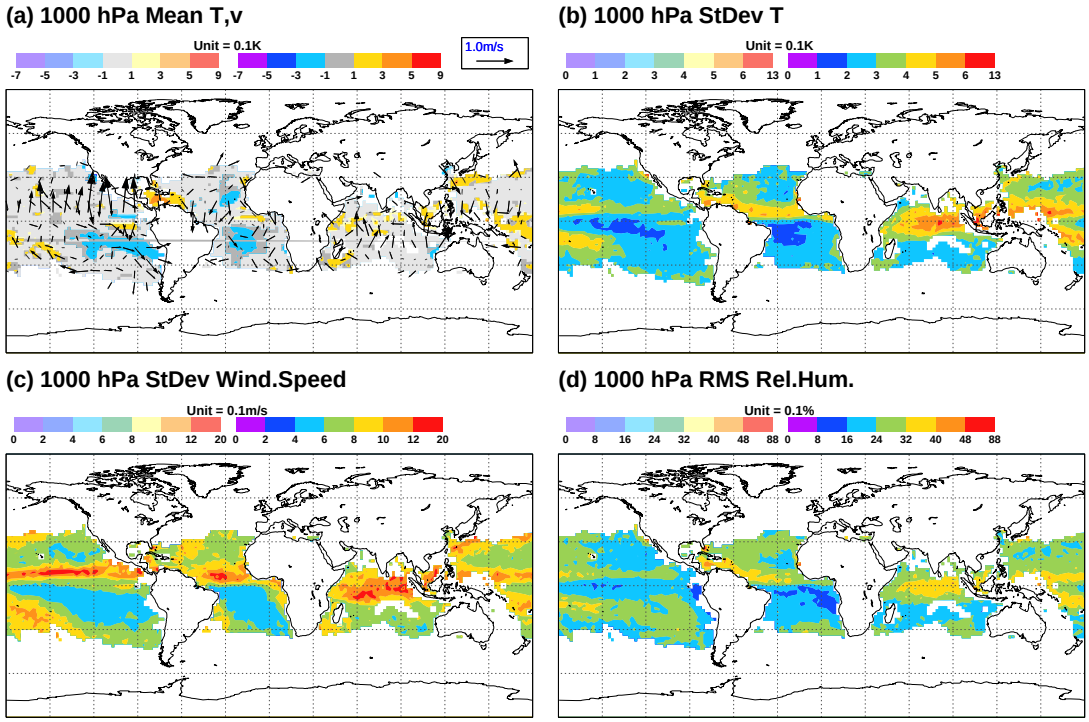

Figure 10: Mean analysis increments and standard deviation for T (K) and wind vector (m s^{-1}), and RMS for RH (%) at 1000 hPa over the period October to December 2011. Statistically significance at the 95% level is denoted by intense colours, pale colours are employed otherwise.

the convective outflow level, wind increments are mainly divergent in convective regions and of O(1-2m s^{-1}), whereas mean and STD of temperature increments are overall < 0.3 K, apart from the region over Amazonia with active convection. Finally, maxima in the RMS of relative humidity at 200 hPa coincide with the climatology of high clouds.

So far the findings can be summarized as follows: Near the surface along the ITCZ the observations tend to increase the convergence, and at 200 hPa there is a consistent divergent signal. Mid-tropospheric temperature and moisture increments show large-scale structures which are consistent with the findings by (De and Chakraborty, 2004; Žagar *et al.*, 2012) who showed that systematic model errors in the Tropics occur at wavenumbers 1-3, whereas random errors occur in the wavenumber 4-7 spectral band. However, a signal that stands out are the strong wind increments at 850 and 700 hPa in the East Pacific. In the Appendix we have produced diagnostics similar to Figures 10-11 for the differences between the ECMWF and UKMO analysis. The STDs of these differences broadly show similar patterns as the increments, however the ECMWF model is colder in the troposphere O(0.5 K) than the UKMO analysis as already indicated in Figure 1. The largest differences with the UKMO analyses occur over Central Africa and in the East Pacific where at 850 hPa the ECMWF winds are more south-southeasterly, while at 700 they correspond to a more north-northeasterly cross equatorial flow. Indeed, the Eastern Pacific is the only tropical region where all year-round, apart from spring, low-level south-southeasterly cross-equatorial flow dominates, and during autumn and winter reverse cross-equatorial flow prevails at 700 hPa that further enhances the vertical wind-shear. As investigated in Graversen *et al.* (2007) and Rodwell *et al.* (2010) errors in the NH mass budget in both analysis and forecasts are due to errors in the cross-equatorial flow, and general circulation models tend to produce large errors in these regions (De Szoeke and Xie, 2008). Philander and Pacanowski (1981) and Okajima *et al.* (2003) explain the particular Pacific wind pattern

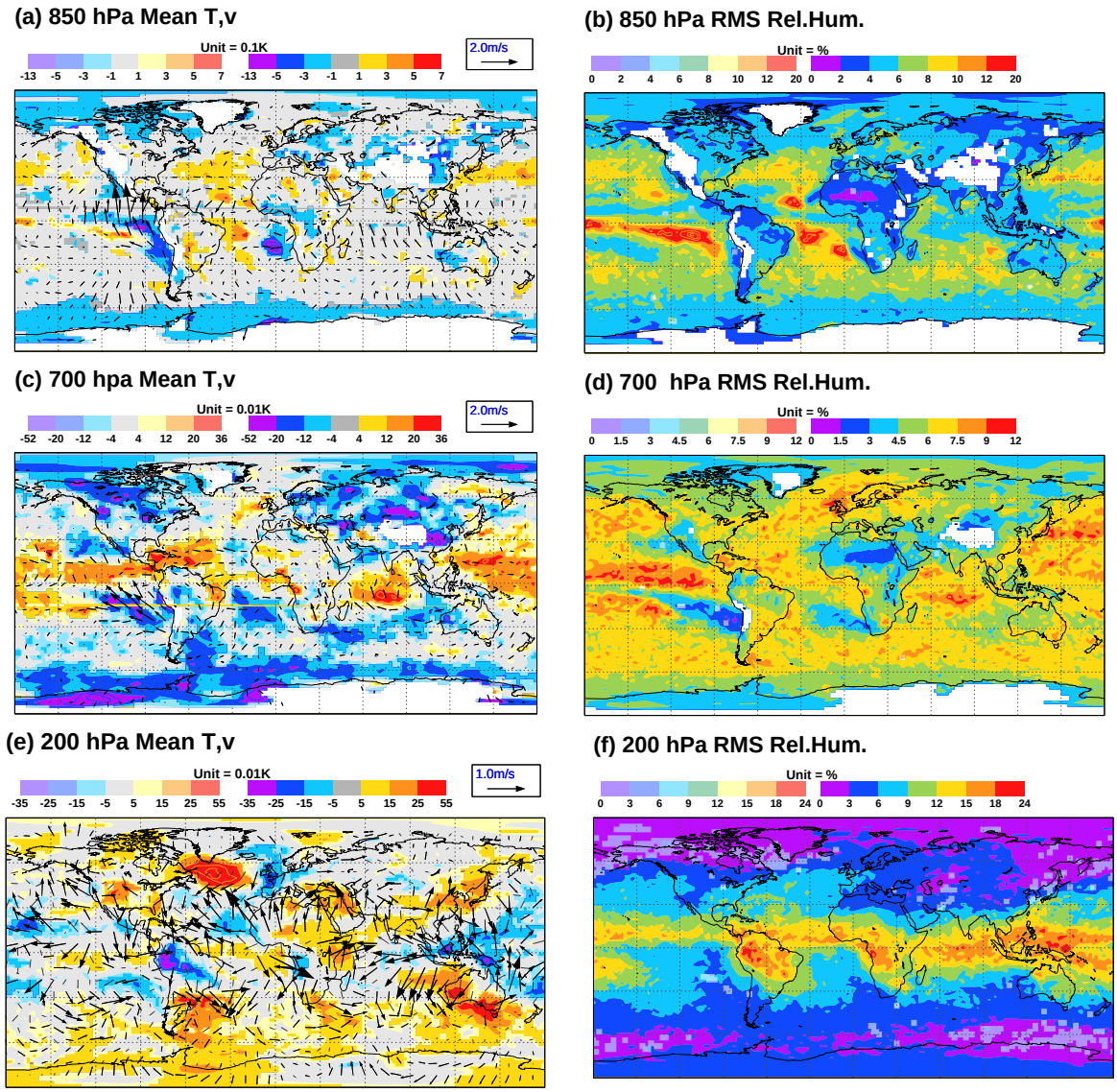

Figure 11: Same as Figure 10 but at 850, 700 and 200 hPa, including only mean increments for T and wind vector (left column), and RMS for RH (right column).

through the position of the ITCZ north of the Equator, the northwest-southeast slant of the American coast, and the Andes orography that break the symmetry, while Rodwell and Hoskins (2001) interpret the anticyclonic flow pattern as a Rossby wave response to the Central and South American Monsoon to the East. In the following we want to assess if the increments in the IFS denote actual model errors and what observation types cause these increments.

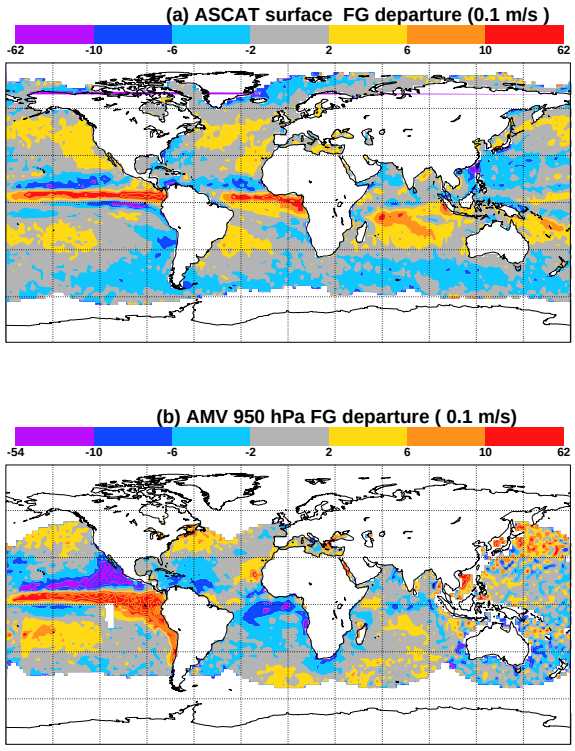

Figure 12: SON 2011 mean first guess departures near the surface from ASCAT, and at 950 hPa from the AMVs.

The observations responsible for the low-level wind increments are mainly near-surface winds from the ASCAT scatterometer, and the AMVs as illustrated in Figure 12 by the first guess departures for the respective observation types. In contrast to ASCAT that has global coverage over the ocean, and therefore globally uniform data quality, the AMVs stem from different products for e.g. the regions covered by METEOSAT and GOES. Nevertheless, both near surface winds from ASCAT, and the AMVs representative for the lowest 50-100 hPa of the atmosphere consistently increase the near-Equator winds (convergence) by O(1 m s^{-1}), apart from the East Pacific, where the AMV analysis increments of up to 5 m s^{-1} are significantly larger than elsewhere. While an international working group on AMVs[2] reports that the AMVs generally improve the analysis there is however an indication that the AMVs for the GOES region have larger 'observation errors' (internal report by Santek and Bormann 2011), probably due to problems with the height assignment of the vector winds and larger wind shear in these regions.

Finally, in Figure 13 day+5 forecast errors against the analysis are depicted. The tropical troposphere cools by about 0.5 K during the first 5 days. The wind patterns show a divergent signal at 1000 hPa all along the ITCZ, large wind errors in the East Pacific at 850 hPa (Figure 13b), smaller errors and no clear pattern at 700 hPa (Figure 13c). At 200 hPa tropical wind errors are largest over South America, the

[2]http://cimss.ssec.wisc.edu/iwwg/iwwg.html

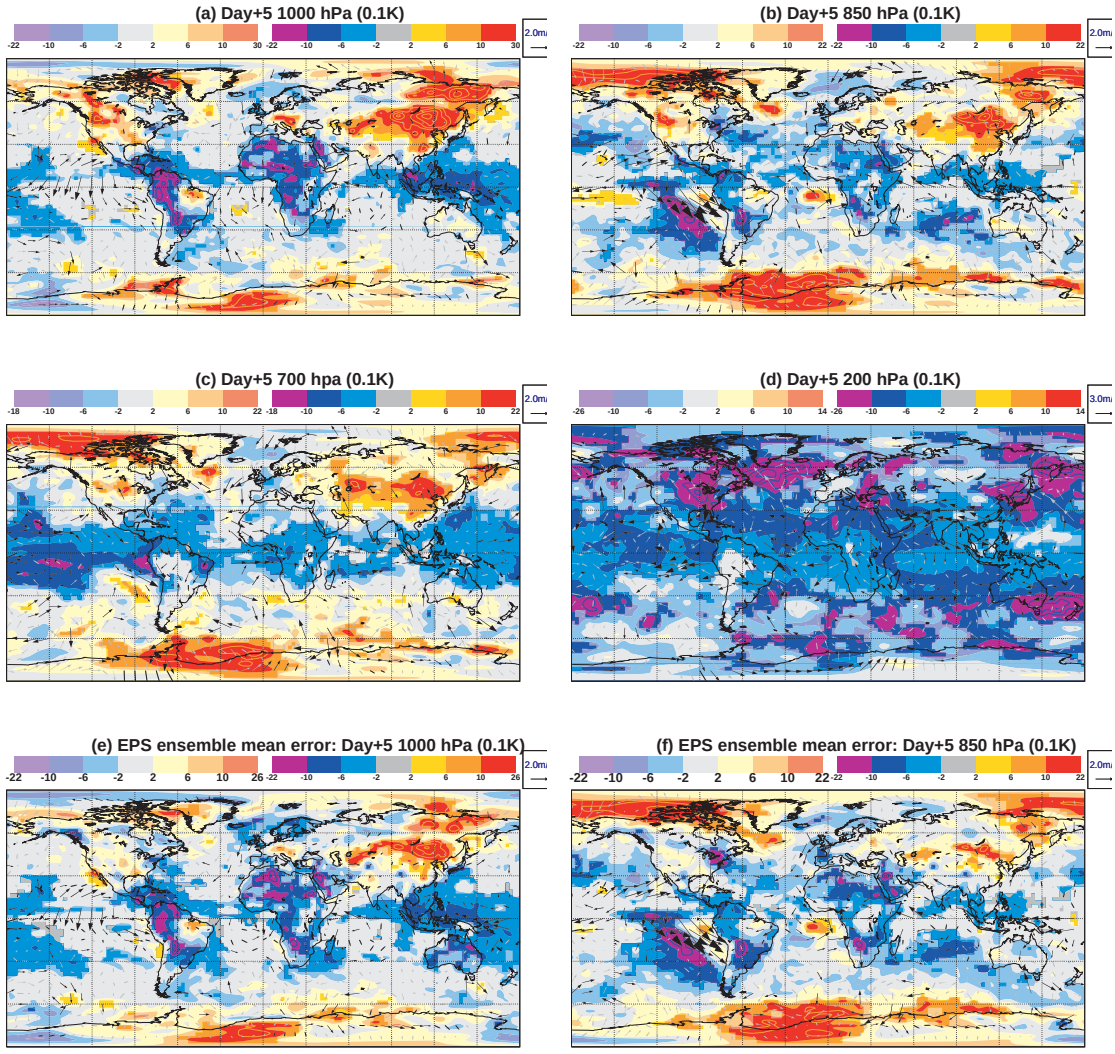

Figure 13: SON 2011 mean day+5 forecast errors against own analysis for T (K) and wind (m s^{-1}) at pressure levels 1000, 850, 700 and 200 hPa from the high-resolution forecasts (a)-(d), and at 1000 and 850 hPa for the ensemble mean error of the EPS (e)-(f).

tropical Atlantic, and the East Pacific south of the Equator, where during late autumn and winter a strong 'tropical westerly jet' is present. Also added are in Figures 13e-f the day+5 errors of the ensemble mean of the EPS at 1000 and 850 hPa. These are very similar to the errors of the high-resolution system Figures 13a-b which suggests that essential information on systematic model errors can already be obtained by an evaluation of the high-resolution system. Finally, comparing Figure 13 to the wind increments at 1000 and 850 hPa (Figure 10) and the observation departures (Figure 12) one can readily identify that wind increments (analysis minus short-range forecast difference) and day+5 forecast errors have similar structure but opposite sign, meaning that the observations tend to correct a model drift towards a weaker Hadley cell (less convergence in the ITCZ) and increase the low-level cross-equatorial flow in the East Pacific.

3.3 East Pacific and Indian Ocean

Over the Tropics, wind data is a very important source of observational information. The two main wind products with global coverage originate from ASCAT and the AMVs. However, observations sensitive to temperature (e.g. infrared/microwave sounders) and moisture (e.g. microwave imagers, selected microwave and infrared sounder channels) can also produce wind increments through the dynamic response to temperature and moisture increments in 4D-Var. These more indirect wind increments are usually broader in scale and thus less specific in height and location.

Focusing on the tropical East Pacific first, Figure 14 shows the mean temperature and wind analysis at levels 700, 850, 925, 1000 hPa over the period October-November 2011. The convergence pattern that crosses the equator and intensifies towards the East where it intersects with the north-easterly flow from the Caribbean is particularly strong at lower levels and the position of the ITCZ is easily identified near 10°N. Between 850 and 700 hPa the wind direction changes drastically from south/south-westerlies to north/north westerlies at the equator, while intensities are fairly similar. As mentioned in the previous Section, these strongly sheared flow patterns intersecting with Central America over areas with large SST gradients are difficult to represent correctly in the model.

The specific impact of wind information derived from observations can be further investigated by observing system experiments (OSE), in which selected data are withdrawn. Figures 15 and 16 show the mean 850 and 700 hPa analysis differences between a control and an experiment in which GOES-13 AMV observations have been withdrawn in the area 30°S-0°/120-150°W for the period October-November 2011. The analysis increments that have been shown in Figs. 10 and 11 are well reproduced here and show a similar maximum of wind increments of O(2 ms^{-1}) near 850 hPa (Fig. 15a). The broad wind impact across the Equator overlaps with a cooling by about 1 K through advection of cooler and drier air masses. The observations therefore amplify low-level convergence across the Equator and thus intensify the Hadley circulation in this area. The observations also move the centre of 850 hPa divergence from 15°S/110°W towards the continent. Into the forecast, the areas with significant temperature increments remain rather stable until day+3. However, in the first 24 hours the enhancement of the cross-Equator convergence changes sign, i.e the model overshoots in response to the large analysis increments. At 700 hPa (Figure 16), the impact of the GOES-13 AMV observations is generally weaker and aims at amplifying the convergence in the 5°S latitude band. The temperature increment shows the opposite sign compared to 850 hPa as a result of the enhancement of opposite-source air mass flow at these levels, and at day+2 a similar wind reversal (overshoot) is observed as at 850 hPa. The enhancement of convergence at the Equator remains fairly stable throughout analysis and day+3 forecast.

Over the Indian Ocean (see Figures 38-40 in the Appendix), the ITCZ is located at the Equator and, in contrast to the East Pacific, lower-level convergence patterns are consistent across all levels but much

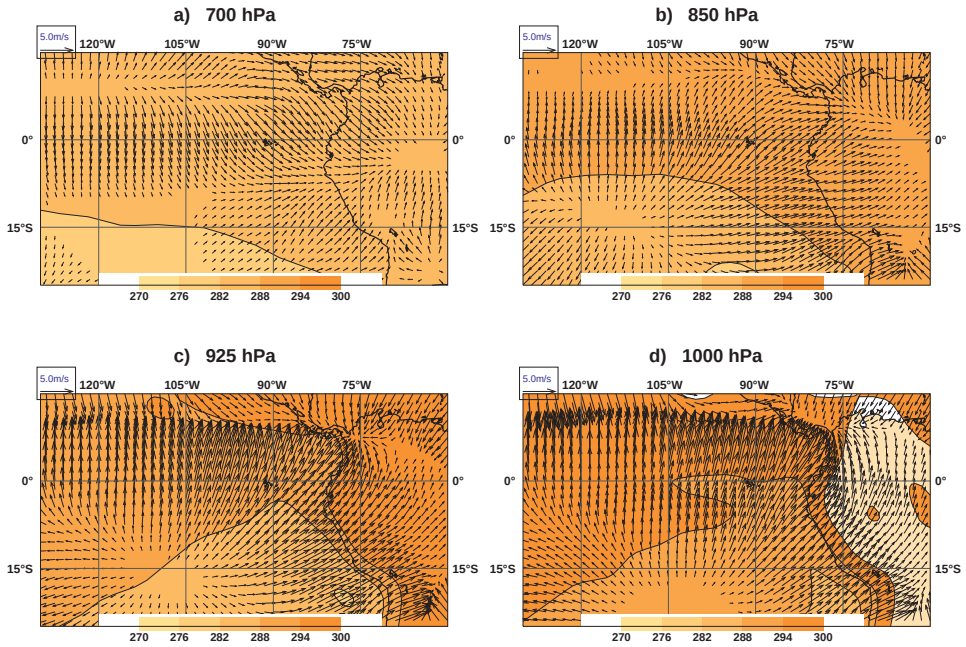

Figure 14: Mean wind and temperature analysis over the East Pacific at 700 (a), 850 (b), 925 (c) and 1000 hPa (d). Period is October-November 2011.

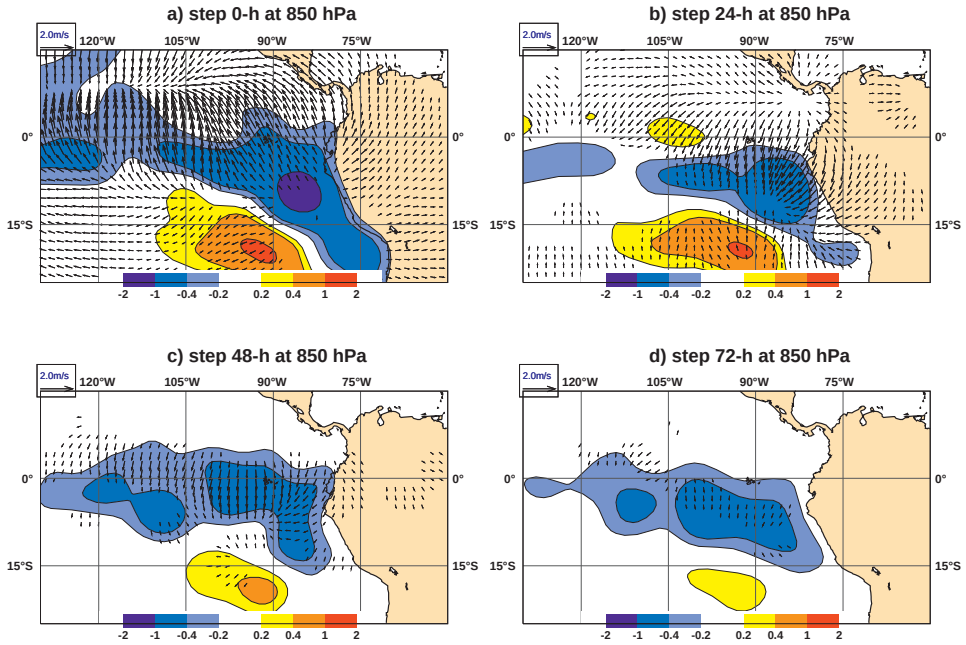

Figure 15: Mean analysis difference between control and GOES-13 AMV denial experiment for wind (arrows) and temperature (colour scale) at 850 hPa and analysis time (a), day+1 (b), day+2 (c) and day+3 (d) forecast time. Period is October-November 2011.

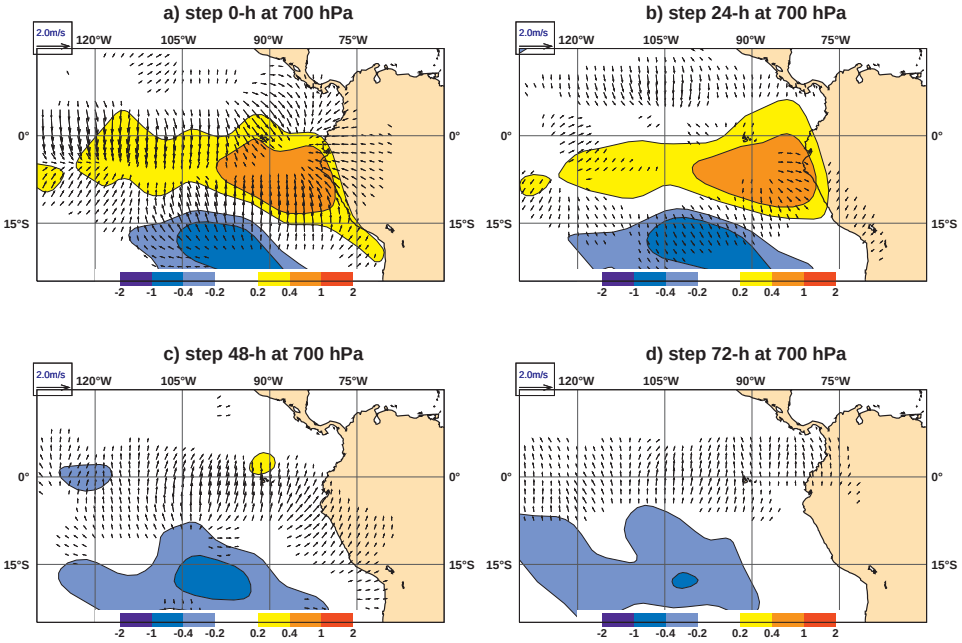

Figure 16: As Fig. 15 but 700 hPa.

weaker than in the Eastern Pacific, as shown in Figure 38. In this case, AMV observations from Meteosat-7 have been removed over the area 30°S-15°N/40°E-100°E. The observations mainly amplify the convergence at 700 hPa (Figure 40b) while their impact at 850 hPa (Figure 40a) is less consistent and dominated by localized track-winds associated with convection. A similar reversal of sign on temperature analysis - as seen in the Eastern Pacific - is found between 850 and 700 hPa (Fig. 40a and Fig. 39a). Interestingly, the 24-hour forecast difference between control and denial experiment shows a relative flow-reversal at 700 hPa as was already seen at 850 hPa in the East Pacific. Again, this is possibly related to the model overshooting in response to large analysis increments. Here, the observational impact dissipates already after 24 hours.

An assessment whether the AMV observation impact is generally beneficial for the 24-hour forecasts by means of FEC is provided in Figure 17, separated into the impact of u-component and v-component observations, respectively. The v-component impact is generally positive (i.e. negative FEC) in the East Pacific, especially in the area where the amplification of the lower-level, cross-equatorial flow, mainly at 850 hPa was noted. Note that most of the GOES-13 AMV observations provide wind information at 850 hPa (5 times more than at levels below and 10 times more than at 700 hPa). However, the negative impact of u-component observations (i.e. positive FEC) further to the south-east coincides with the area of lower-level divergence at 15°S/110°W. Here, wind speeds are very low and it is suspected that the AMV tracking algorithm may produce questionable retrievals in the presence of weak and divergent winds. The situation is different over the Indian Ocean where the negative impact of u-component winds coincides with the area of largest increments in the presence of moderate south-easterlies across all levels. Positive FEC could be related to a significant model bias in this area but this will require further investigation.

While the above investigation focused on AMV observations, other wind-related data also impact the

analysis as mentioned before. ASCAT wind observations most strongly constrain 10-metre winds. Over the East Pacific, they show a more detailed pattern of first-guess departures (Fig. 12a) that is in contradiction to AMVs just south of the Equator. At low levels, the AMV OSE produced very little AMV impact (not shown) so that the results in Fig. 12 should only be interpreted with care. Despite these differences ASCAT winds also enhance lower-level convergence but along a smaller strip south of the ITCZ.

In summary, one can say that the ASCAT and AMV datasets qualitatively agree in that both datasets increase the convergence in the ITCZ and the low-level cross-equatorial flow, therefore pointing to a model bias in these regions. Data denial experiments further show that model forecasts at lead times beyond day+3 have largely 'forgotten' about the AMV analysis increments, and that the forecast adjustment processes between day+0 and day+3 produces a temporary flow reversal. However, given the larger vertical wind-shear and likely larger observation errors of the AMVs in the East Pacific, and the large difference with the UKMO analysis in this region, the flow errors compared to analysis and increments are more uncertain, especially at 850 hPa. Also, experience since Cy32r3 has shown that forecast errors in these regions are very sensitive to the formulation of the momentum transport in the boundary-layer diffusion scheme. The effect of possibly missing convection in the Eastern Pacific warm pool and the Americas on the cross-equatorial flow has not yet been investigated.

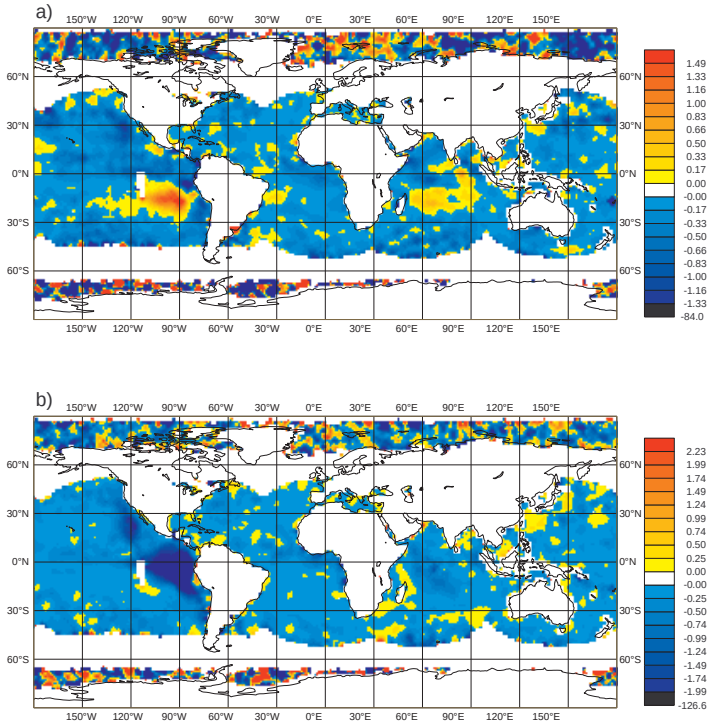

Figure 17: Mean FEC of u-component (a) and v-component (b) AMV observations in the atmosphere between 700 and 1000 hPa. Positive (negative) values denote that the assimilated observations increased (decreased) the global 24-hour forecast error. Units are Joule.

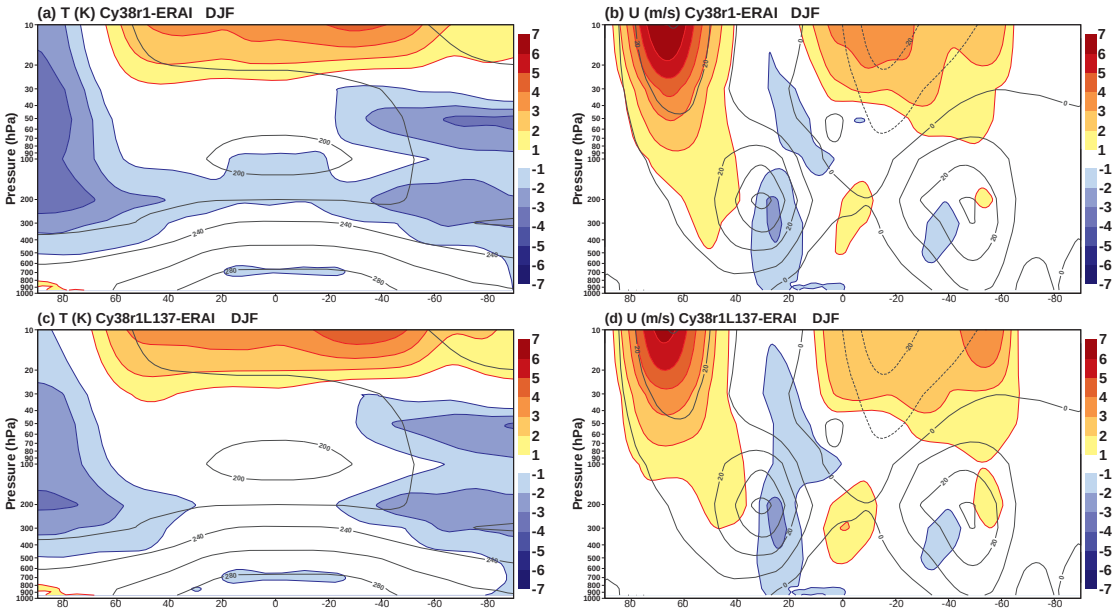

Figure 18: Zonal mean temperature (K) and U wind (m s^{-1}) differences (shaded) for DJF between seasonal integrations with Cy38r1 over a period of 30 years and the ERA-Interim climatology: (a)-(b) 91 vertical levels and (c)-(d) 137 vertical levels. Black isolines denote the climatological background field.

4 Model Climate and Teleconnections

An accurate model climate is fundamental to realistically represent tropical convection. A realistic model convection (parameterization) is however dependent on the model dynamics and physics formulations, and is fundamental to a realistic model climate both in terms of mean state and variability. This is the experience shared by many modellers and has been documented in many studies (Slingo *et al.*, 1994; Jung *et al.*, 2010; Kim *et al.*, 2011; Hourdin *et al.*, 2012; Kim *et al.*, 2012).

The climate of the IFS is evaluated over a period of 30 years based on a 3-member ensemble of either uncoupled or coupled seasonal 7-months integrations at resolution T_L255 (Magnusson *et al.*, 2012). For specific applications like wave or mode diagnostics, the evaluation is based on longer integrations covering either one or up to 10 annual cycles. Here we only present results for the latest IFS cycle 38r1, and, where possible, we apply new diagnostics or observational datasets, not only because tropical features in previous cycles have been reported by Bechtold *et al.* (2008); Jung *et al.* (2010) and Molteni *et al.* (2011), but also because Cy38r1 has the 'best' climate of all cycles so far. We also look ahead and discuss climate impacts of the coming resolution upgrade from 91 to 137 vertical levels. Ocean coupling issues have also been looked at, but it has been found that results from climate simulations in coupled mode are similar but slightly 'worse' with respect to observations compared to the uncoupled simulations (see also Magnusson *et al.*, 2011; Molteni *et al.*, 2011). Therefore, only results from the uncoupled simulations are shown. All results are displayed as seasonal means, and for the sake of brevity only the model fields and season for which either the model error or the signal is largest are shown.

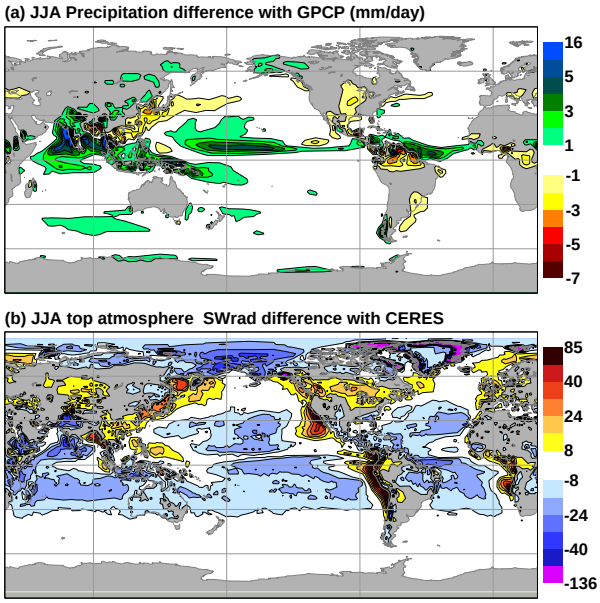

Figure 19: Differences with respect to observations for JJA: (a) total precipitation (mm day^{-1}) against GPCP2.1, and (b) net shortwave radiation at top of atmosphere (W m^{-2}) against CERES, the sign convention is that negative values imply less incoming radiation at the surface.

4.1 Mean state and errors

The zonal mean temperature (K) and U-wind (m s^{-1}) differences for DJF between Cy38r1 and the ERA-Interim are illustrated in Figure 18a-b. The model tends to produce a cold bias in the Tropics of O(0.5 K) attaining O(1 K) at 700 hPa and near the tropopause. These temperature errors are therefore comparable to the day+5 forecast errors in Figure 13. The upper-tropospheric wind bias does not exceed 2 m s^{-1} in the Tropics and 3 m s^{-1} in the subtropical Jets. Model errors are largest in the polar stratosphere and the upper tropical stratosphere. However, these errors are roughly half of what they were a decade ago (see [3] for continuous evaluation). The results from the 137-level run with Cy38r1 (Figure 18c-d) are fairly similar but show a beneficial upper-tropospheric and lower-stratospheric warming of about 0.5 K with respect to the operational 91-levels. The reasons for that are still not fully understood but expected to be due to better numerical accuracy, with better gravity wave handling and a more realistic Brewer-Dobson circulation.

Concerning the comparison of surface fields with observations the two errors that stand out are an overestimation of the Asian summer monsoon rainfall (Figure 19a) and a shortwave radiation bias over the tropical and subtropical oceans (Figure 19b). The Monsoon error has already been discussed in (Jung *et al.*, 2010; Rodwell *et al.*, 2010; Molteni *et al.*, 2011) and has also recently been pointed out by authors external to ECMWF (Chakraborty, 2010). The overestimation of the Asian summer monsoon including an overestimation of precipitation and a too strong diabatically induced low-level circulation, as well as the overestimation of precipitation over the maritime continent leading to too strong easterlies near the Equator, goes back to the revision of the convection scheme in Cy32r3 (Bechtold *et al.*, 2008). In that cycle the convection scheme became decoupled from the dynamics, and the precipitation that previously was heavily overestimated along the Equator, was realistically shifted to the Maritime Continent and India,

[3] http://www.ecmwf.int/products/forecasts/d/inspect/catalog/research/physics_clim/

albeit with a spin-up tendency leading to the overestimation. It is yet not entirely clear how to address this error, but studies (see Section 5) indicate that the lower to mid-tropospheric convective moistening is slightly overestimated. However, other processes like errors in the aerosol climatology, insufficient diffusive damping or errors in the cloud radiation interaction also play a role as indicated by sensitivity studies.

The shortwave radiation biases of O(- 10-20) W m^{-2} in the tropical and subtropical cumulus and trade-cumulus regimes, and of O(+40) W m^{-2} in the stratocumulus areas (Figure 19b) have already been investigated by Ahlgrimm and Köhler (2010). The authors showed that in general stratocumulus cloud amount is underestimated whereas the water content in the trade-cumuli is too high producing clouds that are too reflective. The upcoming 137-level resolution upgrade is not improving these biases but instead slightly increases them (higher vertical resolution is expected to increase the cloud amount by making inversions sharper, the stratocumulus error however is not yet understood). The radiation biases in the cumulus area could possibly be corrected by making the cumuli precipitate more easily. However, this would increase further not only the overestimation of light precipitation in the model (Haiden *et al.*, 2012), see also (Section 5), but also the low-level cold bias (Figure 18). Another possibility would be to make shallow cumulus convection slightly less active, therefore reducing the moistening of the trade wind layer. This modification might be introduced together with adaptions to the boundary-layer turbulence scheme and the cloud schemes. But reductions of the shallow convective mass fluxes and activity must be handled with great care, as this leads to a boundary-layer moistening and consequently to a more convectively unstable atmospheric profile with increased precipitation in long runs.

4.2 Diurnal cycle of convection and variability over land

The simulation of the diurnal cycle of convection is one of the most challenging model problems. A vast amount of observational (Yang and Slingo, 2001; Zhang and Klein, 2010, e.g.) and modeling studies (Chaboureau *et al.*, 2004; Guichard *et al.*, 2004; Khairoutdinov and Randall, 2006; Rio *et al.*, 2009; Schlemmer *et al.*, 2011; Lin *et al.*, 2012; Stirling and Stratton, 2012, e.g.), also with the IFS (Slingo *et al.*, 1992; Bechtold *et al.*, 2004), have been devoted to analyse, understand and resolve the physical processes involved in the temporal behavior of convection. Yet the whole process is not fully understood, but the picture that emerges from these studies can be summarized as follows: The diurnal cycle of convection is a response to diurnal surface heating in the presence of weak large-scale forcing, where the lower to mid-troposphere becomes slowly moistened by shallow and congestus convection before penetrative convection sets in. The latter involves development time scales due to microphysics, convection large-scale interaction, and triggering of cells due to surface cold pools generated by downdraughts. Given its non-equilibrium nature, parameterization schemes have great difficulties in representing the diurnal cycle. They generally produce rainfall in phase with the diurnal cycle of surface fluxes, meaning a maximum rainfall rate around local noon instead of the observed rainfall maximum during late afternoon. Some modelers have reported on success in delaying the convection over land, but at the expense of deteriorated model biases and mean rainfall. However, cloud resolving models (Petch *et al.*, 2002; Sato *et al.*, 2009) are shown to produce a realistic diurnal cycle over land when using horizontal resolutions of O (1 km), but results are still sensitive to numerical formulations like the horizontal mixing.

Here we revisit the diurnal cycle of precipitation in the IFS with the aid of a 1-hourly 9-year rainfall climatology from TRMM recently provided by Y. Takayabu and colleagues. Note that in the IFS 75% of tropical precipitation is of convective origin. Figure 20 displays the amplitude and phase of the diurnal cycle from the first harmonic of precipitation. The amplitude of the model rainfall (Figure 20a) has a maximum between 2.5 and 5 mm day^{-1} over the tropical oceans, and between 5 and up to 15 mm day^{-1}

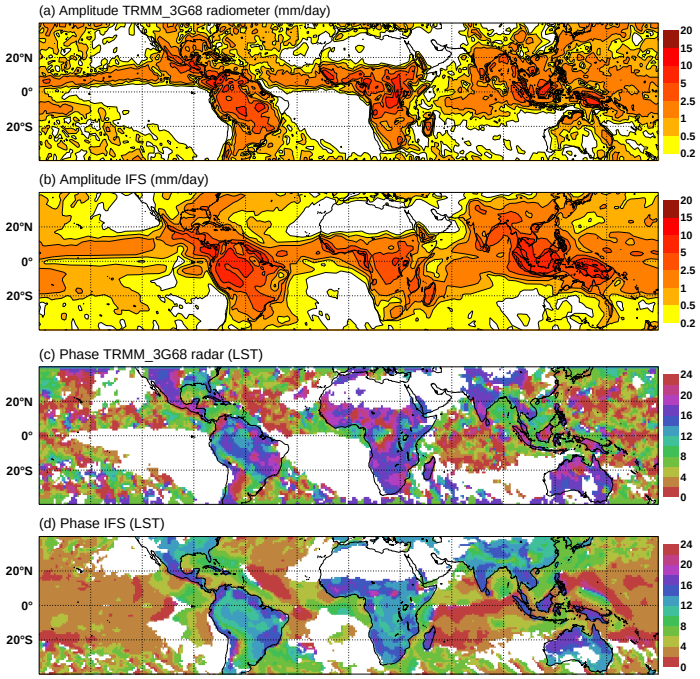

Figure 20: Annual average amplitude (mm day^{-1}) and phase (LST) of the first harmonic of hourly-binned total precipitation: from TRMM radiometer (a) and radar (c), and from model, (b) and (d). Courtesy Yukari Takayabu, Tokyo University, for providing the 9-year TRMM hourly rainfall climatology.

over tropical land which generally agrees with the retrievals from the TRMM radiometer (Figure 20b). Comparing the phase (LST) to the observations from the TRMM radar (Figure 20c-d) it appears that the overall distribution and land-sea contrast is realistic, but the model produces the typical local noon to early afternoon rainfall peak over land that occurs on average 3-4 hours earlier than in the observations. Producing a correct amplitude is most important from a dynamic and energetic point of view, however the phase remains a challenge. There is certainly a requirement to the wider cloud resolving modeling community on further fundamental studies on the diurnal cycle. Possible missing physical processes that could be included in a simple one-dimensional mass flux framework will be discussed in the Conclusions.

We recently received a surface incoming shortwave radiation product from the Climate SAF for the Meteosat-9 area that enables us to look at radiation fluxes and convective cloud variability signals on a daily basis. Comparing the output from the operational forecasts during 2011 to the SAF dataset for the Central Amazon area (Figure 21), where for JJA the climate runs (Figure 22) show an underestimation of downward shortwave radiation of O(15 W m^{-2}), it is recognized that the model indeed overestimates clouds (shallow convection) during the dry season (the biases are comparable to those in the climate runs). During the rainy season in DJF the biases are small, but the radiative variability due to active convection is underestimated (the area mean STD during winter is O(50 W m^{-2})). We consider the convective (radiative) variability over land as satisfying, and our main focus on future model improvement will be the reduction in the SW radiative bias in relation with shallow convection as also present over the oceans.

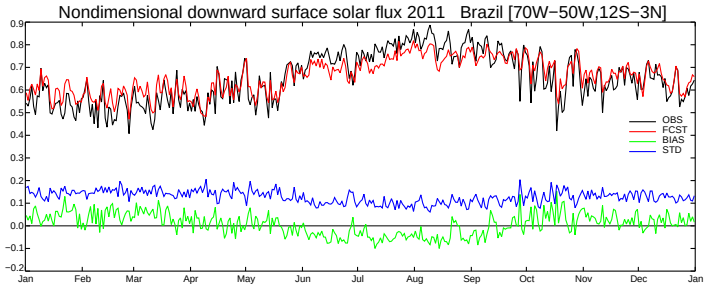

Figure 21: Average nondimensional downward solar fluxes at the surface for central Amazonia during 2011 as observed by Meteosat 9 (climate SAF product), and from the operational day+1 forecasts (red lines). Bias and standard deviation correspond to the green and blue lines, respectively. The fluxes are normalized by the clear sky solar fluxes so that a 5% radiation bias is equivalent to about 15 W m^{-2}.

4.3 Tropospheric teleconnections

A key feature of tropical predictability is the model's ability to appropriately respond to changes in sea-surface temperatures (SSTs) through circulation and convection changes. This is demonstrated in Figure 22 where correlation coefficients and/or regression coefficients between Niño3.4 (Central equatorial Pacific) area-averaged SSTs and either precipitation during JJA or 2-metre temperatures during MAM have been computed for both ERA-Interim and Cy38r1. The seasons have been selected according to the largest signal. Figure 22a-b indicates that the model reproduces the observed covariance between SST and precipitation, where higher Central Pacific SSTs lead to increased precipitation (convection) along the Equator. Note also an equatorially symmetric area of suppressed convection that extends to the West Pacific. The equatorial Atlantic is also affected by increased sinking motion. The model also realistically reproduces the observed relation between Niño3.4 SSTs and 2-metre temperatures during MAM, with an equatorially symmetric warming over large parts of the East Pacific and a cooling in particular over Central and North-West America and Central Asia. These results are in line with Barnston *et al.* (2012) who compared the seasonal prediction skills of several models over the last decade and showed a very favourable ENSO prediction skill of the IFS compared to other models.

4.4 Stratospheric variability and teleconnections

The tropical stratospheric circulation is largely influenced by tropospheric wave activity including convectively coupled large-scale Rossby and Kelvin waves and smaller-scale gravity waves as has been documented for the IFS (Žagar *et al.*, 2005, 2007). It is therefore natural to conclude the climate analysis with a discussion on stratospheric variability and the interaction between the tropo- and stratosphere.

Figure 23 displays the teleconnection between the 2-metre temperature during northern hemispheric winter and the average tropical stratospheric wind at 10 hPa when it is either in the easterly (negative) or westerly (positive) phase of the Quasi-Biennal Oscillation (QBO). There is a clear signal in the ERA-Interim with cooling (warming) over Central Russia and warming (cooling) over Greenland when the mean stratospheric tropical winds are easterly (westerly). Unfortunately, the model produces only very weak signals that do not correspond to the observed teleconnections. This is true for both the operational 91-level version and the 137-level version of Cy38r1.

The reasons behind the lacking teleconnections are unclear, and might reside with internal flow dynam-

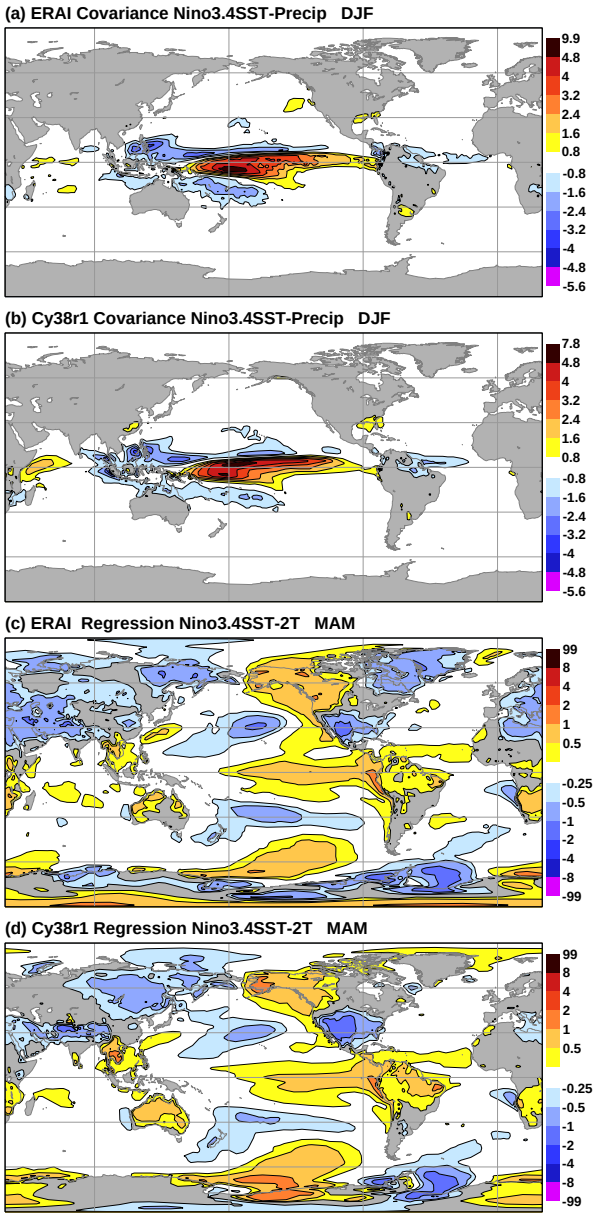

Figure 22: Covariance between SST in Nino3.4 area and precipitation for DJF in (a) ERA-Interim, and (b) Cy38r1 uncoupled, and regression of Nino3.4 SST on 2-metres temperatures during MAM for (c) ERA-Interim and (d)Cy38r1 uncoupled.

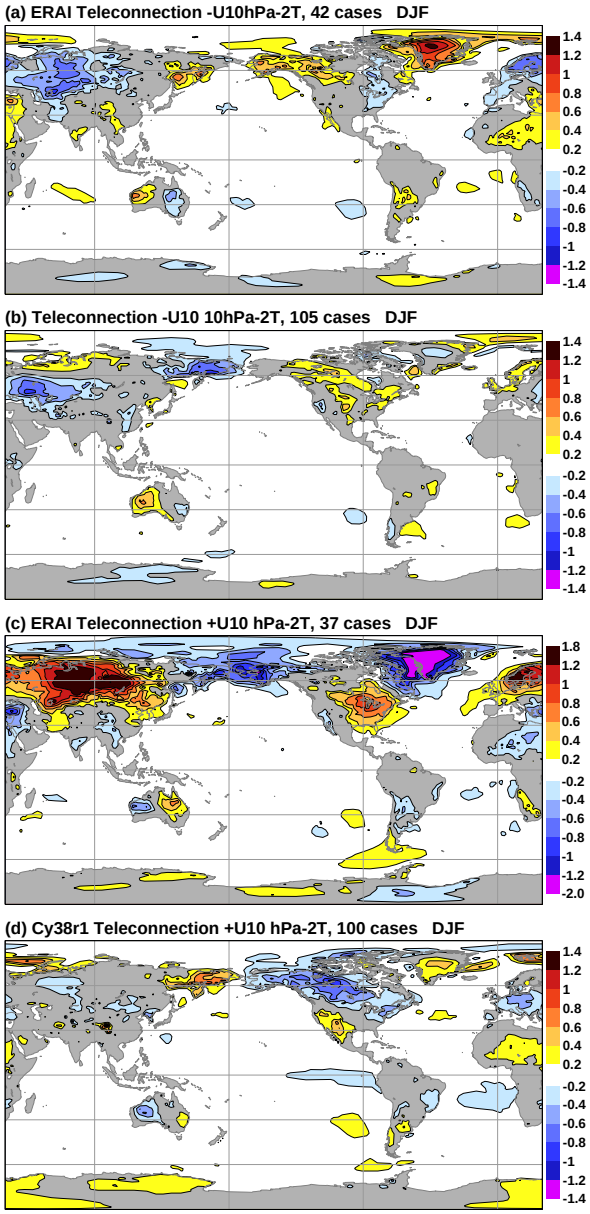

Figure 23: Teleconnection between tropical 10 hPa U wind in easterly phase and 2-metres temperatures during DJF for the ERA-Interim (a) and Cy38r1 uncoupled (b). (c) and (d) same, but for the westerly phase of the 10 hPa zonal wind.

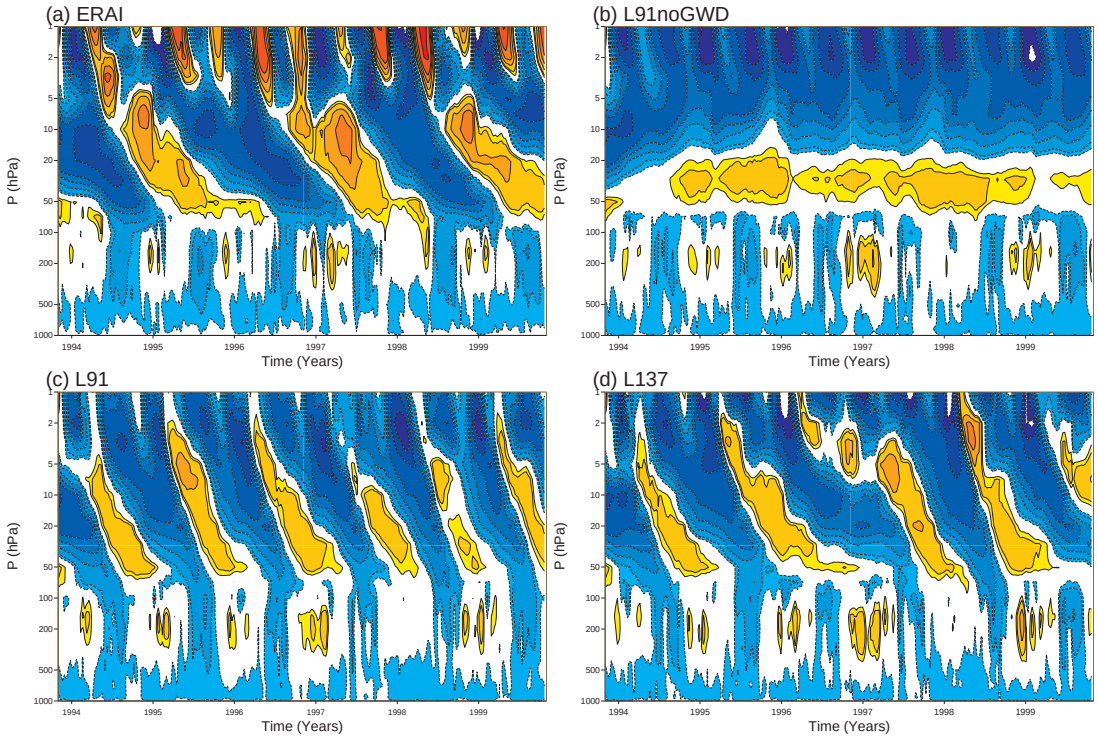

Figure 24: Time-height cross section of the evolution between 1994 and 2000 of the U-wind averaged over the $\pm 10^{\circ}$ tropical band: ERA-Interim (a), Cy38r1 91 and 137 levels (c), (d), and without the non-orographic gravity wave parameterization (b).

ics. However, more importantly the model is expected to reproduce the main modes of stratospheric variability that are the QBO and the semi-annual oscillation of the upper stratosphere/lower mesosphere. The latter are clearly present in ERA-Interim as illustrated in Figure 24a through the evolution during 6-years of u-wind profiles averaged over the tropical band. The current model situation using Cy38r1 and 91-levels and the future version using 137-levels are illustrated in Figures 24c-d. A simulation using Cy38r1 is also shown (Figure 24b), but without the non-orographic gravity wave parameterization (Orr *et al.*, 2010) that was introduced in 2009. Compared to the model versions prior to 2009, which were not able to produce a westerly wind reversal, the current model produces a stratospheric oscillation but with a too short period of roughly one year, and the semi-annual oscillation near the stratopause is absent. Increasing the vertical resolution to 137 levels prodcues a more realistic period of the QBO of roughly 1.5 years, the reasons are a greater numerical accuracy in the handling of resolved gravity waves allowing us to remove the remaining artificial Rayleigh friction term on wavenumber 0 that was necessary before to control the stratospheric wind speeds in the polar night jet. The period of the QBO could be tuned through the non-orographic gravity wave parameterization, but our primary goal is to have realistic mean stratospheric winds. Also, the period of the QBO is rather sensitive to model changes in the tropical troposphere, and is likely to change (shorten) with higher horizontal resolutions due to increased resolved wave drag as demonstrated in the ATHENA project (Jung *et al.*, 2011).

5 The Madden-Julian Oscillation and the Year of Tropical Convection

With the goal of improving the representation of tropical convection in weather and climate prediction, the World Climate Research Program (WCRP) and the World Weather Research Program (WWRP)/THORPEX declared the Year of Tropical Convection (YOTC) [4], with a target period from May 2008 to April 2010, to streamline joint research activities on tropical meteorology and convection (Waliser *et al.*, 2012). ECMWF participated in this activity by providing to the scientific community not only access to the full high-resolution operational data during that period (T_L799 until January 2010 and T_L1279 after), but also by providing model tendencies of all physical processes for the first 36 hours of the forecasts.

5.1 Madden-Julian Oscillation: amplitude and propagation

In collaboration with the University of Reading our focus in YOTC is on the MJO which is the dominant mode in tropical intraseasonal variability (Zhang, 2005), and also provides the major source of predictability in the mid-latitudes on the monthly time scales (Vitart and Molteni, 2009). Numerous studies in the past have evaluated MJO predictions in general circulation models (Slingo *et al.*, 1996; Lin *et al.*, 2006) and tried to relate the quality of the forecasts to biases in the mean state (Inness *et al.*, 2003; Kim *et al.*, 2011), the air-sea interaction (Woolnough *et al.*, 2007), the convection (parameterization) and cloud-radiation interaction (Lin *et al.*, 2006; Kim *et al.*, 2011). All studies agree in that the model resolution is not a determinant factor in the representation of the MJO which can be seen as a projection of the convection on the planetary scales. Rossby wave coupling between the mid-latitudes and the Tropics also plays an important role (Wedi and Smolarkiewicz, 2010). For the IFS Bechtold *et al.* (2008), Jung *et al.* (2010) and Vitart and Molteni (2009) have reported important progress since 2006 in the representation of the MJO that is likely to be related to improvements in the radiation package (Morcrette *et al.*, 2008) and the convection parameterization in particular. Vitart and Molteni (2009) have shown, by comparing monthly hindcasts with ERA-Interim, that the IFS is now able to realistically reproduce tropical and mid-latitude precipitation and height anomalies that are connected to different phases of the MJO.

The quality of the MJO forecasts is documented in Figure 25 based on hindcasts for the period 1995-2001 with all model cycles since 2002. A generally accepted quality measure is the linear correlation coefficient between the forecasted and analysed OLR and wind field projected onto the two leading Empirical Orthogonal Functions (EOFs) (see below). Assuming a meaningful correlation threshold of 0.6, the predictability of the MJO has improved from about 15 days in 2002 to 26 days in 2011. Note that the National Centres for Environmental Prediction (NCEP) hosts a service collecting and evaluating the real-time MJO forecasts from all major Centers [5]. The current predictability limit of the IFS, which is ahead of the other Centers, has to be compared to the theoretical predictability estimate of the MJO, which is one cycle or roughly 50 days (Ding *et al.*, 2010). Judging from this, there is still room for further improvements. Already, model developments showed a strong increase in predictability between 2006 and 2008 in connection with model cycles 32r2 and 33r1. A further increase is noticeable after 2010 in relation to the introduction of the 5-species prognostic microphysics scheme (Forbes *et al.*, 2011). We also have a reduced set of hindcasts with the latest model cycle 38r1 (denoted by the triangle symbols). So far, the results suggest increased predictability by one day through filtering of unrealistic spectral noise in the dynamics, and through tuning of the ice microphysical part as well as the convective detrainment and downdraughts.

[4] http://www.ucar.edu/yotc/

[5] http://www.cpc.ncep.noaa.gov/products/precip/CWlink/MJO/CLIVAR/clivar_wh.shtml

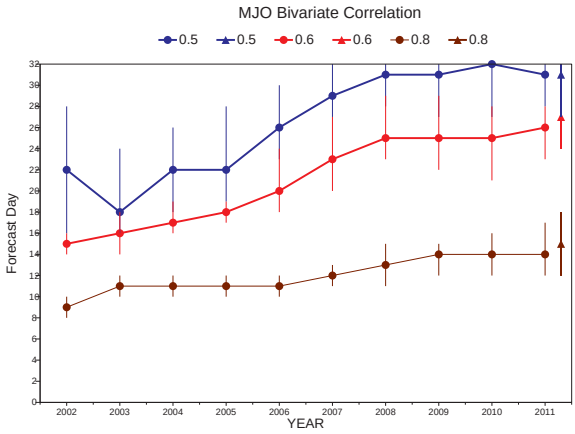

Figure 25: Time series of different thresholds of correlation coefficient between forecasted and anlaysed OLR and wind field projected onto the two leading EOFs. Dots correspond to all operational model cycles between 2002 and 2011 that have been run for the hindcast period 1995 to 2001, triangles denote Cy38r1.

During YOTC our focus is on the role of the physical parameterizations, and in particular the convection, and their projection on forecast errors during the different phases of the MJO. In addition to the available datasets during YOTC, namely the operational forecasts and ERA-Interim dataset using Cy31r1 (2006), a sensitivity forecast experiment (labeled CONV) was completed for the same period. The reforecasts were initialised with the operational analysis and using the then operational cycle Cy35r2, but with the convection scheme reverted to the version before Cy32r3 (November 2007).

MJO events during the period May 2008 to June 2009 are illustrated in Figure 26 with the aid of 1ow-pass filtered OLR anomalies (W m^{-2}) as observed by NOAA satellites (Figure 26a). Also shown are the day+1 and day+10 operational forecasts (Figures 26b,c), day+10 forecasts from ERA-Interim, and the CONV experiment with the reverted convection scheme (Figures 26d,e). The MJO events are characterized by negative OLR anomalies propagating from the Western Indian Ocean to the Central Pacific in about 15-20 days. Clearly, the day+1 operational forecasts closely fit the observations. The operational day+10 forecasts are able to maintain the propagating anomalies, but the amplitude of the convective signals is now overestimated, leading through teleconnections to too strong positive anomalies in the Eastern Pacific. The amplitude error in the convection anomalies is however reduced by roughly 50% in model cycles after 2010 (not shown). In contrast, in both ERA-Interim and CONV forecasts, the amplitude of the anomalies has become rather weak by day 10 and their propagation is compromised.

The propagation characteristics of the MJO can be analysed in further detail with the aid of so called Wheeler and Hendon diagrams (Wheeler and Hendon, 2004) which use the first two Empirical Orthogonal Functions (EOFs) of a multivariate MJO index. As an example the propagation of a MJO event during April 2009 from the Indian Ocean (phase 2/3) to the West Pacific (phase 6/7) is illustrated in Figure 27 following Hirons *et al.* (2012a) for different forecast lead times. These are compared to observations consisting of reanalysis data (wind) and satellite data (OLR). For short lead times all cycles, i.e. operations, ERA-Interim and CONV closely follow the observed propagation. However, for lead times beyond 72 hours there is a strong loss of amplitude in ERA-Interim and CONV leading to a loss of the MJO signal by day+10 compared to the observations. In contrast, the operational forecast is able to maintain a realistic MJO amplitude throughout, but tends to overestimate the amplitude in the short-range over the West Pacific which reflects the model precipitation bias in that region.

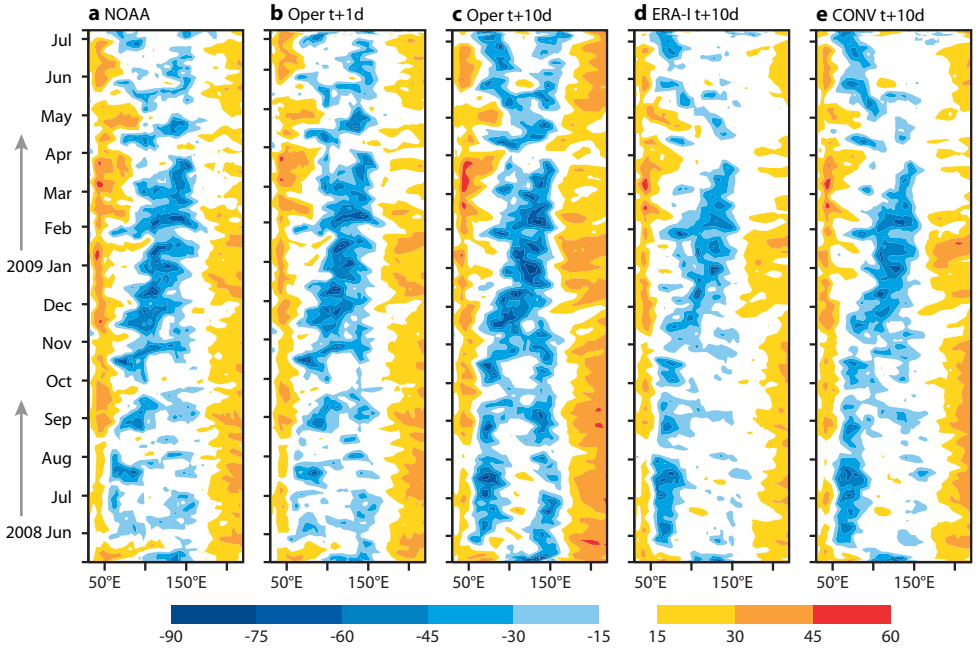

Figure 26: Time versus longitude diagram of 10-day low-pass filtered OLR anomalies (W m^{-2}) averaged over $\pm 10^{\circ}$ latitude for the period May 2008 to July 2009 as observed by NOAA (a), and from operational day-1 (b) and day-10 (c) forecasts, as well as from day-10 forecasts from the ERA-Interim (d), and the operational cycle but using the 'old' convection (e).

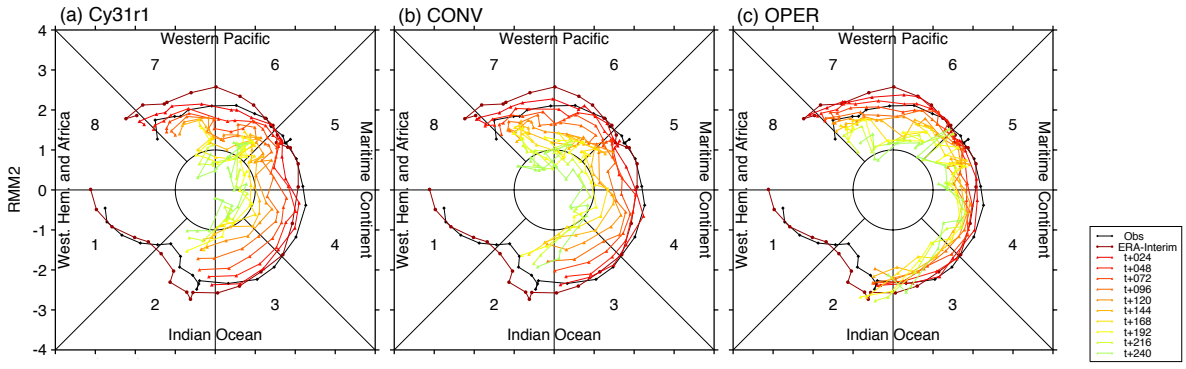

Figure 27: Daily forecasts during April 2009 of multivariate MJO Index consisting of OLR and 850 and 250 hPa zonal wind projected onto the two leading EOFs. The colours distinguish the results for different forecast lead times, from 24 to 240 hours. Black and brown lines denote observations and the ERA-Interim.

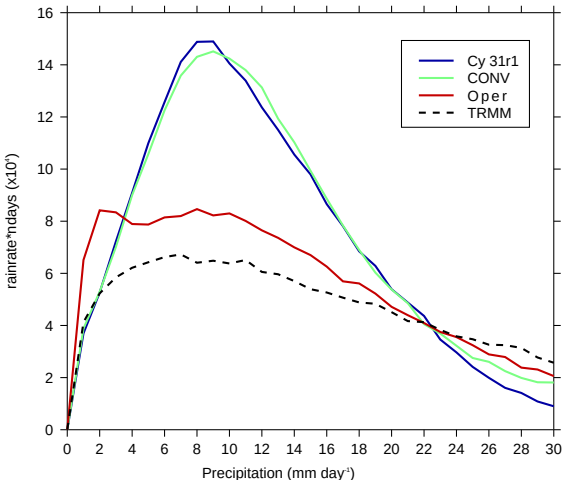

Figure 28: Frequency distribution of tropical rainfall rates averaged over the first 24 h of the forecasts corresponding to ERA-Interim (Cy31r1), the operational forecasts (OPER), the operational cycle but with the 'old' convection scheme (CONV), and the observations from the TRMM radar (dashed).

Finally, following Hirons *et al.* (2012b), more information on the behaviour of the different model versions can be gained by comparing the rainfall distributions of the different models in the $\pm 10^{\circ}$ latitude band during the first 24 hours of the forecasts to the observations from the TRMM radar. Both, ERA-Interim and CONV overestimate the precipitation rate by nearly a factor of two in the 5 to 20 mm day^{-1} rain bins. Interestingly, a similar behaviour has been noted by Holloway *et al.* (2012) for the UKMO model and by Thayer-Calder and Randall (2009) for the NCAR model. In contrast, the operational model reduces the precipitation in the 5 to 20 mm day^{-1} rain bins and increases the precipitation in both low and high-rain bins. This means that in spite of a remaining overall overestimation of precipitation, the current operational model reasonably reproduces the observed rainfall distribution. Chakraborty (2010) has also evaluated the ECMWF operational precipitation forecasts during YOTC. He noticed, consistent with Figure 26, a realistic propagation of convective rain bands up to day+5, smaller precipitation errors over ocean than over land, consistent with Figure 28 an overestimation of small precipitation rates, or an underestimation of dry days, and an underestimation of heavy (> 40 mm day^{-1}) precipitation events. Finally, the striking similarity between ERA-Interim and CONV results shown so far and the fact that the CONV results approach that for ERA-Interim already after 24 hours in spite of them being initialised with the operational analysis, suggests that the main contributor to the improved representation of the MJO and the model tropical precipitation in general is the convection parameterization which produces about 75% of the total tropical precipitation. The most important aspects in the conevctive parameterization to achieve these improvements are a realistic entrainment formulation, a variable convectice adjustment time scale, a numerical solver that supports large mass fluxes, and the trigger formulation.

5.2 Model tendencies

In order to evaluate the contribution of the different model processes in the MJO, composites of the model large-scale advective (dynamics) and physical tendencies have been computed based on the multivariate MJO index (see Figure 27) for the entire YOTC period and individual phases of the MJO. As an illustration of the distribution of the convection for the different phases of the MJO, composites of the tropical OLR anomalies for phase 2/3 of the MJO are given in Figure 29a and OLR anomaly

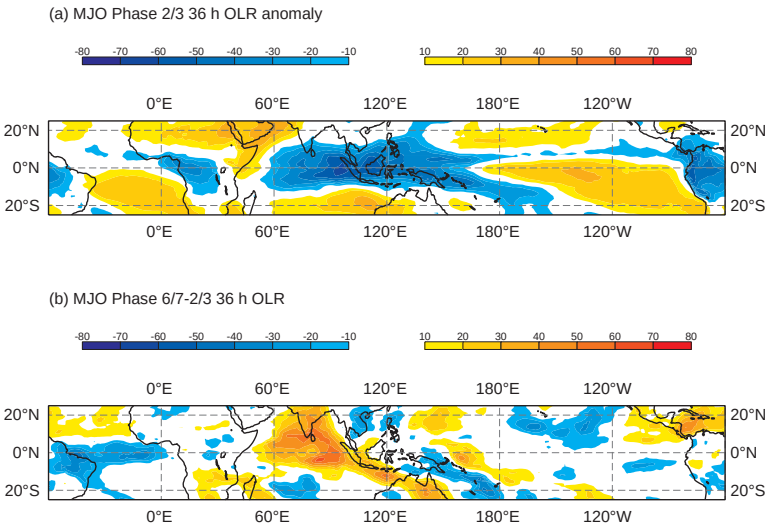

Figure 29: OLR anomalies (W m^{-2}) from 12-36 hour forecasts during YOTC composited for phase 2/3 of the MJO (a) and differences in OLR anomalies between phase 6/7 and 2/3 (b).

differences between phase 6/7 and phase 2/3 are displayed in Figure 29b. Phase 2/3 of the convection implies increased convection over the Indian Ocean, but also increased convection over Central Africa and Western Amazonia. Figure 29b also shows that when the MJO propagates to phase 6/7 that there is increased convection over the Western Pacific, South Pacific convergence and the tropical Atlantic. However, there is only a small modulation of convection over the Maritime Continent as convection over these regions is largely independent of the phase of the MJO, and mainly diurnal-cycle driven (Yang and Slingo, 2001) (see also Figure 20).

Vertical cross-sections of the difference in dynamics, convection, cloud and radiation tendencies between phase 6/7 and phase 2/3 of the MJO during the first 36 hours of the forecasts are depicted in Figure 30. The diffusion tendency is not shown as the phase difference is small. The actual structure and sign of the tendency is roughly consistent with the profiles in the region between 120-160° longitude. Two important observations can be made based on Figure 30. To a first approximation, the MJO is characterised by an equilibrium between a deep dynamic lifting (cooling) mode and convective heating, and the heating rate difference between the different phases of the MJO is on average of O(1-3) K day^{-1}. The actual amplitude is stronger over the Indian Ocean, and it is this region where all tendencies become important. This includes a characteristic heating (condensation) and cooling (evaporation) dipole profile originating from the large-scale cloud scheme, and a remarkable variability of the radiative cooling rate which is O(1) K day^{-1}, and therefore as large as the average radiative cooling rate in the Tropics. The Indian Ocean, which is the region with the largest intraseasonal variability, is therefore also the most sensitive region to any changes in the model. The reason for this strong sensitivity might reside in the relatively uniform sea-surface temperatures (SSTs) distribution in that region (Williamson *et al.*, 2012).

The differences in temperature and moisture tendencies (K day^{-1}) between the operational model and the CONV experiment, i.e. between a recent model version that produces a realistic MJO and a model version representative for the pre-2007 era that does not maintain a realistic MJO are shown in Figure 31 for phase 2/3 of the MJO. Here, similar but less pronounced differences can be observed for the phase

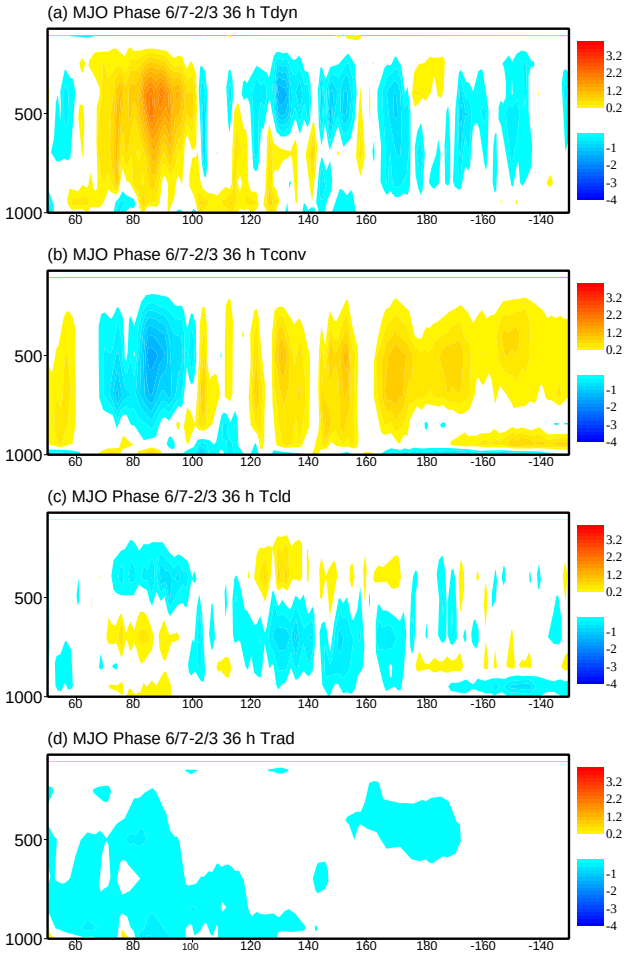

Figure 30: Vertical cross section of differences in unfiltered temperature tendencies (K day^{-1}) for lead time 12-36 hours of the forecasts between phases 6/7 and 2/3 of the MJO: dynamics (a), convection (b), large-scale cloud scheme (c), and radiation (d).

6/7. The results can be summarized as follows. Compared to the CONV experiment there is a distinctive supression of deep convection (less convective heating in Figure 31a) that is compensated by dynamical subsidence (Figure 31b,d). Further, the operational model generates a stronger moistening of the lower to middle troposphere through shallow convection (Figure 31c) producing also more mid-level clouds but less low-clouds (Figure 31e). The impact on the boundary-layer has been compensated by changes in the boundary-layer scheme. We have not shown the momentum tendencies as, apart from the top of the trade wind layer and in the upper-troposphere, cumulus friction by momentum transport is small. Away from the Equator approximate thermal wind balance prevails so that differences in the wind field follow, to the first order, differences in temperature (tendencies).

Furthermore, Hirons *et al.* (2012b) have shown through a time-lag analysis that CONV is producing convective heating/drying that is overestimated and only weakly modulated by the phase of the MJO. In contrast in the operational model deep convection is realistically suppressed in the subsiding branch of the MJO and the middle troposphere is moistenend through shallow and congestus convection, preconditioning the troposphere for the dynamically active phase of the MJO. In this respect the MJO can be interpreted as a moisture mode (Raymond and Fuchs, 2009). Currently, the convective moistening is slightly too strong in the model leading to a drift or an overall overestimation of precipitation with time. Since the pioneering study by Derbyshire *et al.* (2004) the sensitivity of the models' convection to environmental humidity, and their ability to represent a tri-modal distribution of tropical convection including shallow, congestus and penetrative convection is now acknowledged as one of the most important model components for a successful simulation of tropical variability (Lin *et al.*, 2006, 2012; Kim *et al.*, 2012). Many modelling groups currently consider this fact by developing, among others, convective entrainment parameterizations that provide variable and strong entrainment rates in the lower troposphere (Chikira and Sugiyama, 2010; Genio and Wu, 2010; Hourdin *et al.*, 2012; Stirling and Stratton, 2012). An updated version of the IFS entrainment parameterization used in Bechtold *et al.* (2008) is discussed in Rooyde *et al.* (2012) and is shown to compare reasonably to observations. By evaluating the relationship between rain rates and total column water and/or mid-tropospheric humidity from observations and forecasts as advocated by Bretheron *et al.* (2004), Hirons *et al.* (2012b) demonstrated that the operational IFS (but not CONV) realistically represents the observed precipitation dependencies over the Indian and Pacific Ocean basins for a large range of atmospheric humidities, but that it overestimates rain rates when the atmosphere is very moist (total column water > 55 kg m^{-2}).

We have not discussed yet the interaction between heating and the MJO. It was only in 2000 that Yanai *et al.* demonstrated that for the MJO with its vertical westward tilted structure, the amplification occurs through potential to kinetic energy conversion in the upper troposphere when the dynamically warm phase of the MJO coincides with the convective or condensational heating. This principle has also been demonstrated for the Kelvin wave by Shutts (2008), and for the global energy cycle of the IFS by Steinheimer *et al.* (2008). It is therefore crucial for a realistic simulation of the MJO that the model's convection parameterization produces a realistic heating profile in the right phase of the background or 'dry' wave. Or, in other words, $-\overline{T\omega} > 0$, i.e the correlation between the heating anomaly and vertical velocity in pressure coordinates must be negative in the upper troposphere. This explains the decrease in MJO amplitude through negative energy conversion in the CONV experiment where convection is active irrespective of the phase of the large-scale wave.

6 Towards global resolved deep convection

The ECMWF plans foresee a horizontal resolution upgrade to T_L2047 (10 km) in 2015, and towards T_L3999 (5 km) in 2020. This means that deep convective motions become gradually more resolved so

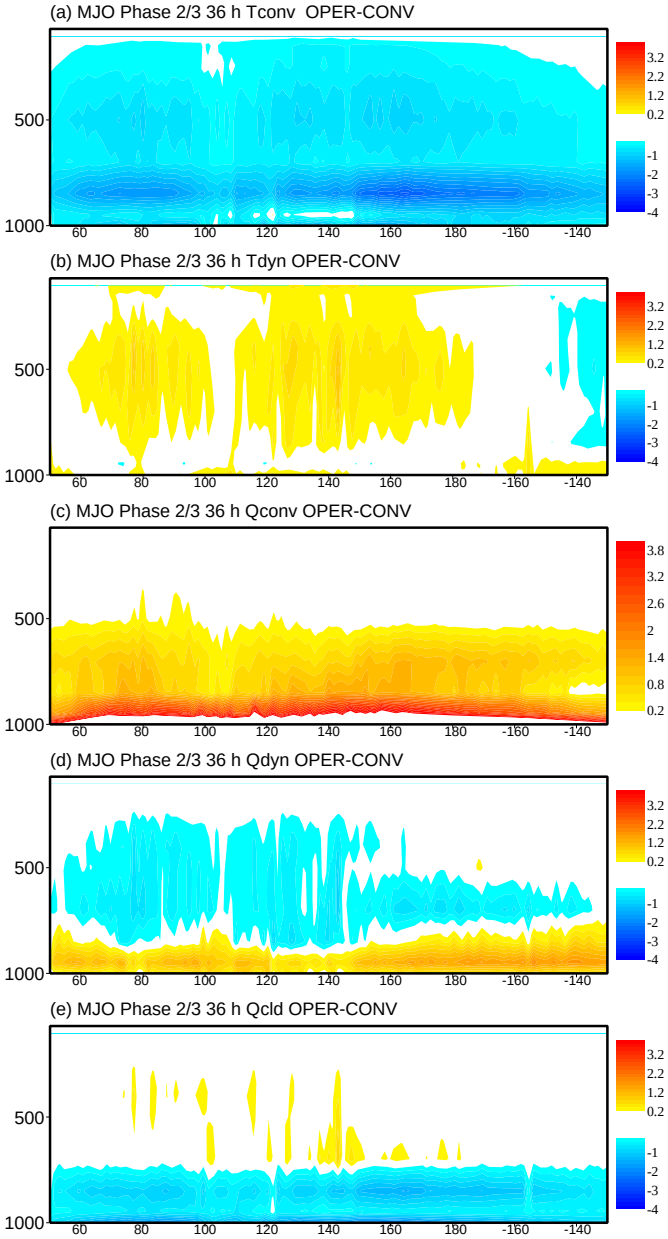

Figure 31: Same as Figure 30 but for differences in unfiltered temperature (a)-(b) and moisture (c)-(e) tendencies (K day^{-1}) between operations and old convection (CONV) when the MJO is in phase 2/3.

that the optimal partitioning in the model between resolved and sub-grid vertical motions and condensation processes has to be revisited. Also some assumptions inherent to the mass-flux convection scheme like column independent convection, stationarity and the equilibrium hypothesis between the large-scale forcing and the convection have to be reevaluated (e.g. Gerard and Geleyn, 2005). And finally, one wants to estimate, from which horizontal resolution onwards the global forecasting system could eventually be run without a deep convection parameterization and, at the same time, maintaining or improving the forecast skill on the medium to monthly time scales for both mid-latitude and tropical regions.

An ideal testbed for these exploratory studies on high-resolution global convection is the so-called Aqua-planet experiment (AQUA) defined in Blackburn *et al.* (2012) and Williamson *et al.* (2012). In this setup, models are run with a specified SST distribution that is close to the observed mean SST distribution peaking at the Equator. The sun is held fixed over the Equator thus removing any seasonal cycle. The advantage of this setup is that it further removes complications due to land-surface/atmosphere interactions like e.g. soil hydrology and the diurnal cycle of convection over land. It also avoids problems due to possibly unknown surface fields at very high resolutions.Williamson *et al.* (2012) showed that in Aqua-planet mode the models produce a realistic global circulation and characteristic tropical wave features after a spin-up time of roughly 6 months.

We have reproduced the Aqua-planet mode with Cy38r1 at linear spectral truncation T_L159 (125 km) by starting from a balanced state, using a 6 months spin-up forecast, generating a 4-member ensemble by applying to each member random perturbations at initial time, and running the ensemble for one year. The SST corresponds to 'QOBS' in Williamson *et al.* (2012) (their Figure 1), which means that it peaks at 27°C at the Equator and decreases to 0°C at $\pm 60^\circ$. A comparison of the Aqua-planet simulation with the corresponding real-globe simulation for 2000/2001 and observations has been produced. Figure 32 shows annual mean total column water content and surface latent heat flux, and Figure 33 shows annual mean daily precipitation and the symmetric component of the OLR wavenumber-frequency spectra as derived from daily data averaged over $\pm 10^\circ$ latitude. It is shown that the mean climatology of the Aqua-planet represents a latitude structure that is fairly close to the real Earth for both the tropical band and the mid-latitude storm tracks. It also reproduces similar tropical wave activity, e.g the global mean daily precipitation rate from the Aqua-planet simulations amounts to 3.2 mm day^{-1} compared to 2.9 mm day^{-1} for the true-globe integration and 2.7 mm day^{-1} from the observations. The largest differences are found in polar regions. However, the Kelvin wave activity in the Aqua-planet simulation is stronger than in reality as these waves can circle the globe undisturbed by surface heat contrasts, and the tropospheric mid-latitude temperatures are generally colder (not shown). We also take advantage of Figure 33 to illustrate the progress in the representation of convectiveley coupled waves since Cy31r1 (2006). Indeed in that cycle, and earlier, the convective precipitation is concentrated along the Equator and no significant Kelvin wave and MJO signals are preesnt in the spectra Figure 33g-h.

6.1 Full planet

The next step is to use this experimental setup and run the model on increasingly higher horizontal resolutions with and without deep convection parameterization, say from T_L159 (125 km) to T_L1279 (15 km) and higher. This is to monitor the effect of increasingly resolved scales on the general climate performance of the model as was done in the ATHENA project (Jung *et al.* (2011); Dirmeyer *et al.* (2011)).

The first results of the project are illustrated in Figure 34. Similar to Figure 33, the annual mean total precipitation rate (mm day^{-1}) and the symmetric part of the wavenumber frequency spectrum are used to characterize the effects of parameterized convection versus grid-scale 'convective' overturning (the deep convection is switched off and only shallow convection is active) on the Aqua-planet when going from

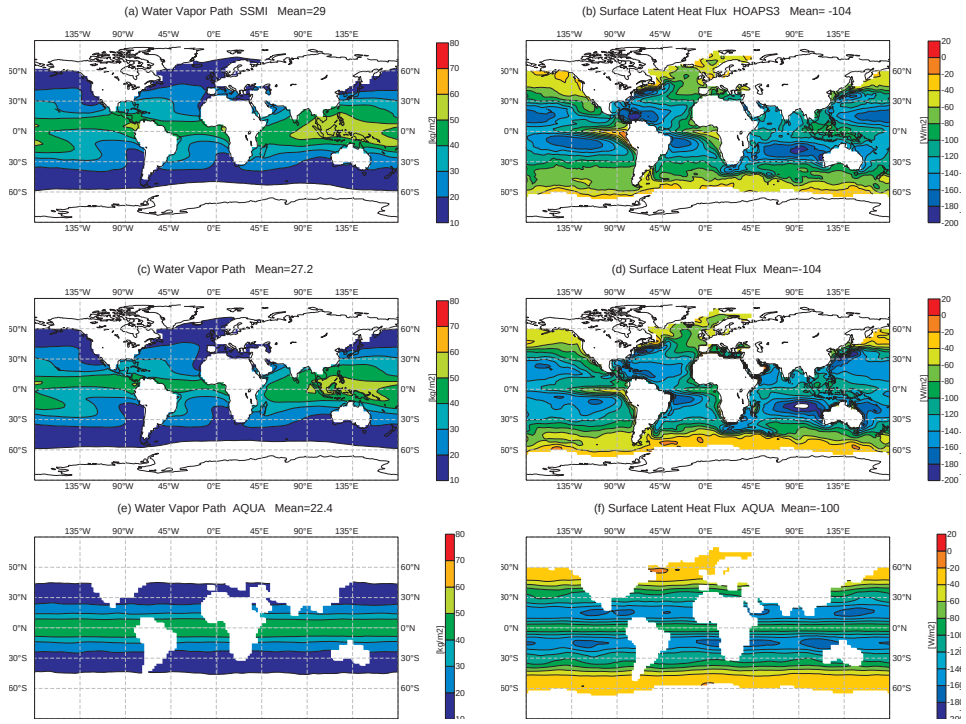

Figure 32: Annual mean total column water content (kg m^{-2}), left column, and surface latent heat flux (W m^{-2}), right column, from observations: SSM/I (a) and HOAPS (b), and from an ensemble of 1-year integrations at T_L159 on the real Earth (c)-(d), and the Aqua-planet (e)-(f).

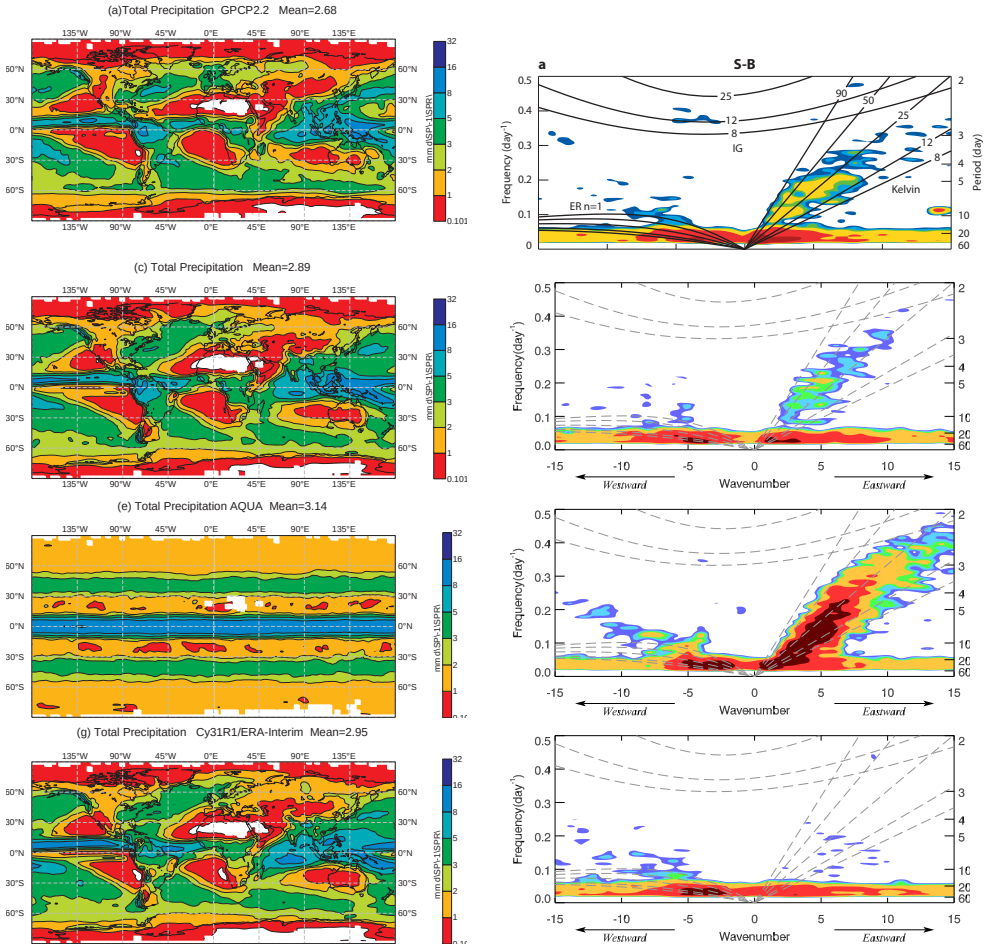

Figure 33: Similar to Figure 32 but for annual mean daily precipitation, left column, and the symmetric wavenumber frequency spectra of the OLR, right column. For comparison are also added the results for Cy31r1 (ERA-Interim). Spectra include the theoretical dispersion relations for Kelvin, equatorial Rossby, and inertial gravity waves with equivalent depths of 8,12, 25, 50, and 90 m. Observations are from the GPCP2.2 (a) and NOAA satellites (b).

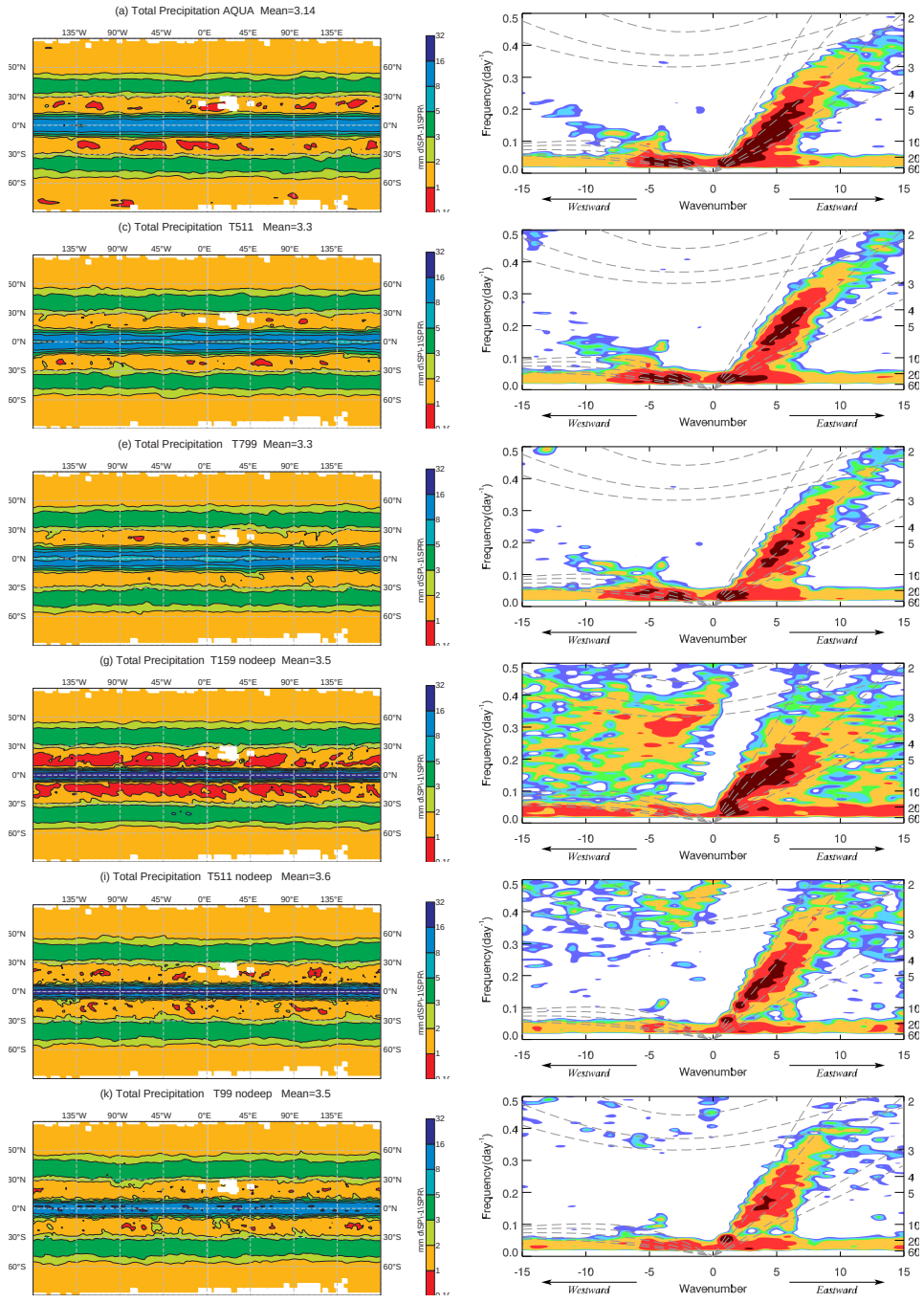

Figure 34: Same as Figure 33, but for full planet simulations at T_L159, T_L511, T_L799 with, (a)-(f), and without deep convection, (g)-(l).

T_L159 (125 km) to T_L799 (25 km) (Figures 34a-l). In particular, one observes in the run without deep convection (Figures 34c-d) at T_L159 an ITCZ with heavy precipitation peaking around 24 mm day^{-1} at the Equator compared to the baseline run with deep convection (Figures 34a-b) producing around 11 mm day^{-1}. Furthermore, without deep convection the wave spectra become nearly red so that the Kelvin and Rossby signal present in the run with deep convection is blurred.

However, when increasing the resolution further to T_L511 and T_L799 one notes two interesting features. The results in the runs with deep convection only weakly depend on resolution. E.g. the peak precipitation rate at the Equator decreases by about 0.5 mm day^{-1} at T_L799 compared to T_L159, and the precipitation in the mid-latitude storm tracks increases by about 0.2 mm day^{-1}. The ratio of convective to total precipitation is for all resolutions around 68%. This is by construction of the convection scheme where the convective adjustment time scale ($\tau = H_c/w^u$, with H_c being the depth of the convective cloud, and w^u denoting the mean updraught velocity) is modulated by a resolution dependent factor (Bechtold *et al.*, 2008) to offset the increase in the large-scale forcing (convergence). There is however a slight tendency to form a split ITCZ with increasing resolution. A tendency for models to produce a split ITCZ with a QOBS SST distribution has also been noticed by (Williamson *et al.*, 2012). This is in contrast to a SST distribution with a sharp peak at the Equator for which all models tend to produce a single ITCZ.

However, the runs without deep convection parameterization strongly depend on resolution, but with increasing resolution the maximum zonal mean tropical precipitation rate decreases from 22 mm day^{-1} at T_L159 to 19 mm day^{-1} at T_L511, and 15 mm day^{-1} at T_L799, and the wave amplitudes decrease as well. In particular the wavenumber frequency spectra at T_L799 become comparable to the corresponding run with parametrised deep convection, but the Kelvin wave phase speed is still too high and the MJO signal is missing.

6.2 Small planet

The high-resolution approach on the full planet becomes quickly too costly with present computer power, especially for model development and data analysis. Therefore, we have chosen the small planet approach where the Earth radius R is divided by a factor γ_r, and a dynamic rescaling is performed, so that the global circulation and the dynamic forcing of the convection is realistically represented. This approach has been pioneered by Smolarkiewicz and Margolin (1997), Kuang *et al.* (2005), and Garner *et al.* (2007) and bears the distinctive advantage over traditional high-resolution equatorial channel simulations (Shutts, 2006; Holloway *et al.*, 2012) that it also permits to simulate (emulate) the global climate and in particular the wave interaction between the Tropics and the middle latitudes.

The dynamical scaling we have used is as follows: Conserving the large-scale dynamics and the wavenumber of large-scale waves amounts to conserving the Rossby number $Ro = U/(fR_a)$, where R_a is the Earth radius, U is a horizontal velocity (to be conserved) depending on the meridional temperature gradient, and f the Coriolis parameter or inverse time scale. Therefore, if $R'_a = R_a/\gamma_r$ then, in order to conserve Ro, f has to be scaled as $f' = f\gamma_t$, with $\gamma_t = \gamma_r$. This is equivalent to reducing the length of the day by a factor γ_t. However, in this system the vertical to horizontal aspect ratio is distorted with respect to the full planet, as is the continuity equation which can be illustrated in simplified form by

$$\frac{\partial u}{\partial x'} + \frac{\partial v}{\partial y'} = \gamma_r \left(\frac{\partial u}{\partial x} + \frac{\partial v}{\partial y} \right) = -\frac{\partial w}{\partial z} = -\frac{\partial \omega}{\partial p} \tag{1}$$

All notations are standard. In the small-Earth system denoted by primes the left-hand side (lhs) of (1)

increases by a factor γ_r so that the vertical derivative and both w and ω change by the same factor. This has important consequences for the global circulation as is illustrated in Figures 35a,b for a T_L159 small-planet run with $\gamma_r = \gamma_t = 4$, and active deep convection. This simulation should be in principle directly comparable to the T_L511 full-planet simulation (Figures 34c,d). The small-planet run produces broad tropical and midlatitude precipitation zones, with the latter being shifted poleward, and an unrealistic zonal mean temperature and wind structure (not shown). Furthermore, the tropical wave spectra are distorted exhibiting a too intense and too slow Kelvin mode and a distorted Rossby mode.

However, the correct aspect ratio can be simply reestablished by scaling the gravity $g' = \gamma_g g$, with $\gamma_g = \gamma_r = \gamma_t = 4$. This in turn adjusts the atmospheric scale height $H' = R\overline{T}/g' = R\overline{T}/(\gamma_g g)$, where R is the gas constant, and $\overline{T}$ a mean tropospheric temperature. Under this scaling the vertical velocity w is conserved but z is reduced and ω is still augmented (pressure is conserved) as follows from (1), so that for the entire system time is shortened in both the horizontal (increased rotation) and the vertical. Note that the subscript notation for the factor γ distinguishes as in the computer code between horizontal, vertical, and time scales. Conserved variables include therefore the geopotential, pressure, and density, but the total mass is not conserved (reduced) as is the volume. The gravity wave speed $c = \sqrt{gH}$, and the ratio between the buoyant (convective) frequency and the Coriolis parameter $N/f = N'/f'$ with $N'^2 = g'\theta^{-1}d\theta/dz = \gamma_g^2 N^2$ are also conserved with respect to the full planet, and therefore the Richardson number $Ri = N^2H^2/U^2$. As shown by Verkley and van der Velde (2010) for the shallow water equation system on the equatorial β-plane, the non-dimensional scaling of the dynamical equations can be summarized by one single parameter, the Lamb parameter $R_\gamma = 4(\Omega R_a)^2/(gH)$, with $f = 2\Omega sin\Phi = \beta y = 2\Omega/R_a y$. The Lamb parameter can be interpreted as the ratio of the Earth's rotational speed and the gravity wave phase speed, and contains both the *Ro* and *Ri* number.

While we have chosen a small planet system with scaled gravity dubbed SASE, 'shallow atmosphere small earth', which has the advantage of leaving the dynamical core of the model untouched, and being applicable to different planets, other groups have chosen to increase the vertical velocity instead and keep the scale height untouched. The two systems however, imply different scalings of the physics. Scaling the gravity is a simple operation, though this necessitated a major and beneficial cleaning of the IFS. However, scaling of the physics under modified gravity is far from obvious and probably one of the reasons why a fully scaled moist atmospheric system has only found relatively little attention. Changing the scale height of the atmosphere requires to scale physical 'constants' and 'procedures' that imply absolute values of height like the definition of the standard atmosphere, the convective entrainment/detrainment rates, and the turbulent length-scales. This scaling can be done exactly and be verified by single column model runs. Furthermore, the radiative heating rate also has to be adjusted through scaled optical thicknesses, but not the microphysical 'constants' like the terminal fall velocities for rain drops and snow, as it is necessary for the alternative system. The scaling of the microphysics is particularly important to avoid unrealistically high liquid water and ice contents.

The corresponding small planet run using $\gamma_r = \gamma_t = \gamma_g = 4$ (equivalent to $T_L630 \approx$ 30 km) is shown in Figures 35c,d. An equivalent run but with $\gamma = 8$ (equivalent to $T_L1279 \approx$ 15 km) is shown in Figures 35e,f. The mean climate is shown to become quasi-invariant of the value of γ, and the results for both the global precipitation and the wave spectra now reasonably match that for the full planet runs with deep convection and this for a large range of γ (Figures 34a-f). Obtaining these results is far from obvious; the circulation is very sensitive and small errors or neglects in the scaling very easily lead to a pronounced double ITCZ structure. Note that graphical output also requires scaling (which is done automatically), in particular scaling the gravity and reducing the atmospheric scale height requires scaling of the total column quantities like total column water etc. by a factor γ_g, a reduction in the length of the day must be taken into account in the frequency spectra which are representative of 'daily mean' data, and wind

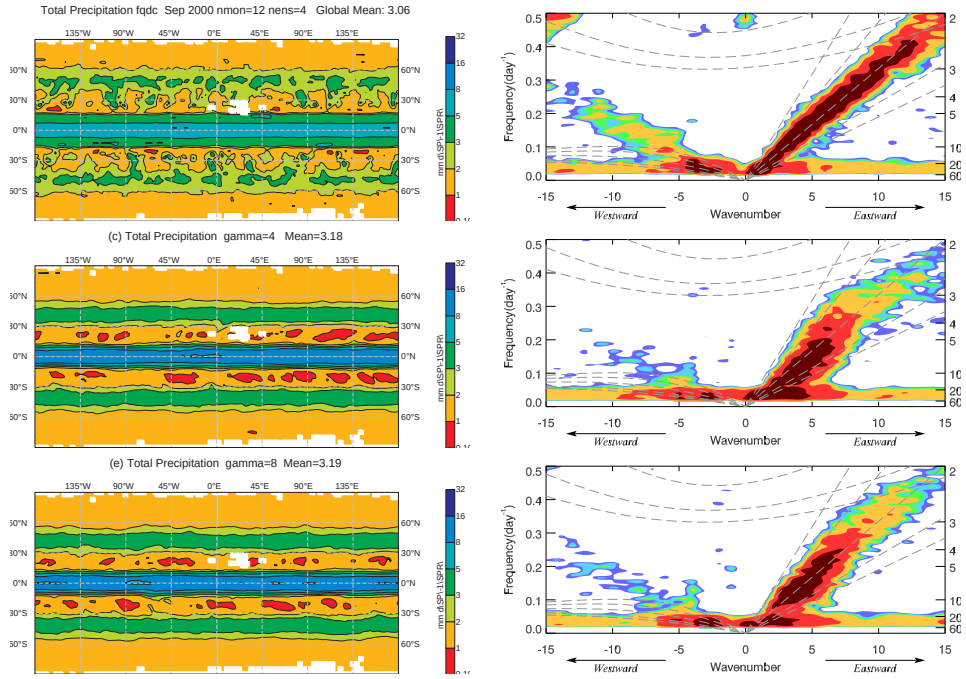

Figure 35: Same as Figure 34, but for small planet simulations at T_L159 with $\gamma_r = \gamma_t = 4$, using deep convection and standard gravity, (a)-(b), and in addition gravity and related physical parameters scaled by $\gamma_g = 4$, (c)-(d). (e)-(f) is equivalent to (c)-(d) but using $\gamma = 8$.

speeds must be scaled by a factor γ_r^{-1} when computed from the vorticity and divergence field to account for the reduced radius of the planet.

We now have achieved within the last 6 months a small-planet system that is an approximate small-scale version of the full planet system. It constitutes a generally scalable and very efficient system ('prototype') for high-resolution studies and studies of other planetary atmospheric systems. The final challenge of the small planet system is to bring the synoptic-scales closer to the convective scales while preserving a realistic large-scale forcing, and a realistic wave interaction between the middle latitudes and the Tropics. Further scale and data analysis is necessary to assess if the prototype system is able to also represent deep convection explicitly, or if, by scaling the whole Earth system down, the 'convective scales' are also downscaled and therefore become out of reach for resolution increases. Depending on the outcome we might therefore also evaluate the alternative 'deep atmosphere system' where the scale height of the atmosphere remains unchanged.

7 Conclusions and Perspectives

We have evaluated the quality of the high-resolution IFS forecast system and the convection in the Tropics during the last decade, and in the latest operational cycle on the basis of available observational data sets, the IFS analysis, and a comparison with analysis from other Centres. The challenge of the exercise was to quantify 'forecast error' which is particularly difficult in the Tropics due to the sparseness of in situ data over the tropical oceans. Further, relatively large differences exist between analyses from different systems which can amount to an average temperature difference of 0.5 K in the troposphere and a relative humidity difference of O(20%) in the upper-tropical troposphere.

Taking all measures into account, i.e. precipitation data, low-level wind data, cyclone tracks, model climate biases and variability, one can say that the tropical errors during the last decade have roughly been reduced by 20% for wind, and up to 50% for precipitation over oceans, cyclone track errors and climate biases. This is due to improvements in the model, in observational data and data assimilation scheme, as well as due to resolution upgrades, allowing ECMWF to maintain its lead in tropical prediction among the weather Centres. The most prominent improvement in the last decade is probably the gain from 15 to 25 days in MJO predictability in the monthly forecasts that is mainly due to improvements in the convection. The latter resulted in improvements of both the mean atmospheric state and the tropical variability, which are a result of a more realistic responsiveness (phase relationship and energy conversion) of the convective heating/drying to the large-scale vertical-velocity and moisture field.

However, it turned out that forecast improvements can be spatially rather variable. The largest improvements have been obtained for the equatorial Indian Ocean which is also shown to be the area with the largest sensitivity to changes in any part of the model physics and the dynamics, and also with a large sensitivity to the observations. On the other hand, there has been very little forecast improvement in areas like the East Pacific. Indeed, this area is exceptional in the sense that the vertical wind-shear is large and a cross-equatorial flow prevails throughout most of the year. Analysis differences are also large in this area, as is the uncertainty in observational products like the Atmospheric Motion Vectors.

The major remaining systematic forecast errors that are valid for the high-resolution forecast system and also largely for the EPS can be summarized as follows (in order of importance):

- A spin-down of the Hadley cell.
- An overestimation of the South-East Asian Monsoon, and an overestimation of rainfall over the Maritime Continent, leading to too strong easterlies near the Equator.
- A too strong onset of the Indian Monsoon during June (*not discussed*).
- Low-level wind errors in the East tropical Pacific.
- A weakening of the African Easterly jet, predominantly in its entry region, by 10-15% during the first 24 hours of the forecast (*not discussed*).
- A diurnal cycle of convection over land that produces maximum convective activity roughly 3-4 hours too early.
- An overestimation of the frequency of light precipitation and an underestimation of the frequency of heavy precipitation.
- Too little incoming shortwave radiation at the surface over tropical oceans, but an overestimation in subtropical stratocumulus regions .
- Over Amazonia a 5% (15 W m^{-2}) underestimation of shortwave downward radiation during the dry season due to overestimated low clouds, and too little variability during the rainy season at the surface.
- A too short period of the Quasi-Biennial Oscillation.

whereas from the analysis side, the major uncertainty stems from:

- The absence of sufficient temperature observations in the presence of clouds and precipitation.

- Moisture observations producing little impact on the medium-range and being restricted to oceanic areas.
- Few direct wind observations originating from scatterometers for near-surface oceanic winds and Atmospheric Motion Vectors with issues associated to height-assignment and observation error definition. The latter is particularly important in areas with strong vertical wind shear.
- The data assimilation system running at lower resolution and with background error definitions that require optimization for tropical areas.

As demonstrated, these errors will be barely altered by the coming vertical resolution upgrade to 137-levels, apart from a beneficial warming of roughly 0.5 K in the upper troposphere and the stratosphere, and a more realistic QBO due to better resolved gravity wave driving.

Concerning the convection parametrization scheme, the major contributions to improved forecasts over the last decade include a trigger mechanism that responds to surface fluxes but also can detect elevated convection, a strong entrainment rate producing realistic sensitivity to environmental humidity, a variable convective adjustment time-scale, an implicit numerical procedure supporting large mass-fluxes, and an overall linearity of the scheme allowing more easily global optimisations (see Bechtold, 2012, for an overview).

Options for further improvements of the scheme are somewhat limited, though between Cy36r4 (2010) and Cy38r1 (2012) tuning of the detrainment rates and the strength of the downdraughts produced a further improvement of O(5%) in lower-level tropical winds and temperatures. This gives also an estimate of possible further improvements through parameter optimisation. We are currently testing, in collaboration with the Finnish Meteorological Institute, an automated statistical procedure based on perturbed parameters in the Ensemble Prediction System (Laine *et al.*, 2011; Järvinen *et al.*, 2011).

After many years of efforts we do not yet see a robust solution to address the diurnal precipitation cycle over land problem with the current mass flux scheme. Some authors (e.g. Gerard and Geleyn, 2005; Piriou *et al.*, 2007) suggest to include some convective memory through additional prognostic equations. Though, a simplified prognostic closure has been tested, it has the drawback of adding one more degree of freedom and making the 'global optimal control' of convection more difficult.

The representation of upgradient subgrid convective momentum transport as occuring in line convection is also a problem. But there too, no general solution is in sight, in spite of theoretical work by Zhang and Cho (1991), as it is practically impossible to distinguish between organized and unorganized convection on the subgrid-scale. Instead, we intend to test a possible solution to the other main limitation of the operational mass flux scheme, namely its column independent formulation, where mass exchange between neighboring columns can only occur via the grid-scale circulation, which might become a limiting factor at higher horizontal resolutions. Kuell *et al.* (2007) proposed to increase the communication between the subgrid-scale convection and the dynamics through the export of the entrainment and detrainment mass sources. This is certainly an attractive framework for a non-hydrostatic code though it is difficult to assure formal mass conservation.

Lastly, we have not yet evaluated the possible benefits of a more stochastic formulation of the convection. However, the current scheme is shown to reproduce, when sampled over certain space and time scales, the theoretical exponential mass flux distribution (Cohen and Craig, 2006), and the correct scaling of the Pdfs of convective tendencies as a function of horizontal resolution.

Overall, we think that the largest potential for model improvements is in the prediction of the MJO. This implies contributions from the microphysical scheme, concerning in particular the representation of

the ice phase that determines the upper-tropsopheric stability, the cloud-radiation interaction, as well as the boundary-layer and turbulent diffusion scheme, as well as the implicit diffusion and problems with water vapor conservation inherent to the semi-Lagrangian advection scheme. As shown in Sandu *et al.* (2012) there is also potential for improvements of the upper-tropical jets and the subtropical jet through optimisations of the vertical diffusion in free atmospheric shear layers. Preliminary work also indicates potential for improving the western branch of the Indian Monsoon circulation with the Somalia jet, and the Eastern tropical Atlantic through an improved aerosol climatology. Concerning the analysis we think that further improvements in tropical analysis will be achieved through improvements in the background error formulation (Bonavita *et al.*, 2012) as already achieved in Cy38r1 (Holm et al., internal report), the treatment of all-sky radiances, and in particular through the assimilation of tropical wind data from the ADM-Aeolus wind lidar[6] that is expected in the 2015 time frame.

Finally, there is no demonstration yet that cloud resolving or convection permitting models will deliver more accurate tropical forecasts during the next decade neither on the medium-range nor in climate prediction. Nevertheless, we already prepare for the future high-resolution IFS system where the deep convection will become more resolved. The numerical framework adopted is a small Aqua-planet with scaled gravity. Most of the physical scaling issues implied by this system named 'Shallow Atmosphere Small Earth' have been solved, so that we now have a numerically efficient and generally scalable system applicable to planets of different sizes and gravity. The small-Earth system should also be an interesting tool for idealised data assimilation experiments. Having shown that the mean climate and tropical variability of the small-scale system is similar to that of the full Aqua planet and the real Earth system, we now need to address the question about the scale of the convection, before we can proceed to convection resolving resolutions, and/or start experiments on how to adjust the amplitude (adjustment time-scale) of the current convection parameterization for higher resolutions.

Acknowledgements

Our sincere gratitude goes to King-Fai Li from CalTech for providing the wavenumber frequency package, to Yukari Takuyabu from Tokyo University for providing the hourly TRMM climatology dataset, to Linda Hirons form Reading University for providing the MJO/observations comparison, to Nicholas Klingamann from Reading University for providing the NOAA daily OLR data, and to Jörg Trentmann from DWD for providing the climate SAF radiation products. We also warmly thank Sylvie Malardel for her help in developing the small planet system, Anton Beljaars, Roberto Buizza, Elias Holm, Lars Isaksen, Erland Källén, Martin Leutbecher, Adrian Simmons and Alan Thorpe for many helpful discussions and corrections improving earlier versions of the manuscript, and Anabel Bowen, Rob Hine and Els Kooij Connally for graphical editing.

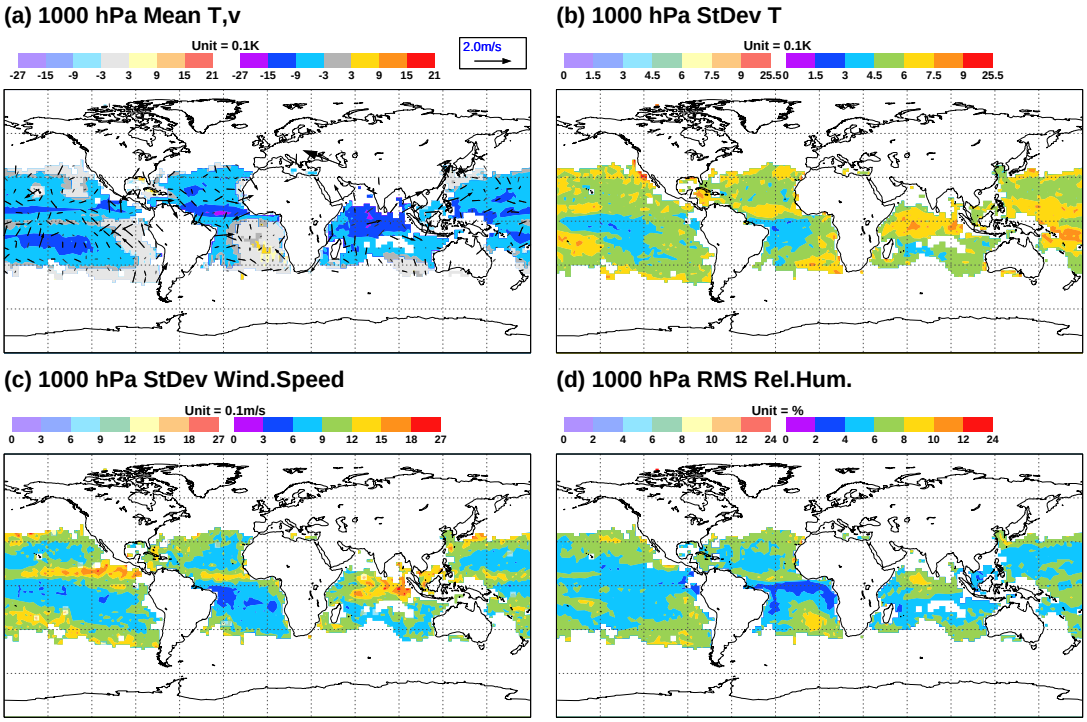

Figure 36: Same as Figure 10 but for the analysis difference between ECMWF and UKMO.

Appendix

Analysis ECMWF versus UKMO

Observing system experiments, Indian Ocean

Description of model cycles

Observation types

[6] http://esamultimedia.esa.int/.../SP-1311_ADM-Aeolus_FINAL_low-res.pdf

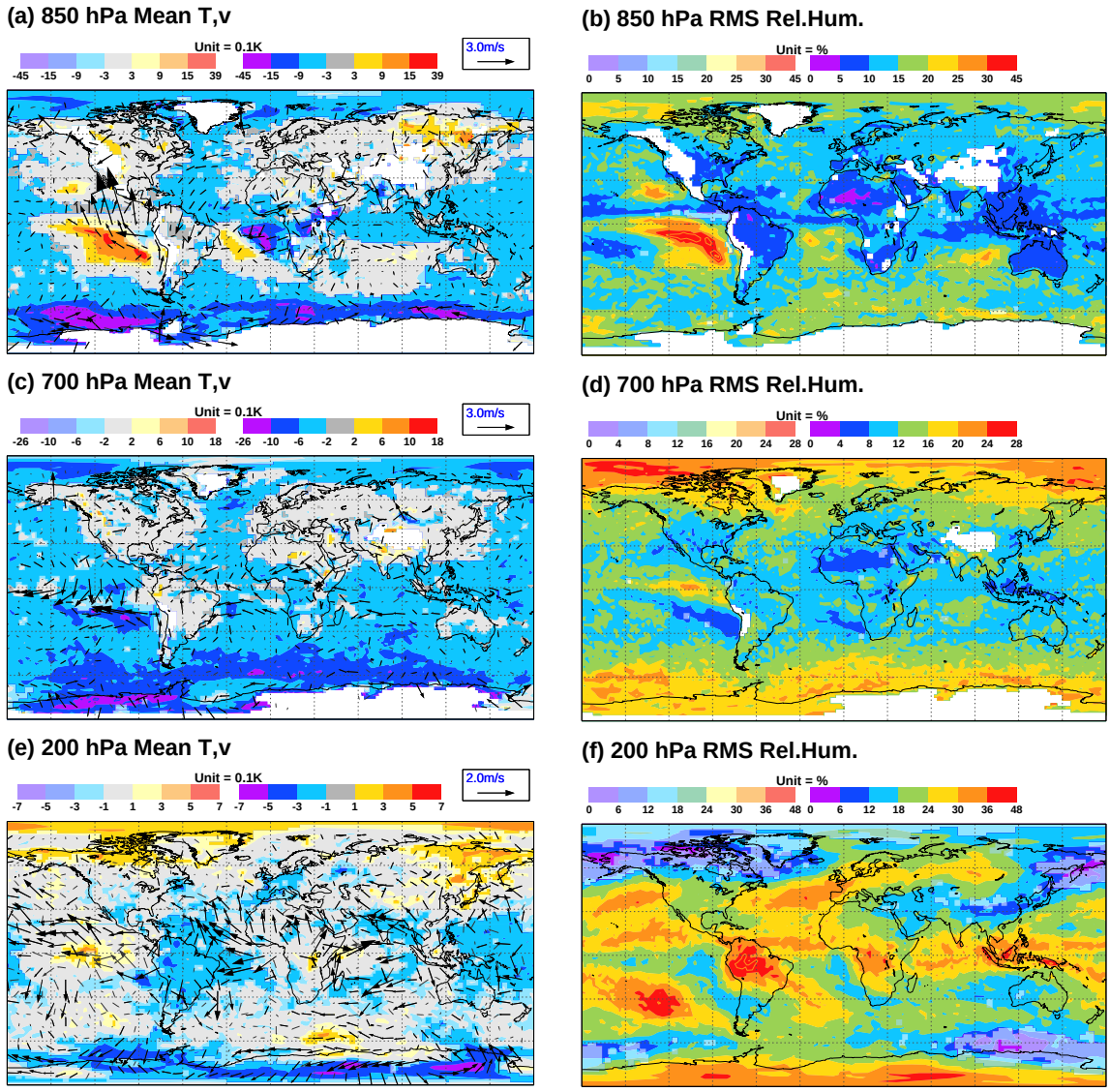

Figure 37: Same as previous but at 850, 700 and 200 hPa showing only mean T and wind vector differences and RMS of RH.

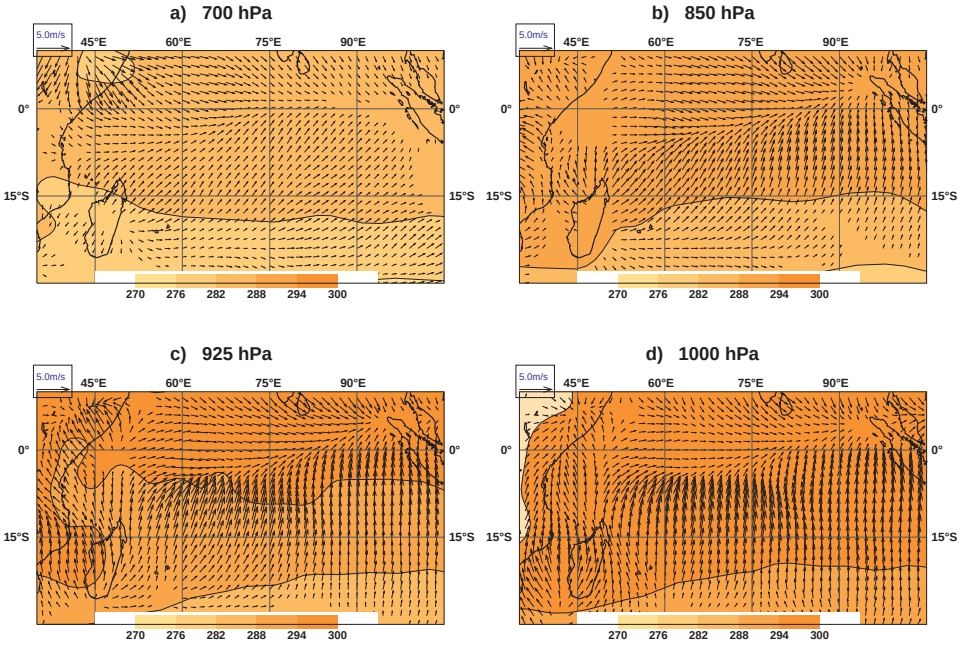

Figure 38: Mean wind and temperature analysis over the Indian Ocean at 700 (a), 850 (b), 925 (c) and 1000 hPa (d). Period is October-November 2011.

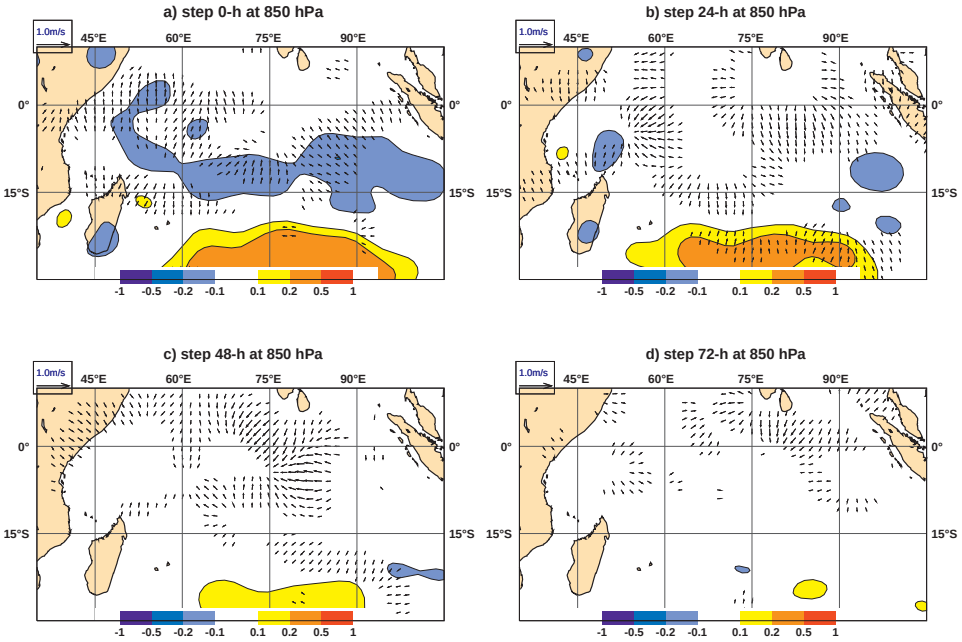

Figure 39: Mean analysis difference between control and Meteosat-7 AMV denial experiment for wind (arrows) and temperature (colour scale) at 850 hPa and analysis time (a), day+1 (b), day+2 (c) and day+3 (d) forecast time. Period is October-November 2011.

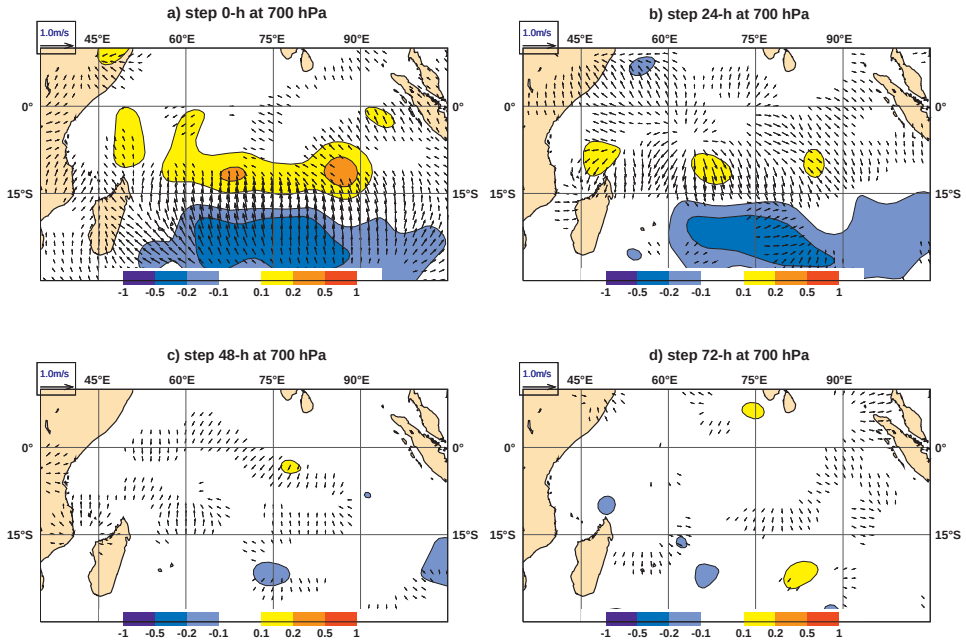

Figure 40: As Fig. 39 but 700 hPa.

Table 1: List of some major model cycles during the last decade and decription of model changes affecting Tropics.

Model Cycle	Introduction Date	Description
Cy23r3	21 November 2000	**T511**
Cy24r3	22 January 2002	SSMI bias correction, active QuikSCAT data, preconditioning of 4DVAR minimization, new radiative transfer model
Cy25r4	14 January 2003	Multi-incremental 4D-Var, GOES WV radiances, HIRS channels, new convective triggering, revised cloud numerics
Cy26r3	7 October 2003	AMSU-B, MSG, GOES9/12 radiances, new humidity analysis
Cy28r3	28 September 2004	Revised convection numerics and call of cloud scheme, radiation called hourly, MSG clear-sky radiances and GOES AMVs
Cy29r2	28 June 2005	Assimilation of rain-affected SSMI radiances, use of MSG winds, humidity analysis changes affecting spinup.
Cy30r1	1 February 2006	**T799 L91**, model top raised to 1 Pa, inner loop upgrade from T95/T159 to T95/T255.
Cy31r1	12 September 2006	**ERA-Interim**: Revised cloud scheme, ice supersaturation, implicit computation of convective transports, modified orographic drag, ocean surface rel. hum reduced from 100% to 98%, revised assimilation of rain-affected radiances, variational bias correction of satellite radiances
Cy32r2	5 June 2007	3 outer loops 4D-Var, new moist linear physics,new SW radiation and McICA
Cy32r3	6 November 2007	Convection revision, new soil hydrology, revision of vertical diffusion, radiosonde bias correction, increased radio occultation data, assimilate TMI and SSMIS window channels, increased radio occultation data
Cy33r1	3 June 2008	Increased vertical diffusion, retuned entrainment and convective scaling bugfix, change in surface roughness and orographic form drag, active assimilation of rainy radiances
Cy35r3	8 September 2009	Non-orogr. gravity wave scheme and new trace gas climatology, improved background error statistics for humidity, Huber norm, weak constraint strato 4D-Var
Cy36r2	26 January 2010	**T1279**
Cy36r4	9 November 2010	5-species prognostic microphysics, new simplified convective entrainment/detrainment, diffusion in stable boundary-layer, all-sky improvements to microwave assimilation, base of Seasonal System 4 (2011)
Cy37r2	18 May 2011	Fix condensation term in cloud scheme, adjustments to MODIS AMVs, and AMSU-A errors
Cy37r3	15 November 2011	New RTTOV, aircraft bias correction, revised convective detrainment, revised ice microphysics
Cy38r1	19 June 2012	Filtering of spectral noise, revised convective downdraught strength, revised ice melting and fall speed.

Table 2: List of observation types assimilated in October 2011. The total number of data in one 12-hour assimilation cycle is on average 5,000,000.

Name	Data type	Variable/region
OZONE (O_3)	Backscattered solar UV radiation, retrievals	Ozone, stratosphere
GOES-Rad	US geostationary satellite infrared sounder radiances	Moisture, mid/upper troposphere
MTSAT-Rad	Japanese geostationary satellite infrared sounder radiances	Moisture, mid/upper troposphere
MET-rad	EUMETSAT geostationary satellite infrared sounder radiances	Moisture, mid/upper troposphere
AMSU-B	Microwave sounder radiances	Moisture, troposphere
MHS	Microwave sounder radiances	Moisture, troposphere
MERIS	Differential reflected solar radiation, retrievals	Total column water vapour
TMI	Microwave imager radiances	Total column water vapour, cloud liquid water, precipitation
SSMIS	Microwave imager radiances	Total column water vapour, cloud liquid water, precipitation
GPS-RO	GPS radio occultation bending angles	Temperature, surface pressure
IASI	Infrared sounder radiances	Temperature, moisture, ozone
AIRS	Infrared sounder radiances	Temperature, moisture, ozone
AMSU-A	Microwave sounder radiances	Temperature
HIRS	Infrared sounder radiances	Temperature, moisture, ozone
ASCAT	Microwave scatterometer backscatter coefficients	Surface wind
MODIS-AMV	US polar Atmospheric Motion Vectors, retrievals	Wind, troposphere
Meteosat-AMV	(Meteosat-7 and 9) EUMETSAT geostationary Atmospheric Motion Vectors, retrievals	Wind, troposphere
MTSAT-AMV	Japanese geostationary Atmospheric Motion Vectors, retrievals	Wind, troposphere
GOES-AMV	(GOES-11 and 13) US geostationary Atmospheric Motion Vectors, retrievals	Wind, troposphere
PROFILER	US, European and Japanese Wind profiles	Wind, troposphere
PILOT	Radiosondes from land stations	Wind, troposphere
DROP	Dropsondes from aircrafts	Wind, temperature, moisture, pressure
TEMP	Radiosondes from land and ships	Wind, temperature, moisture, pressure
Aircraft	Aircraft measurements	Wind, temperature, troposphere
DRIBU	Drifting buoys	Surface pressure, moisture, wind
SYNOP	Surface Observations at land stations and on ships	Surface pressure, moisture, wind

References

Agusti-Panareda, A., A. Beljaars, C. Cardinali, L. Genkova, and C. D.Thorncroft, 2010: Impact of assimilating AMMA SOP soundings on ECMWF analyses and forecasts. *Wea. Forecast.*, **25**, 1142–1160.

Ahlgrimm, M., and M. Köhler, 2010: Evaluation of Trade Cumulus in the ECMWF Model with Observations from CALIPSO. *Mon. Weather Rev.*, **138**, 3071–3083.

Andersson, E., E. Hólm, P. Bauer, A. Beljaars, G. A. Kelly, A. P. McNally, A. J. Simmons, J. N. Thépaut, and A. Tompkins, 2007: Analysis and forecast impact of the main humidity observing systems. *Q. J. R. Meteorol. Soc.*, **133**, 1473–1485.

Baker, N., and R. Daley, 2000: Observation and background adjoint sensitivity in the adaptive observation targeting problem. *Q. J. R. Meteorol. Soc.*, **126**, 1431–1454.

Barnston, A., M. K. Tippett, M. L. L'Heureux, S. Li, and D. G. DeWitt, 2012: Skill of real-time seasonal model predictions during 2002-11. is our capability increasing?

Bauer, P., T. Auligné, W. Bell, A. Geer, V. Guidard, S. Heilliette, M. Kazumori, M.-J. Kim, E. H.-C. Liu, A. P. McNally, B. Macpherson, K. Okamoto, R. Renshaw, and L.-P. Riishoegaard, 2011: Satellite cloud and precipitation assimilation at operational NWP centres. *Q. J. R. Meteorol. Soc.*, **137**, 1934–1951.

Bauer, P., P. Lopez, D. Salmond, A. Benedetti, S. Saarinen, and M. Bonazzola, 2006: Implementation of 1D+ 4D-Var assimilation of precipitation affected microwave radiances at ECMWF. Part II: 4D-Var. *Q. J. R. Meteorol. Soc.*, **132**, 2307–2332.

Bechtold, P., 2012: Atmospheric Moist Convection. ECMWF Lecture Note, available under http://www.ecmwf.int/newsevents/training/lecture_notes/LN_PA.html, 81 pp.

Bechtold, P., M. Köhler, T. Jung, F. Doblas-Reyes, M. Leutbecher, M. Rodwell, F. Vitart, and G. Balsamo, 2004: The simulation of the diurnal cycle of convective precipitation over land in global models. *Q. J. R. Meteorol. Soc.*, **130**, 3119–3137.

Bechtold, P., M. Köhler, T. Jung, F. Doblas-Reyes, M. Leutbecher, M. Rodwell, F. Vitart, and G. Balsamo, 2008: Advances in simulating atmospheric variability with the ECMWF model: From synoptic to decadal time-scales. *Q. J. R. Meteorol. Soc.*, **134**, 1337–1351.

Blackburn, M., D. L. Williamson, K. Nakajima, W. Ohfuchi, O. Takahashi, Y.-Y. Hayashi, H. Nakamura, M. Ishiwatari, J. McGregor, H. Borth, V. Wirth, H. Frank, P. Bechtold, N. P. Wedi, H. Tomita, M. Satoh, M. Zhao, I. M. Held, M. J. Suarez, M.-I. Lee, M. Watanabe, M. Kimoto, Y. Liu, Z. Wang, A. Molod, K. Rajendran, A. Kitoh, and R. Stratton, 2012: The Aqua Planet Experiment (APE): CONTROL SST Simulation. *J. Meteorol. Soc. Jpn,*, to appear.

Bonavita, M., L. Isaksen, and E. Holm, 2012: On the use of EDA background error variances in the ECMWF 4D-Var. *Q. J. R. Meteorol. Soc.,*, to appear.

Bougeault, P., Z. Toth, C. Bishop, B. Brown, D. Burridge, D.-H. Chen, B. Ebert, M. Fuentes, T. Hamill, K. Mylne, J. Nicolau., T. Paccagnella, Y.-Y. Park, D. Parsons, B. Raoult, D. Schuster, P. S. Dias, R. Swinbank, Y. Takeuchi, W. Tennant, L. Wilson, and S. Worley, 2010: The THORPEX interactive grand global ensemble. *Bull. Am. Meteorol. Soc.*, **91**, 1059–1072.

Bretheron, C. S., M. E. Peters, and L. E. Back, 2004: Relationships bewteen water vapor path and precipitation over the tropical oceans. *J. Climate*, **17**, 1517–1528.

Bretherton, C. S., and P. Smolarkiewicz, 1989: Gravity waves, compensating subsidence and detrainment around cumulus clouds. *J. Atmos. Sci.*, **46**, 740–759.

Cardinali, C., 2009: Monitoring the forecast impact on the short-range forecast. *Q. J. R. Meteorol. Soc.*, **135**, 239–250.

Cardinali, C., and R. Buizza, 2004: Observation sensitivity to the analysis and the forecast: a case study during ATreC targeting campaign. Proceedings of the First THORPEX International Science Symposium, Montreal, Canada, WMO TD 1237 WWRP/THORPEX N. 6.

Cardinali, C., S. Pezzulli, and E. Andersson, 2004: Influence matrix diagnostics of a data assimilation system. *Q. J. R. Meteorol. Soc.*, **130**, 2767–2786.

Cardinali, C., and F. Prates, 2011: Performance measurement with advanced diagnostic tools of all-sky microwave imager radiances in 4D-Var. *Q. J. R. Meteorol. Soc.*, **137**, 2038–2046.

Chaboureau, J.-P., F. Guichard, J.-L. Redelsperger, and J.-P. Lafore, 2004: The role of stability and moisture in the diurnal cycle of convection over land. *Q. J. R. Meteorol. Soc.*, **130**, 3105–3117.

Chakraborty, A., 2010: The skill of ecmwf medium-range forecasts during the year of tropical convection 2008. *Mon. Weather Rev.*, **138**, 3787–3805.

Chikira, M., and M. Sugiyama, 2010: A cumulus parameterization with state-depdent entrainment rate. part i: Description and sensitivity to temperature and humidity profiles. *J. Atmos. Sci.*, **67**, 2171–2193.

Cohen, B., and G. C. Craig, 2006: Fluctuations in an equilibrium convective ensemble. part i: Theoretical formulation. *J. Atmos. Sci.*, **63**, 1996–2004.

De, S., and D. R. Chakraborty, 2004: Tropical systematic and random error energetics based on NCEP (MRF) analysis-forecast system - A barotropic approach part II: in wavenumber. *Proc. Indian Acad. Sci.*, **113**, 167–195.

De Szoeke, S. P., and S.-P. Xie, 2008: The tropical eastern Pacific seasonal cycle: Assessment of errors and mechanisms in IPCC AR4 coupled ocena-jas,atmosphere general circulation models. *J. Climate*, **21**, 2573–2590.

Dee, D., 2005: Bias and data assimilation. *Q. J. R. Meteorol. Soc.*, **131**, 3323–3343.

Dee, D. P., S. M. Uppala, A. J. Simmons, P. Berrisford, P. Poli, S. Kobayashi, U. Andrae, M. A. Balmaseda, G. Balsamo, P. Bauer, P. Bechtold, A. C. M. Beljaars, L. van de Berg, J. Bidlot, C. Delsol, R. Dragani, M. Fuentes, L. A. Geer, Haimberger, S. Healy, H. Hersbach, E. V. Hólm, L. Isaksen, P. Kalberg, M. Køhler, M. Matricardi, A. P. McNally, B. M. Monge-Sanz, J.-J. Morcrette, B.-K. Park, C. Peuby, P. de Rosnay, C.Tavolato, J.-N. Thépaut, and F. Vitart, 2011: The era-interim reanalysis: Configuration and performance of the data assimilation system. *Q.J.R. Meteor. Soc.*, **137**, 553–597.

Derbyshire, S. H., I. Beau, P. Bechtold, J.-Y. Grandpeix, J.-M. Piriou, J.-L. Redelsperger, and P. M. M. Soares, 2004: Sensitivity of moist convection to environmental humidity. *Q.J.R. Meteor. Soc.*, **130**, 3055–3080.

Ding, R., J. Li, and K.-H. Seo, 2010: Predictability of the Madden-Julian Oscillation estimated using observational data. *Mon. Weather Rev.*, **138**, 1004–1013.

Dirmeyer, P. A., B. A. Cash, J. L. Kinter, T. Jung, L. Marx, M. Satoh, C. Stan, H. Tomita, P. Towers, N. Wedi, D. Achuthavarier, J. M. Adams, E. L. Altshuler, B. Huang, E. K. Jin, and J. Manganello, 2011: Simulating the diurnal cycle of rainfall in global climate models: Resolution versus parameterization. *Climate Dyn.,*, DOI: 10.1007/s00382–011–1127–9.

Fiorino, M., 2009: Record-setting performance of the ecmwf ifs in medium-range tropical cylone prediction. *ECMWF Newsletter,* (118).

Forbes, R., A. M. Tompkins, and A. Untch, 2011: A new prognostic bulk microphysics scheme for the ifs. ECMWF Technical Memorandum No. 649, 30 pages, available from ECMWF, Reading, UK.

Garner, S. T., D. M. W. Frierson, I. M. Held, O. Pauluis, and G. K. Vallis, 2007. *J. Atmos. Sci.*, **64**, 2061–2075.

Geer, A., P. Bauer, and P. Lopez, 2010: Direct 4D-var assimilation of all-sky radiances. Part II: Assessment. *Q. J. R. Meteorol. Soc.*, **136**, 1886–1905.

Genio, A. D. D., and J. Wu, 2010: Sensitivity of moist convection to environmental humidity. *J. Climate,* **23**, 2722–2738.

Gerard, L., and J.-F. Geleyn, 2005: Evolution of a subgrid deep convection parametrization in a limited-area model with increasing resolution. *Q. J. R. Meteorol. Soc.*, **131**, 2293–2312.

Graversen, R. G., E. Källén, M. Tjernström, and H. Körnich, 2007: Atmospheric mass-transport inconsistencies in the era-40 reanalysis. *Q. J. R. Meteorol. Soc.*, **133**, 673–680.

Guichard, F., J. C. Petch, J.-L. Redelsperger, P. Bechtold, J.-P. Chaboureau, S. Cheinet, W. Grabowski, H. Grenier, C. G. Jones, M. Koehler, J.-M. Piriou, R. Tailleux, and M. Tomasini, 2004: Modelling the diurnal cycle of deep precipitating convection over land with CRMs and SCMs.

Haiden, T., M. J. Rodwell, D. S. Richardson, A. Okagaki, T. Robinson, and T. Hewson, 2012: Intercomparison of global model precipitation forecast skill in 2010/11 using the SEEPS score. *Mon. Weather Rev.*, **140**, in press.

Held, I. M., R. S. Hemler, and V. Ramaswamy, 1993: Radiative-convective equilibrium with explicit two-dimensional moist convection. *J. Atmos. Sci.*, **50**.

Hilburn, K. A., and F. J. Wentz, 2008: Intercalibrated passive microwave rain products from the unified microwave ocean retrieval algorithm (UMORA). *J. Appl. Meteor. Clim.*, **47**, 778–794.

Hirons, L., P. Inness, F. Vitart, and P. Bechtold, 2012a: Understanding advances in the simulation of intraseasonal variability in the ECMWF model. Part I: The representation of the MJO. *Q. J. R. Meteorol. Soc.,*, submitted.

Hirons, L., P. Inness, F. Vitart, and P. Bechtold, 2012b: Understanding advances in the simulation of intraseasonal variability in the ecmwf model. part ii: The application of process based diagnostics. *Q. J. R. Meteorol. Soc.,*, submitted.

Holloway, C. E., S. J. Woolnough, and G. M. S. Lister, 2012: Precipitation distributions for explicit versus parametrized convection in large-domain high-resolution tropical case study. *Q. J. R. Meteorol. Soc.,*, available online.

Hourdin, F., J.-Y. Grandpeix, C. Rio, S. Bony, A. Jam, F. Cheruy, N. Rochetin, L. Fairhead, A. Idelkadi, and I. Musat, 2012: Lmdz5b: the atmospheric component of the ipsl climate model with revisited parameterizations for clouds and convection. *Climate Dyn.*,, DOI: 10.1007/s00382–012–1343–y.

Inness, P. M., J. M. Slingo, E. Guilyardi, and J. Cole, 2003: Simulation of the madden-julian oscillation in a coupled general circulation model: Part ii: The role of the basic state. *J. Climate*, **16**, 365–382.

Järvinen, H., M. Laine, A. Solonen, and H. Haario, 2011: Ensemble prediction and parameter estimation system: the concept. *Q. J. R. Meteorol. Soc.*, **138**, 281–288.

Jung, T., G. Balsamo, P. Bechtold, A. Beljaars, M. Köhler, M. Miller, J.-J. Morcrette, A. Orr, M. Rodwell, and A. Tompkins, 2010: The ecmwf model climate: recent progress through improved physical parametrizations. *Q. J. R. Meteorol. Soc.*, **136**, 1145–1160.

Jung, T., M. J. Miller, T. N. Palmer, P. Towers, N. Wedi, D. Achuthavarier, J. M. Adams, E. L. Altshuler, B. A. Cash, J. L. K. III, L. Marx, C. Stan, and K. I. Hodges, 2011: High-resolution global climate simulations with the ecmwf model in the athena project: Experimental design, model climate and seasonal forecast skill. *J. Climate*, **25**, 3155–3172.

Kamga, A. F., S. Fongang, and A. Viltard, 2000: Systematic errors of the ECMWF operational model over tropical Africa. *Mon. Weather Rev.*, **128**, 1949–1959.

Kanamitsu, M., 1985: A study of predictability of ECMWF operational forecast model in the tropics. *Rev. Geophys.*, **63**, 779–804.

Kelly, G., P. Bauer, A. J. Geer, P. Lopez, and J.-J. Thépaut, 2007: Impact of SSM/I observations related to moisture, clouds and precipitation on global NWP forecast skill. *Mon. Weather Rev.*, **138**, 3071–3083.

Khairoutdinov, M., and D. A. Randall, 2006: High-resolution simulations of shallow-to-deep convection transition over land. *J. Atmos. Sci.*, **63**, 3421–3436.

Kim, D., A. H. Sobel, A. D. Genio, Y.-H. Chen, S. J. Camargo, M.-S. Yao, M. Kelley, and L. Nazarenko, 2012: The tropical subseasonal variability simulated in the nasa giss general circulation model. *J. Climate*,, in press.

Kim, D., A. H. Sobel, and L.-S. Kang, 2011: A mechanism denial study on the madden-julian oscillation. *J. Adv. Model. Earth Syst.*, **3**, doi:10.1029/2011MS000081.

Kim, D., A. H. Sobel, E. D. Maloney, D. M. W. Frierson, and L.-S. Kang, 2011: A systematic relationship between intraseasonal variability and mean state bias in agcm simulations. *J. Climate*, **24**, 5506–5520.

Kuang, Z., P. N. Blossey, and C. S. Bretherton, 2005: A new approach for 3d cloud-resolving simulations of large-scale atmospheric circulation. *Geophys. Res. Letters*, **32**, L02809.

Kuell, V., A. Gassmann, and A. Bott, 2007: Towards a new hybrid cumulus parametrization scheme for use in non-hydrostatic weather prediction models. *Q. J. R. Meteorol. Soc.*, **133**, 479–490.

Laine, M., A. Solonen, H. Haario, and H. Järvinen, 2011: Ensemble prediction and parameter estimation system: the method. *Q. J. R. Meteorol. Soc.*, **138**, 289–297.

Langland, R. H., and N. L. Baker, 2004: Estimation of observation impact using the NRL atmospheric variational data assimilation adjoint system. *Tellus*, **56**.

Langland, R. H., R. N. Maue, and C. H. Bishop, 2008: Uncertainty in atmospheric temperature analyses. *Tellus*, **60**.

Lin, J. L., G. N. Kiladis, B. E. Mapes, K. E. Weickmann, K. R. Sperber, W. Lin, M. C. Wheeler, S. D. Schubert, A. D. Genio, L. J. Donner, S. Emori, J. F. Gueremy, F. Hourdin, P. J. Rasch, E. Roeckner, and J. F. Scinocca, 2006: Tropical intraseasonal variability in 14 ipcc ar4 climate models. part i: Convective signals. *J. Climate*, **19**, 2665–2690.

Lin, Y., L. J. Donner, J. Petch, P. Bechtold, J. Boyle, S. Klein, T. Komori, K. Wapler, M. Willett, X. Xie, M. Zhao, S. Xie, S. A. McFarlane, and C. Schumacher, 2012: Twp-ice global atmospheric model intercomparison: convection responsiveness and resolution impact. *J. Geophys. Res.*, **117**, D09111,doi:10.1029/2011JD017018.

Lupu, C., P. Gauthier, and S. Laroche, 2011: Evaluation of the impact of observations on analyses in 3d- and 4d-var based on information content. *Mon. Weather Rev.*, **139**, 726–737.

Madden, R. A., and P. R. Julian, 1971: Detection of a 40-50 day oscillation in the zonal wind in the tropical pacific. *J. Atmos. Sci.*, **28**, 702–708.

Magnusson, L., M. Alonso-Balmaseda, S. Corti, F. Molteni, and T. Stockdale, 2011: On the dependence of enso simulation on the coupled model mean state. ECMWF Technical Memorandum No. 658, 29 pages, available from ECMWF, Reading, UK.

Magnusson, L., M. Alonso-Balmaseda, S. Corti, F. Molteni, and T. Stockdale, 2012: Evaluation of forecast strategies for seasonal and decadal forecasts in presence of systematic model errors. ECMWF Technical Memorandum No. 676, 30 pages, available from ECMWF, Reading, UK.

Molteni, F., T. Stockdale, M. Balmaseda, G. Balsamo, R. Buizza, L. Ferranti, L. Magnusson, K. Mogensen, T. Palmer, and F. Vitart, 2011: The new ECMWF seasonal forecast system (System 4). ECMWF Technical Memorandum No. 656, 30 pages, available from ECMWF, Reading, UK'.

Morcrette, J.-J., H. Barker, J. N. S. Cole, M. H. Iacono, and R. Pincus, 2008: Impact of a new radiation package, McRad, in the ECMWF integrated forecasting system. *Mon. Weather Rev.*, **136**, 4773–4798.

Okajima, H., S. P. Xie, and A. Numaguti, 2003: Interhemispheric coherence of tropical climate variability: Effect of the climtological ITCZ. *J. Meteorol. Soc. Jpn*, **81**, 1371–1386.

Orr, A., P. Bechtold, J. Scinoccia, M. Ern, and M. Janiskova, 2010: Improved middle atmosphere climate and analysis in the ECMWF forecasting system through a non-orographic gravity wave parametrization. *J. Climate*, **23**, 5905–5926.

Park, Y.-Y., R. Buizza, and M. Leutbecher, 2008: TIGGE: preliminary results on comparing and combining ensembles. *Q. J. R. Meteorol. Soc.*, **134**, 2029–2050.

Peng, G., H.-M. Zgang, H. Frank, J.-R. Bidlot, M. Higaki, S. Stevens, and W. R. Hankins, 2012: Evaluation of various surface wind products with oceansites buoy measurements. *Weather Forecast.*,.

Petch, J. C., A. R. Brown, and M. E. B. Gray, 2002: The impact of horizontal resolution on the simulations of convective development over land. *Q. J. R. Meteorol. Soc.*, **28**, 2031–2044.

Philander, S. G. H., and R. C. Pacanowski, 1981: The oceanic response to cross-equatorial winds (with application to coastal upwelling in low latitudes). *Tellus*, **33A**, 201–210.

Piriou, J.-M., J.-L. Redelsperger, J.-F. Geleyn, J.-P. Lafore, and F. Guichard, 2007: An Approach for Convective Parameterization with Memory: Separating Microphysics and Transport in Grid-Scale Equations. *J. Atmos. Sci.*, **64**, 4127–4139.

Plu, M., 2011: A new assessment of the predictability of tropical cyclone tracks. *Mon. Weather Rev.*, **139**, 3600–3608.

Raymond, D. J., and Z. Fuchs, 2009. *J. Atmos. Sci.*, **22**, 3031–3046.

Rio, C., F. Hourdin, J.-Y. Grandpeix, and J. P. Lafore, 2009: Shifting the diurnal cycle of parameterized-deep convection over land. *Geoph. Res. Let.*, **36**, L07809,doi:10.1029/2008GL036779.

Rodwell, M. J., and B. J. Hoskins, 2001: Subtropical anticyclones and summer Monsoons. *J. Climate*, **14**, 3192–3211.

Rodwell, M. J., T. Jung, P. Bechtold, P. Berrisford, N. Bormann, C. Cardinali, L. Ferranti, T. Hewson, F. Molteni, M. B. N. Wedi, G. Balsamo, M. Bonavita, R. Buizza, M. Dahoui, A. Garcia-Mendez, M. Leutbecher, P. Lopez, Y. Trémolet, and F. Vitart, 2010. ECMWF Technical Memorandum No. 637, 49 pages, available from ECMWF, Reading, UK.

Rodwell, M. J., D. S. Richardson, T. D. Hewson, and T. Haiden, 2010: A new equitable score suitable for verifying precipitation in numerical weather prediction. *Q. J. R. Meteorol. Soc.*, **136**, 1344–1363.

Rooyde, W., P. Bechtold, K. Fröhlich, C. Hohenegger, H. Jonker, S. Mironov, J. Teixeira, and J.-I. Yano, 2012: Entrainment and detrainment in cumulus convection: An overview. *Q. J. R. Meteorol. Soc.*,, to appear.

Sandu, I., A. Beljaars, P. Bechtold, T. Mauritsen, and G. Balsamo, 2012: Why is it so difficult to represent stably stratified conditions in nwp models ? *J. Adv. Model. Earth System*,.

Sato, T., H. Miura, M. Satoh, Y. N. Takayabu, and Y. Wang, 2009: Diurnal cyle of precipitation in the tropics simulated in a global cloud-resolving model. *J. Climate*, **22**.

Schlemmer, L., C. Hohenegger, J. Schmidli, C. Bretherton, and C. Schär, 2011: An idealized cloud-resolving framework for the study of summertime midlatitude diurnal convection over land. *Q. J. R. Meteorol. Soc.*, **68**.

Shutts, G. J., 2006: Upscale effects in simulations of tropical convection on an equatorial beta-plane. *Dyn. Atmos. Oceans*, **42**, 30–58.

Shutts, G. J., 2008: The forcing of large-scale waves in an explicit simulation of deep tropical convection. *Dyn. Atmos. Oceans*, **45**, 1–25.

Simmons, A. J., 1982: The forcing of stationary wave motion by tropical diabatic heating. *Q. J. R. Meteorol. Soc.*, **108**, 503–534.

Simmons, A. J., and A. Hollingsworth, 2002: Some aspects of the improvement in skill of numerical weather prediction. *Q. J. R. Meteorol. Soc.*, **128**.

Slingo, J., M. Blackburn, A. Betts, R. Brugge, K. Hodges, B. Hoskins, M. Miller, L. Steenman-Clark, and J. Thuburn, 1994: Mean climate and transience in the tropics of the ugamp gcm: Sensitivity to convective parametrization. *Q. J. R. Meteorol. Soc.*, **120**, 881–922.

Slingo, J., K. R. Sperber, J. S. Boyle, J. P. Ceron, M. Dix, B. Dugas, W. Ebisuzaki, J. Fyfe, D. Gregory, J. F. Gueremy, J. Hack, A. Harzallah, P. Inness, A. Kitoh, W. K. M. Lau, B. McAvaney, R. A. Madden, A. J. Matthews, T. N. Palmer, C. K. Park, D. A. Randall, and N. Renno, 1996: Intraseasonal oscillations in 15 atmospheric general circulation models: results from an amip diagnostic subproject. *Climate Dyn.*, **12**, 325–357.

Slingo, J. M., K. Sperber, J.-J. Morcrette, and G. L. Potter, 1992: Analysis of the temporal behavior of convection in the tropics of the European Centre for Medium-range Weather Forecast model. *J. Geophys. Res.*, **97**, 119–135.

Smolarkiewicz, P. K., and L. G. Margolin, 1997: On forward-in-time differencing for fluids: An eulerian/semi-lagrangian nonhydrostatic model for stratified flows. *Atmos. Ocean Special*, **35**, 127–152.

Steinheimer, M., M. Hantel, and P. Bechtold, 2008: Convection in Lorenz 92s global cycle with the ECMWF model. *Tellus*, **60A**, 1001–1022.

Stirling, A., and R. A. Stratton, 2012: Entrainment processes in the diurnal cycle of deep convection over land. *Q. J. R. Meteorol. Soc.*,, to appear.

Thayer-Calder, K., and D. A. Randall, 2009: The role of convective moistening in the Madden-Julian oscillation. *J. Atmos. Sci.*, **67**, 3297–3312.

Tompkins, A. M., P. Bechtold, A. C. M. Beljaars, A. Benedetti, S. Cheinet, M. Janisková, M. Köhler, P. Lopez, and J.-J. Morcrette, 2004: Moist physical processes in the ifs: Progress and plans. ECMWF Technical Memorandum No. 452, 93 pages, available from ECMWF, Reading, UK.

Tukey, J. W., 1977: Exploratory data analysis. Addison-Wesley.

Uppala, S. M., P. W. Kallberg, A. J. Simmons, U. Andrae, V. M. Costa-Bechtold, M. Fiorino, J. K. Gibson, J. Haseler, A. Hernandez, G. A. Kelly, X. Li, K. Onogi, S. Saarinen, N. Sokka, R. P. Allan, E. Andersson, K. Arpe, M. A. Balmaseda, A. C. M. Beljaars, L. V. D. Berg, J. Bidlot, N. Bormann, S. Caires, F. Chevallier, A. Dethof, M. Dragosavac, M. F. M. Fisher, E. H. S. Hagemann, B. J. Hoskins, L. Isaksen, P. A. Janssen, R. Jenne, A. P. McNally, J. F. J.-F. Mahfouf, J.-J. Morcrette, N. A. Rayner, R. W. Saunders, P. Simon, A. Sterl, K. E. Trenberth, A. Untch, D. Vasiljevic, P. Viterbo, and J. Woollen, 2005: The ERA-40 re-analysis. *Q. J. R. Meteorol. Soc.*, **131**, 2961–3012.

Velleman, P. F., and R. E. Welsch, 1981: Efficient computing of regression diagnostics. *The American Statisticians*, **35**, 234–242.

Verkley, W. T. M., and I. R. van der Velde, 2010: Balanced dynamics in the tropics. *Q. J. R. Meteorol. Soc.*, **136**, 41–49.

Vitart, F., and F. Molteni, 2009: Simulation of the MJO and its teleconnections in an ensemble of 46-day hindcasts. *Q. J. R. Meteorol. Soc.*, **136**, 842–856.

Wahba, G., D. R. Johnson, F. Gao, and J. Gong, 1995: Adaptive tuning of numerical weather prediction models: Randomized GCV in three- and four-dimensional data assimilation. *Mon. Weather Rev.*, **123**, 3358–3369.

Waliser, D. E., M. Moncrieff, D. Burridge, A. H. Fink, D. Gochis, B. N. Goswami, B. Guan, P. Harr, J. Heming, H.-H. Hsu, C. Jakob, M. Janiga, R. Johnson, S. Jones, P. Knippertz, J. Marengo, H. Nguyen, M. Pope, Y. Serra, C. Thorncroft, M. Wheeler, R. Wood, and S. Yuter, 2012: The year of tropical convection: Climate variability and weather highlights. *Bull. Am. Meteorol. Soc.*,, to appear.

Wedi, N. P., and P. K. Smolarkiewicz, 2010: A nonlinear perspective on the dynamics of the mjo: Idealized large-eddy simulations. *J. Atmos. Sci.*, **67**, 1202–1217.

Wei, M., Z. Toth, and Y. Zhu, 2010: Analysis differences and error variance estimates from multi-centre analysis. *Austral. Meteor. Ocean. J.*, **59**, 25–34.

Wheeler, M. C., and H. H. Hendon, 2004: An all-seasonal real-time multivariate MJO Index: development of and Index for monitoring and prediction. *Mon. Wea. Rev.*, **132**, 1917–1932.

Williamson, D. L., M. Blackburn, K. Nakajima, W. Ohfuchi, O. Takahashi, Y.-Y. Hayashi, H. Nakamura, M. Ishiwatari, J. McGregor, H. Borth, V. Wirth, H. Frank, P. Bechtold, N. P. Wedi, H. Tomita, M. Satoh, M. Zhao, I. M. Held, M. J. Suarez, M.-I. Lee, M. Watanabe, M. Kimoto, Y. Liu, Z. Wang, A. Molod, K. Rajendran, A. Kitoh, and R. Stratton, 2012: The Aqua Planet Experiment (APE): Response to changed meridional SST profile. *J. Meteorol. Soc. Jpn*,, to appear.

Woolnough, S. J., F. Vitart, and M. A. Balmaseda, 2007: The role of the ocean in the Madden-Julian Oscillation: Implications of MJO prediction. *Q. J. R. Meteorol. Soc.*, **133**, 117–128.

Yanai, M., B. Chen, and W.-W. Tung, 2000: The Madden-Julian oscillation observed during the TOGA COARE IOP: Global view. *J. Atmos. Sci.*, **57**, 2374–2396.

Yang, G.-Y., and J. Slingo, 2001: The diurnal cycle in the tropics. *Mon. Weath. Rev.*, **129**, 784–801.

Ẑagar, N., E. Andersson, and M. Fisher, 2005: Balanced tropical data assimilation based on a study of equatorial waves in ecmwf short-range forecast errors. *Q. J. R. Meteorol. Soc.*, **131**, 987–1011.

Ẑagar, N., E. Andersson, M. Fisher, and A. Untch, 2007: Influence of the QBO on the ECMWF model short-range forecast errors in the tropical stratosphere. *Q. J. R. Meteorol. Soc.*, **133**, 1843–1853.

Ẑagar, N., L. Isaksen, D. Tan, and J. Tribbia, 2012: Balance properties of the short-range forecast errors in the ECMWF 4D-Var ensemble. *Q. J. R. Meteorol. Soc.*, **138**, to appear.

Zhang, C., 2005: Madden-Julian oscillation. *Rev. Geophys.*, **43**, 1–36.

Zhang, G. J., and H.-R. Cho, 1991: Parameterization of the vertical transport of momentum by cumulus clouds. Part I: Theory. *J. Atmos. Sci.*, **48**, 1483—2539.

Zhang, Y., and S. A. Klein, 2010: Mechanisms affecting the transition from shallow to deep convection over land: Interferences from observations of the diurnal cycle collected at the ARM Southern Great Plains site. *J. Atmos. Sci.*, **67**, 2943–2959.

Zhu, Y., and R. Gelaro, 2008: Observation sensitivity calculations using the adjoint of the gridpoint statistical interpolation (gsi) analysis system. *Mon. Weather Rev.*, **136**, 335–351.